Automation of one-loop corrections for multi-particle processes

RODGERS, MARK

Automation of one-loop corrections for multi-particle processes

Mark Rodgers

A Thesis presented for the degree of
Doctor of Philosophy

Institute for Particle Physics Phenomenology
Department of Physics
Durham University
United Kingdom

July 2012

Automation of one-loop corrections for multi-particle processes

Mark Rodgers

Submitted for the degree of Doctor of Philosophy
July 2012

Abstract

With the advent of the Large Hadron Collider, we are in a new era in Particle Physics, in which unprecedented energy scales can be probed. Although it is a discovery machine, it has already been shown to be able to produce experimental precisions at the percent level, and so our theoretical calculations must match that, which requires (at least) calculations to next-to-leading order (NLO). In this thesis, we explain and develop new techniques for the evaluation of one-loop integrals, which have historically been the bottleneck in NLO calculations. After introducing Quantum Field Theory and NLO calculations, we explain the process of tensor reduction and the `golem95` method for avoiding its numerical instabilities. We follow this by discussing the techniques used to improve the stability of a library of scalar integrals (for two- and three-point integrals), and then we discuss the extension of the `golem95` library to include complex internal masses, along with the reasons for doing so. We then bring together the `GoSam` project with the event generator `Sherpa`, in order to calculate the process $pp \to e^+e^-\mu^+\mu^-$ by diboson production to NLO, including the (formally higher order) loop-induced process with gluons in the initial state.

Declaration

The work in this thesis is based on research carried out at the Institute for Particle Physics Phenomenology, Department of Physics, Durham University, United Kingdom. No part of this thesis has been submitted elsewhere for any other degree or qualification and it is all my own work unless referenced to the contrary in the text.

Acknowledgements

I am very grateful to everyone who has helped and supported me over the course of this PhD: my supervisor (in reality) Gudrun Heinrich, for her continuing help, particularly during my stays in Munich; and our collaborators, particularly Gionata Luisoni and Jean-Philippe Guillet – their help has been invaluable. There are too many supportive people at the IPPP to list them all, but I'd like to mention Mike Johnson, whose computing effort was always beyond the call of duty, Peter Richardson, Nigel Glover, Frank Siegert, and my shorter-term supervisors Adrian Signer and Daniel Maître. My officemates, particularly Jon Carter, made the process much more enjoyable. And of course I'd like to thank my family and Clare, who've managed both to put up with me over the course of this time and to keep me sane.

This work was funded by an STFC fellowship.

Contents

List of Figures

List of Tables

Chapter 1

Introduction

Particle Physics has its roots in a long tradition of probing the types of matter of which the universe is made and the interactions between them. From its study, we gain insights not only into very fundamental, small scale phenomena, but also into the very early history of the universe, and with theories that are applicable at ever higher energy, we probe ever closer to the Big Bang. All modern Particle Physics is built on Quantum Field Theories (QFTs), which trace their origins back to the 1920s, to descriptions of the quantised interaction between light and the electron by Dirac [1], which Fermi later reformulated into Quantum Electrodynamics (QED) [2].

The concept of a non-abelian local gauge theory was introduced in 1954 by Yang and Mills [3], and a mechanism to introduce masses to such theories was postulated in 1964 by three independent teams: Higgs [4,5]; Englert and Brout [6]; and Guralnik, Hagen and Kibble [7]. In the 1960s, Glashow [8], Weinberg [9] and Salam [10] used these theories to expand QED, including it and the weak force in a single framework.

As regards nuclear matter, the quark description was developed in 1964, independently by Gell-Mann [11] and Zweig [12]. It held that the hadrons were composed of a more fundamental set of particles, the quarks, with each meson composed of a quark pair and each baryon a quark triplet. At the time, only the u, d and s quarks were needed to explain the system of particles: the J/ψ meson, the first charmed hadron, was discovered in 1974 [13,14].

It soon became clear in studies of the baryons known at the time that there was a need for an additional interaction: for example, the Δ^{++}-baryon had spin $\frac{3}{2}$ and

isospin $\frac{3}{2}$ [15], and so according to the model it should have been composed of three up-quarks with aligned spins. However, it was a fermion, and therefore required an additional antisymmetric degree of freedom for consistency. Greenberg [16], and Han and Nambu [17] postulated an SU(3) charge, later to be termed colour, and the latter also noted that there could be 8 vector bosons, which would later be termed the gluons.

This completed the components required to build the Standard Model (SM), in which all of the calculations of this thesis are given. The SM is a neat model which, using only 19 free parameters[1], gives a very good description of all particle physics phenomena observed to date[2]: specifically, it is a QFT which describes all known particles and their three lower-scale interactions (i.e. not gravity). These fundamental forces are written in the combined gauge group $\mathrm{U}(1)_Y \times \mathrm{SU}(2)_L \times \mathrm{SU}(3)_C$, and the first two groups are spontaneously broken to $\mathrm{U}(1)_{QED}$ by the Higgs mechanism, allowing the W and Z bosons to be massive, and the photon massless.

However, although it seems pleasantly self-contained, we should not imagine that the Standard Model is a complete theory, as there are still aspects, from both experimental and theoretical points of view, which are not yet satisfactory.

Experimental Status of the SM

At the time of writing, it may well be that all components of the SM have been observed experimentally: it was announced this month [18, 19] that a particle consistent with the Higgs boson, the final part of the SM, has been observed by the two largest detectors at the Large Hadron Collider (LHC), at around 125 GeV.

From experiments previous to the LHC, most notably from SM fits from the precision studies at the Large Electron-Positron Collider (LEP) [20], there have been hints of tensions, which could be an indication of physics beyond the Standard

[1] The masses of the Higgs and Z, 9 fermion masses, 3 mixing angles, 1 mixing phase, 3 coupling strengths, and the CP-violating topological term θ_{QCD}.

[2] An exception being that the SM in its standard form does not include neutrino masses, which have been observed and can be added in (with the addition of another 3 masses, 3 mixing angles and a phase).

Model (BSM) within the reach of direct searches at the LHC. Although the LHC has been performing such searches, there have not so far been any such observations.

Theoretical Status of the SM

The SM is an extremely successful theory, but it is clear that it cannot be valid in all cases at all scales: the most obvious example being that it does not include gravity, which only becomes relevant at scales far larger than we can probe in currently-conceivable collider experiments.

There is also a problem of apparent arbitrariness: there is no clear reason why Nature would choose $\mathrm{U}(1)_Y \times \mathrm{SU}(2)_L \times \mathrm{SU}(3)_C$, nor why there are three generations, nor why there should be such a large range of scales, such as between the electron and Z-boson masses.

The SM also suffers from the hierarchy problem, that it is not clear what protects the Higgs boson from radiative corrections which would act to raise its mass. Many BSM theories have been proposed which would solve this problem, for example supersymmetry and extra dimensions, and the work of the LHC, to observe or constrain these models, continues.

1.1 Outline of Thesis

In Chapter 2, we discuss the theoretical background to particle physics and the Standard Model, and in Chapter 3 we discuss next-to-leading order calculations in general. In Chapter 4, we discuss the treatment of tensor integrals by tensor reduction. In Chapter 5, we detail the specific work on a library for scalar integrals, particularly in terms of certain difficult limits, and in Chapter 6 we discuss the implementation of such a library with complex masses, in order to be able to include the effects of unstable particles. In Chapter 7 we describe a particular calculation, $pp \to e^+e^-\mu^+\mu^-$ by diboson production, which was performed by linking the `GoSam` and `Sherpa` programmes, before concluding in Chapter 8.

Chapter 2

Particle Physics and The Standard Model

The fundamental machinery of the Standard Model is Quantum Field Theory (QFT): a set of techniques in which we begin with a Lagrangian $\mathcal{L}$ representing our fields and their interactions, and calculate from it physical quantities such as the cross section, in a way briefly reviewed in this chapter.

2.1 Scattering

In particle physics, we are interested in scattering processes, that is we wish to describe processes at colliders where there are (usually) two incident particles and a number of resultant particles[1]. To do this, we need to consider the momentum states of the incoming particles at large negative time, denoted $|i\rangle_{in}$, and those of the outgoing states at large positive time, denoted $|f\rangle_{out}$, so that we are far from the scattering interaction. We can then describe the amplitude for the transition between them, as we would in quantum mechanics, by calculating their overlap:

$$\langle f|_{out} |i\rangle_{in} \,, \tag{2.1.1}$$

[1]Much of the detail for this section and throughout the thesis draws on the excellent literature around the subject, including [21–26].

but the evolution of states in time can be described by the Hamiltonian, so we can evolve them to a common time (say, $t = 0$):

$$\langle f|_{out} |i\rangle_{in} = \lim_{T\to\infty} \langle f(T)| \, |i(-T)\rangle \tag{2.1.2}$$

$$= \lim_{T\to\infty} \langle f|e^{iH(2T)}|i\rangle \, . \tag{2.1.3}$$

We rewrite this double time translation matrix between the states as a Scattering matrix $\mathtt{S}$:

$$\langle f| \, \mathtt{S} \, |i\rangle \tag{2.1.4}$$

and so the probability of a scattering from $|i\rangle$ to $|f\rangle$, remembering the normalisation, will be

$$P = \frac{|\langle f| \, \mathtt{S} \, |i\rangle|^2}{\langle i|i\rangle \, \langle f|f\rangle}. \tag{2.1.5}$$

In scattering, we have the uninteresting case where nothing happens and $|i\rangle = |f\rangle$. To exclude this, we often work with the matrix $(\mathtt{S} - 1)$. We will also always have overall four-momentum conservation, so we can remove it in the definition of a process-specific quantity, the invariant matrix element $\mathcal{M}$:

$$\langle f| \, (\mathtt{S} - 1) \, |i\rangle = (2\pi)^4 \delta^{(4)} \left(\sum_i p_i \right) \mathcal{M}_{i\to f}, \tag{2.1.6}$$

where factors of 2π are included for convenience.

2.1.1 Cross-section σ

Let us consider two collinear colliding beams of particles a and b, with a number of particles per unit beam area $\rho_a(x, y)$ and $\rho_b(x, y)$. We define the integrated luminosity[2] $\mathcal{L}$, which is similar to the flux of a fixed-target experiment, by

$$\mathcal{L} = \int dA \rho_a(x, y) \rho_b(x, y) \tag{2.1.7}$$

with dA the element of the beam collision area.

Now we can express the number of the scattering interactions that we are interested in N using a more general quantity, the cross-section σ:

$$N = \mathcal{L}\sigma. \tag{2.1.8}$$

[2]Its time-derivative being called the *instantaneous* luminosity.

It is this σ which we can treat as the fundamental quantity to measure and calculate. By dimensional analysis, it is an area, which gives rise to its name.

We can examine the relationship between σ and $\mathcal{M}$ by considering the infinitesimal probability for a known initial state[3], with beams along the z-direction, scattering into n particles with three-momenta in the small region $d^3\mathbf{p}_1 d^3\mathbf{p}_2 \dots d^3\mathbf{p}_n$. As shown in Chapter 4 of [21], we arrive at:

$$\begin{aligned} d\sigma =& \frac{1}{2E_a E_b} \left| \frac{p_{a,z}}{E_a} - \frac{p_{b,z}}{E_b} \right|^{-1} \left(\prod_{j=1}^{n} \frac{d^3\mathbf{p}_j}{2E_{\mathbf{p}_j}} \right) |\mathcal{M}(p_a, p_b \to p_1, p_2, \dots, p_n)|^2 \\ & \times (2\pi)^4 \delta^{(4)} \left(p_a + p_b - \sum_{j=1}^{n} p_j \right) \end{aligned} \tag{2.1.9}$$

and this can be used in differential form as a differential cross-section, or integrated over all outgoing momenta to obtain the total cross-section.

2.1.2 The Langrangian and Perturbative Calculations

Now that we have related physical observables to the matrix element, we would like to be able to calculate it. Rather than using the Hamiltonian to evolve our states in time, we will use a formulation based on a related quantity called the Lagrangian L, or rather its density $\mathcal{L}$,[4] with $L = \int d^3x \mathcal{L}$. We will develop the very intuitive method used to perform this perturbative expansion, introduced by Feynman [27], which we come to in Section 2.2.3. As in classical field theory, we will apply the principle of least action $\mathcal{S}$:

$$\mathcal{S} = \int dt L = \int d^4x \mathcal{L}, \tag{2.1.10}$$

henceforth we will only consider $\mathcal{L}$, so we will drop the word "density" from its description. From the minimisation of $\mathcal{S}$, we gain an Euler-Lagrange equation for

[3] i.e. one with a specific number of particles, usually two, which have known particle type (*flavour*) and known momenta and polarisation.

[4] We can connect this to the Hamiltonian density using $\mathcal{H} = \dot{\phi}_i \dfrac{\partial \mathcal{L}}{\partial \dot{\phi}_i} - \mathcal{L}$, with the dot denoting differentiation with respect to time. There is an implied sum over i, as we use the Einstein summation convention (except where we note otherwise) in this thesis.

each field ϕ_i in the Lagrangian:

$$\partial_\mu \frac{\partial \mathcal{L}}{\partial(\partial_\mu \phi_i)} = \frac{\partial \mathcal{L}}{\partial \phi_i}. \tag{2.1.11}$$

We will split this Lagrangian:

$$\mathcal{L} = \mathcal{L}_{free} + \lambda \mathcal{L}_{int} \tag{2.1.12}$$

such that $\mathcal{L}_{free}$ is that part of the theory whose solutions are plane-waves, and $\mathcal{L}_{int}$, the interaction Lagrangian, contains the interactions between the fields of the model. We will expand our matrix elements in this small parameter[5] λ. This will be done using the method of Feynman diagrams, a pictorial representation which relies on rules derived from $\mathcal{L}$. In particular, this thesis is devoted to techniques for the calculation of the second term in this expansion.

Spinors

Before we go any further, we must first introduce the concept of a spinor, which is an object representing a spin-$\frac{1}{2}$ particle, coming from solving the Euler-Lagrange equation (2.1.11) for $\bar{\psi}$, defined by $\bar{\psi} = \psi^\dagger \gamma^0$, in the free Dirac particle Lagrangian[6]

$$\mathcal{L}_{free,Dirac} = \bar{\psi}(i\not{\partial} - m)\psi \tag{2.1.13}$$

so

$$i\not{\partial}\psi - m\psi = 0 \tag{2.1.14}$$

$$(\not{p} - m)\psi = 0, \tag{2.1.15}$$

where we have used the momentum operator $p^\mu = i\partial^\mu$, and introduced Feynman slash notation $\not{p} = \gamma^\mu p_\mu$. We solve this for plane-waves and spin s with $\psi(x) = u^s(p)e^{-ip\cdot x}$. We call this four-component object $u^s(p)$ a spinor, and choose the normalisation:

$$\bar{u}^s(p)u^r(p) = 2m\delta^{sr} \tag{2.1.16}$$

[5] In this thesis, we will restrict ourselves to the perturbative regime: the case in which the coefficient λ is a small parameter, so that it will make sense to expand in it.

[6] The Dirac matrices γ^μ are introduced in Appendix B.1.

and we also have the useful property:

$$\sum_s u^s(p)\bar{u}^s(p) = \not{p} + m. \tag{2.1.17}$$

We have a similar (orthogonal) object for the antifermion:

$$\bar{\psi}(x) = v^s(p)e^{+ip\cdot x} \tag{2.1.18}$$

$$\bar{v}^s(p)v^r(p) = -2m\delta^{sr} \tag{2.1.19}$$

$$\sum_s v^s(p)\bar{v}^s(p) = \not{p} - m \tag{2.1.20}$$

$$\bar{u}^s(p)v^r(p) = 0 \tag{2.1.21}$$

$$\bar{v}^s(p)u^r(p) = 0. \tag{2.1.22}$$

2.2 Quantum Electrodynamics

Now that we have set up the framework, let us consider Quantum Electrodynamics, historically the first component of the Standard Model to be formulated. We start by writing down a free Lagrangian for a massive electron field ψ

$$\mathcal{L}_e = i\bar{\psi}\gamma^\mu\partial_\mu\psi - m\bar{\psi}\psi. \tag{2.2.23}$$

This Lagrangian is invariant under a global U(1) transformation, defined here as:

$$\psi \to e^{i\theta}\psi, \tag{2.2.24}$$

with θ being a constant:

$$\mathcal{L}_e \to ie^{-i\theta}\bar{\psi}\gamma^\mu e^{i\theta}\partial_\mu\psi - me^{-i\theta}\bar{\psi}e^{i\theta}\psi = \mathcal{L}_e. \tag{2.2.25}$$

Now let us consider instead a local U(1) transformation, under which we allow θ to be a function of position:

$$\psi \to e^{i\theta(x)}\psi \tag{2.2.26}$$

so

$$\partial_\mu\psi \to e^{i\theta(x)}\partial_\mu\psi + i\left(\partial_\mu\theta(x)\right)e^{i\theta(x)}\psi \tag{2.2.27}$$

and the Lagrangian (2.2.23) is not invariant under this transformation

$$\mathcal{L}_e \to ie^{-i\theta(x)}\bar{\psi}\gamma^\mu\left(e^{i\theta(x)}\partial_\mu\psi + i\left(\partial_\mu\theta(x)\right)e^{i\theta(x)}\psi\right) - me^{-i\theta(x)}\bar{\psi}e^{i\theta(x)}\psi \tag{2.2.28}$$

$$\to \mathcal{L}_e - \bar{\psi}\gamma^\mu\left(\partial_\mu\theta(x)\right)\psi. \tag{2.2.29}$$

If we wish to make the Lagrangian invariant under this transformation, we must introduce a new field, a U(1) gauge field A_μ, in a term $-e\bar{\psi}\gamma^\mu A_\mu\psi$, and require that it transform according to:

$$A_\mu \to A_\mu - \frac{1}{e}\partial_\mu\theta, \tag{2.2.30}$$

so
$$\begin{aligned}\mathcal{L}_e - e\bar{\psi}\gamma^\mu A_\mu\psi &\to \mathcal{L}_e - \bar{\psi}\gamma^\mu\left(\partial_\mu\theta(x)\right)\psi - e\bar{\psi}\gamma^\mu A_\mu\psi - e\bar{\psi}\gamma^\mu\left(-\frac{1}{e}\partial_\mu\theta\right)\psi \\ &\to \mathcal{L}_e - e\bar{\psi}\gamma^\mu A_\mu\psi \end{aligned} \tag{2.2.31}$$

and we have a Lagrangian invariant under our transformation. It will turn out that this new field, which we introduced merely to keep our invariance, is the photon, and that this extra term is nothing other than the interaction between the electron and the photon. If we are to promote the A_μ-field to be a true particle, however, we will need one more term to describe its propagation[7], involving the *field-strength tensor* $F^{\mu\nu}$:

$$\mathcal{L}_F = -\frac{1}{4}F^{\mu\nu}F_{\mu\nu} \tag{2.2.32}$$

with
$$F^{\mu\nu} = \partial^\mu A^\nu - \partial^\nu A^\mu. \tag{2.2.33}$$

We can check the gauge invariance of this term easily: indeed the field-strength tensor is individually gauge invariant:

$$F^{\mu\nu} \to \partial^\mu\left(A^\nu - \frac{1}{e}\partial^\nu\theta\right) - \partial^\nu\left(A^\mu - \frac{1}{e}\partial^\mu\theta\right) \tag{2.2.34}$$

$$\to \partial^\mu A^\nu - \frac{1}{e}\partial^\mu\partial^\nu\theta - \partial^\nu A^\mu + \frac{1}{e}\partial^\nu\partial^\mu\theta \tag{2.2.35}$$

$$\to F^{\mu\nu}. \tag{2.2.36}$$

So we have a Lagrangian describing the propagation and interaction of the electron and the photon:

$$\mathcal{L}_{QED} = i\bar{\psi}\gamma^\mu\partial_\mu\psi - m\bar{\psi}\psi - e\bar{\psi}\gamma^\mu A_\mu\psi - \frac{1}{4}F^{\mu\nu}F_{\mu\nu}. \tag{2.2.37}$$

[7]Note that without this kinetic term, its Euler-Lagrange equation (2.1.11) is $\frac{\partial\mathcal{L}}{\partial A} = 0$.

It is convenient to combine the first and third terms by writing a covariant derivative

$$D_\mu = \partial_\mu + ieA_\mu \tag{2.2.38}$$

which has the property that $D_\mu\psi$ transforms in the same way as ψ

$$\begin{aligned} D_\mu\psi = \partial_\mu\psi + ieA_\mu\psi \quad &\to \partial_\mu e^{i\theta(x)}\psi + ie\left(A_\mu - \frac{1}{e}\partial_\mu\theta(x)\right)e^{i\theta(x)}\psi \\ &\to e^{i\theta(x)}\partial_\mu\psi + e^{i\theta(x)}i\left(\partial_\mu\theta(x)\right)\psi + ieA_\mu e^{i\theta(x)}\psi - ie^{i\theta(x)}\psi\partial_\mu\theta(x) \\ &\to e^{i\theta(x)}D_\mu\psi \end{aligned} \tag{2.2.39}$$

so that $$\mathcal{L}_{QED} = i\bar{\psi}\gamma^\mu D_\mu\psi - m\bar{\psi}\psi - \frac{1}{4}F^{\mu\nu}F_{\mu\nu}. \tag{2.2.40}$$

Incidentally, it is worth noting at this point that a photon mass term $\frac{1}{2}m_A^2A^\mu A_\mu$ cannot be trivially included as it is not gauge invariant under this U(1):

$$m_A^2A_\mu A^\mu \to m_A^2\left(A_\mu - \frac{1}{e}\partial_\mu\theta\right)\left(A^\mu - \frac{1}{e}\partial^\mu\theta\right) \tag{2.2.41}$$

$$\to m_A^2A_\mu A^\mu - \frac{2}{e}A^\mu\partial_\mu\theta + \frac{1}{e^2}\partial_\mu\theta\partial^\mu\theta. \tag{2.2.42}$$

2.2.1 Dimensions in the Lagrangian

Given that the action $\mathcal{S} = \int d^4x\mathcal{L}$ is dimensionless, the Lagrangian must have mass dimension[8] 4. We then have:

$$[\partial_\mu] = 1 \qquad [m_0] = 1 \qquad [\psi] = \frac{3}{2} \qquad [A^\mu] = 1 \qquad [e] = 0. \tag{2.2.43}$$

We will revisit these dimensions in Section 2.3.5.

2.2.2 Gauge-fixing

So far, we have a gauge-invariant theory, which means that there are different conformations of our fields possible which are not physically distinguishable. We wish to remove this degeneracy, and in the process make our propagators well defined, by making the kinetic terms uniquely invertible. In order to do this, we can add a

[8] We work in natural units, $\hbar = c = 1$ throughout, see Appendix A.1.

gauge-fixing term to our Langrangian. The most common choice restricts the theory to the R_ξ *gauges*, which are Lorentz invariant:

$$\mathcal{L}_{GF} = -\frac{(\partial_\mu A^\mu)^2}{2\xi}. \tag{2.2.44}$$

We can either leave ξ in our calculation, and check that the final result does not depend on it, or we can fix it before we start to a value we choose for our convenience, simplifying the calculation. The three main choices are: $\xi \to 0$ (Landau gauge); $\xi = 1$ (Feynman gauge); $\xi \to \infty$ (Unitary gauge). Different gauge choices can simplify different calculations, and we will choose the Feynman gauge throughout this thesis, for reasons that will become apparent in the following section.

2.2.3 QED Feynman Rules

We can take QED as our first example of a set of Feynman rules. There are four types of such rule:

External Particle Objects: Incoming and outgoing particles give an object, which might be a spinor, a polarisation vector, or unity[9].

Outgoing fermion	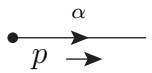	$\bar{u}_\alpha(s,p)$
Incoming fermion	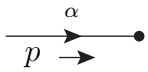	$u_\alpha(s,p)$
Outgoing antifermion	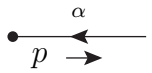	$v_\alpha(s,p)$
Incoming antifermion	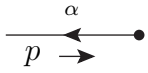	$\bar{v}_\alpha(s,p)$
Outgoing photon	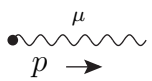	$\epsilon^{*\mu}(\lambda,p)$
Incoming photon	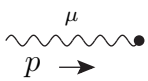	$\epsilon^\mu(\lambda,p)$

[9]For a scalar particle, none of which appear in QED.

Internal Particle Propagators: For lines on which particles propagate entirely within the diagram, the diagram receives a factor of the inverse of its momentum-space free particle operators.

Internal photon line 

$$\frac{-i}{p^2+i\lambda}\left(g^{\mu\nu}-(1-\xi)\frac{p^\mu p^\nu}{p^2}\right)$$

Internal fermion line 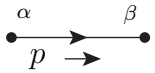

$$\frac{i(\not{p}+m)_{\beta\alpha}}{p^2-m^2+i\lambda}$$

where $i\lambda$ is an infintesimal displacement from the real axis. We can now see the virtue of the Feynman gauge: the second term in the photon propagator is set to zero, simplifying the calculation.

Vertex Factors: The interaction Lagrangian will give a certain set of permitted vertices and the prefactors associated with them. In QED, the expansion is in the small parameter e, with the fermion carrying a charge qe.

Vertex 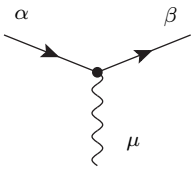

$$-iqe\gamma^\mu_{\beta\alpha}$$

Overall Factors: Certain features of a diagram can lead to overall factors: having n indistinguishable particles in the final state gives a factor of $\frac{1}{n!}$; closed fermion loops give factor of (-1); diagrams involving Majorana fermions must be treated with care due to an overall sign[10].

2.2.4 Example: $e^+e^- \to \mu^+\mu^-$ at Leading Order

We can now investigate a specific example: $e^+e^- \to \mu^+\mu^-$, with massless (and on-shell) electrons and muons, to leading order (LO) in QED (drawing on [21]). There is only one possible diagram at this order, shown in Figure 2.1[11].

[10] This is laid out carefully in [28, 29].

[11] The diagrams in this thesis are drawn with axodraw [30]. The jaxodraw [31] interface was used for the larger diagrams such as this one.

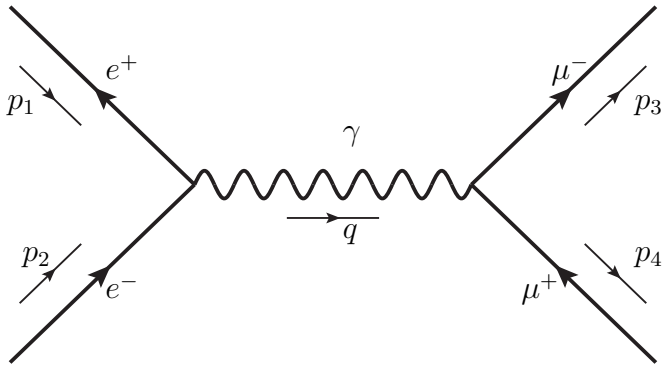

Figure 2.1: Leading order diagram for $e^+e^- \to \mu^+\mu^-$.

Using the Feynman rules in Section 2.2.3, we write down:

$$i\mathcal{M}_{LO} = \bar{v}_2(-i(-1)e\gamma^\mu)u_1\frac{-ig_{\mu\nu}}{q^2}\bar{u}_3(-i(-1)e\gamma^\nu)v_4, \tag{2.2.45}$$

where spinors are marked with the subscript of their momentum, and the $+i\lambda$ can be neglected. We can square this:

$$|\mathcal{M}_{LO}|^2 = \frac{e^4}{q^4}\left(\bar{v}_2\gamma^\mu u_1\bar{u}_3\gamma_\mu v_4\right)\left(\bar{u}_1\gamma^\rho v_2\bar{v}_4\gamma_\rho u_3\right), \tag{2.2.46}$$

and after averaging over initial spins and summing over final ones, remembering that we are working with massless electrons and muons, we have

$$|\mathcal{M}_{LO}|^2 = \frac{e^4}{4q^4}\mathrm{Tr}\left(\gamma_\mu \not{p}_4\gamma_\rho \not{p}_3\right)\mathrm{Tr}\left(\gamma^\mu \not{p}_1\gamma^\rho \not{p}_2\right). \tag{2.2.47}$$

Now we use the identity[12]

$$\mathrm{Tr}\left(\gamma^\mu\gamma^\nu\gamma^\rho\gamma^\sigma\right) = 4\left(g^{\mu\nu}g^{\rho\sigma} - g^{\mu\rho}g^{\nu\sigma} + g^{\mu\sigma}g^{\nu\rho}\right) \tag{2.2.48}$$

to find

$$|\mathcal{M}_{LO}|^2 = \frac{e^4}{4q^4}p_4^\sigma p_3^\rho 4\left(g_{\mu\sigma}g_{\nu\rho} - g_{\mu\nu}g_{\sigma\rho} + g_{\mu\rho}g_{\sigma\nu}\right)p_{1\alpha}p_{2\beta}4\left(g^{\mu\alpha}g^{\nu\beta} - g^{\mu\nu}g^{\alpha\beta} + g^{\mu\beta}g^{\alpha\nu}\right), \tag{2.2.49}$$

which we can simplify to

$$|\mathcal{M}_{LO}|^2 = \frac{8e^4}{q^4}p_4^\sigma p_3^\rho p_{1\alpha}p_{2\beta}\left(\delta_\sigma^\alpha\delta_\rho^\beta - \delta_\sigma^\beta\delta_\rho^\alpha\right) \tag{2.2.50}$$

$$|\mathcal{M}_{LO}|^2 = \frac{8e^4}{q^4}\left((p_4\cdot p_1)(p_3\cdot p_2) - (p_4\cdot p_2)(p_3\cdot p_1)\right), \tag{2.2.51}$$

[12]For an LO calculation, we can work in four dimensions, rather than the d of Section 2.3.5.

and given that we are in the massless case, so, e.g.

$$s_{13} = (p_1 + p_3)^2 = p_1^2 + 2p_1 \cdot p_3 + p_3^2 = 2p_1 \cdot p_3, \tag{2.2.52}$$

we have

$$|\mathcal{M}_{LO}|^2 = \frac{2e^4}{q^4}\left(s_{23}^2 + s_{13}^2\right). \tag{2.2.53}$$

We introduce a parameter $\alpha = \frac{e^2}{4\pi}$, which will be our way of referring to the coupling constants in the results of calculations, and so we write:

$$|\mathcal{M}_{LO}|^2 = \frac{32\pi^2\alpha^2}{q^4}\left(s_{23}^2 + s_{13}^2\right) \tag{2.2.54}$$

and we talk of the the LO squared matrix element as being $\mathcal{O}(\alpha^2)$. The next-to-leading order (NLO) calculation of this process is explored in Section 3.2.

2.3 Divergences

We can use QED to highlight a more general aspect of QFTs which becomes clear when we start trying to calculate loop diagrams[13], namely that the results are divergent and we need to deal with these divergences in a consistent manner. The divergences are of two types:

Ultraviolet (UV) divergences: These occur in the short-distance or high-energy behaviour of a loop integral, and result from our attempt to apply our theory to an energy scale beyond its applicability.

Infrared (IR) divergences: These occur in the long-distance or low-energy behaviour of a loop integral, or else from a soft or collinear divergence in a real emission process. They are only present if we are using a theory which includes massless particles.

We will need first to *regularise* both of these divergences, that is to develop a scheme in which they can be described mathematically. The UV divergences will

[13]Or real emission diagrams, as we will see in Section 2.3.2.

also need a redefinition of the theory, *renormalisation*, to allow us to find physical results, but the IR divergences will cancel within the model, leaving finite measurable quantities.

2.3.1 Ultraviolet Divergences

To illustrate the appearance of a UV divergence, let us consider the two-point function for a fermion of mass m_0: at leading order, this is just the propagator $\mathcal{P}_{LO} = \frac{i}{\not{p}-m_0+i\lambda}$, and at next-to-leading order there is a correction from the loop diagram:

Figure 2.2: A loop correction to the fermion propagator.

Naïvely, the loop diagram would give a contribution:

$$\frac{i}{\not{p}-m_0+i\lambda} iqe\gamma^\mu \left(\int d^4k \frac{-ig_{\mu\nu}}{(p-k)^2+i\lambda} \frac{i(\not{K}+m_0)}{k^2-m_0^2+i\lambda} \right) iqe\gamma^\nu \frac{i}{\not{p}-m_0+i\lambda} \quad (2.3.55)$$

at large k, the integral[14] will be of the form $\int d^4k \frac{1}{k^4}$. But this integral is ill-defined: it will have logarithmic-type behaviour, that is it will diverge at the infinite upper limit. We can think of this divergence as due to our hubris in assuming that QED will be valid up to infinite energy, when physics at that scale is not known (and it would be very surprising if it were similar to QED!).

2.3.2 Infrared Divergences

We can demonstrate the appearance of an infrared divergence in a real emission using the simplified diagram in Figure 2.3, where the fermion is taken to be massless and the dark blob is understood to be all other components of the full diagram:

We will have in our expression some terms from the blob, which we will denote

[14]The $\not{k}$ in the numerator gives an odd term which vanishes on symmetric integration.

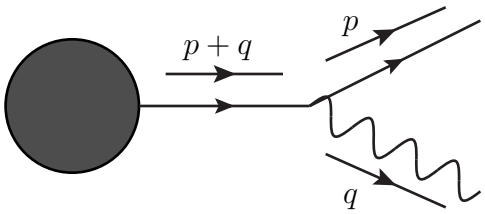

Figure 2.3: Simplified diagram used to illustrate the appearance of an IR divergence.

with $\mathcal{B}$ [15]:

$$i\mathcal{M} = \bar{u}(p)\frac{\not{p}+\not{q}}{(p+q)^2}(ie\gamma^\mu)\mathcal{B}\epsilon^*_\mu(q) \tag{2.3.56}$$

now the denominator of the propagator will be

$$(p+q)^2 = 2p\cdot q = 2(p^0q^0 - |p||q|\cos\theta) = 2|p||q|(1-\cos\theta) \tag{2.3.57}$$

where we have used the fact that for massless particles, $E^2 = |p|^2$, and where θ is the angle between the external particles' 3-momenta. We can see that there are two circumstances in which the denominator will become small: when $|p| \to 0$ or $|q| \to 0$, which we can call a soft divergence; and when $\cos\theta \to 1$, that is when the particles' paths become parallel, which we will call a collinear divergence. These are the two possibilities for an IR divergence.

2.3.3 Regularisation

In order to treat the IR and UV divergences in our theory, we need to find a way of writing them such that they appear not merely as infinities, but as the limit of some finite expression.

Let us start with our integral (2.3.55):

$$\frac{i}{\not{p}-m_0+i\lambda}iqe\gamma^\mu\left(\int d^4k\frac{-ig_{\mu\nu}}{(k+p)^2+i\lambda}\frac{i(\not{K}+m_0)}{k^2-m_0^2+i\lambda}\right)iqe\gamma^\nu\frac{i}{\not{p}-m_0+i\lambda}. \tag{2.3.58}$$

An immediate way of regularising the UV divergence would be simply to assert that we do not know the physics above some scale Λ, and so to decide to cut off our integral at that point[16]. This will leave us with a $\log(\Lambda)$-term in our result. Although

[15] Notably, $\mathcal{B}$ will have to carry a suppressed fermion index.

[16] A related, but more sophisticated, method is Pauli-Villars regularisation [32].

simple, this method is not desirable as it preserves neither Lorentz invariance nor gauge invariance.

Other schemes exist, including the introduction of a small photon mass into QED[17] (which covers IR divergences only), which will not be discussed here. The method used throughout this thesis is Dimensional Regularisation.

2.3.4 Dimensional Regularisation

In Dimensional Regularisation [34, 35], we consider integrations that would naïvely be 4-dimensional in $\mathcal{d} = 4 - 2\epsilon$ dimensions. The advantages of this scheme are that it can be used to regularise both IR and UV divergences, and that it respects the Lorentz and gauge invariance that were broken by the simple cutoff regulator.

Consider a simplified form of a UV-divergent loop integral[18]:

$$\int_{-\infty}^{\infty} d^4k \frac{1}{(k^2 - m_0^2)^2} = \Omega_4 \int_0^{\infty} \frac{k^3 dk}{m_0^4 \left(\left(\frac{k}{m_0} \right)^2 + 1 \right)^2} \tag{2.3.59}$$

$$= \frac{\Omega_4}{2} \int_0^{\infty} \frac{\kappa d\kappa}{(\kappa + 1)^2} \tag{2.3.60}$$

$$= \frac{\Omega_4}{2} \frac{\Gamma(2)\Gamma(0)}{\Gamma(2)} \to \infty, \tag{2.3.61}$$

where the Γ-functions arise from the results in Appendix B.4, which are explored in more detail in Section 4.1.6. We have used $\kappa = \left(\frac{k}{m_0} \right)^2$, and the constant factor Ω_4 comes from the angular integrations and is not crucial to the argument.

But in $\mathcal{d}$ dimensions,

$$\int_0^{\infty} d^{\mathcal{d}}k \frac{1}{(k^2 - m_0^2)^2} = \Omega_{\mathcal{d}} \int_0^{\infty} \frac{k^{\mathcal{d}-1} dk}{m_0^4 \left(\left(\frac{k}{m_0} \right)^2 + 1 \right)^2} \tag{2.3.62}$$

$$= \frac{\Omega_{\mathcal{d}}}{2} \int_0^{\infty} m_0^{\mathcal{d}-4} \frac{\kappa^{\frac{\mathcal{d}-2}{2}} d\kappa}{(\kappa + 1)^2} \tag{2.3.63}$$

[17] This is used in some modern electroweak calculations, for example in [33].

[18] In the first line, we move to Euclidean space without giving the detail, for simplicity of illustration. This is the cause of the sign change in the denominator. This process is explained in Section 4.1.6.

$$= \frac{\Omega_{\not d}}{2} m_0^{\not d-4} \frac{\Gamma(\frac{\not d}{2})\Gamma(1-\frac{\not d}{2})}{\Gamma(2)} \tag{2.3.64}$$

$$= \frac{\Omega_{\not d}}{2} m_0^{\not d-4} \frac{\Gamma(2-\epsilon)\Gamma(\epsilon)}{\Gamma(2)}, \tag{2.3.65}$$

so the divergence appears as a pole in the Γ-function (see Appendix B.3):

$$\Gamma(\epsilon) = \frac{1}{\epsilon} - \gamma_E + \mathcal{O}(\epsilon). \tag{2.3.66}$$

2.3.5 Revisiting Dimensions

At this point, we must revisit Section 2.2.1: $\mathcal{S}$ must still be dimensionless, but now $\mathcal{S} = \int d^{\not d}x\mathcal{L}$, so that

$$[\partial_\mu] = 1 \qquad [m_0] = 1 \qquad [\psi] = \frac{\not d - 1}{2} \qquad [A^\mu] = \frac{\not d - 2}{2}. \tag{2.3.67}$$

The coupling e would have dimension $\frac{4-d}{2} = \epsilon$, but we do not wish our coupling to be dimensionful, so we introduce a regularisation scale μ_{Reg}, and redefine $e \to \mu_{Reg}^{\epsilon} e$ [19]. A further choice that comes at this point, the dimensionality of vector bosons, is explored in detail in [36] but need not concern us here.

2.3.6 Renormalisation

The concept of renormalisation is a remedy to the fact that our first attempt at writing down a Lagrangian gives an insufficient description. In the bubble diagram in Figure 2.2, we have a correction to the fermion two-point function. Let us continue this example to illustrate the functioning of renormalisation, by the absorption of divergent quantities into parameters of the Lagrangian (although a full discussion of the mass renormalisation is beyond the scope of this work).

We can imagine continuing the correction to ever higher order, with a more general sum (a *Dyson sum* [37]) of all loops[20], represented by a grey circle, whose

[19] As we will see in Section 2.3.7, this dimensionless quantity will be μ_{Reg}-dependent

[20] Technically the loops have to be one particle irreducible to avoid double-counting.

value we represent as $-i\delta m$, a notation that will become clearer later[21]:

$\mathcal{P}_{N\infty LO} =$  (2.3.68)

$$= \frac{i}{\not p - m_0 + i\lambda} + \frac{i}{\not p - m_0 + i\lambda}(-i\delta m)\frac{i}{\not p - m_0 + i\lambda}$$
$$+ \frac{i}{\not p - m_0 + i\lambda}(-i\delta m)\frac{i}{\not p - m_0 + i\lambda}(-i\delta m)\frac{i}{\not p - m_0 + i\lambda} + \dots \quad (2.3.69)$$

but this is a simple geometrical series:

$$\mathcal{P}_{N\infty LO} = \frac{i}{\not p - m_0 + i\lambda}\sum_{j=0}^{\infty}\left(\frac{\delta m}{\not p - m_0 + i\lambda}\right)^j \quad (2.3.70)$$
$$= \frac{i}{\not p - m_0 + i\lambda}\frac{1}{1 - \left(\frac{\delta m}{\not p - m_0 + i\lambda}\right)} \quad (2.3.71)$$
$$= \frac{i}{\not p - (m_0 + \delta m) + i\lambda}, \quad (2.3.72)$$

that is to say that we can absorb this infinite string of divergent integrals if we perform a redefinition of the mass[22] to $m_r = m_0 + \delta m$. This will make sense because, although m_0, which we call the bare mass, is the parameter entered in our Lagrangian, the measured value of the mass – the pole in the propagator[23] – will be at m_r.

The Renormalised Lagrangian

We now wish to incorporate this renormalised parameter into our QED Lagrangian, which we will do by adding and subtracting a *counter term*, which involves δm and is formally of higher order in the coupling, and writing

$$m_0 = Z_m m_r = m_r - \delta m. \quad (2.3.73)$$

We will also need to renormalise the other components: in order to remove the divergence from the diagram in Figure 2.4 we will need to renormalise the fields

[21] For the purposes of this illustration, we will treat this quantity as if it were a simple number. In fact it will be a function of $\not p$ (and p^2, but we remember that $p^2 = (\not p)^2$).

[22] r for renormalised.

[23] We will revisit this for unstable particles in Section 6.1.

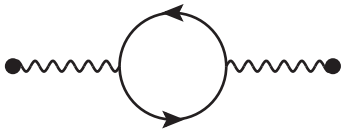

Figure 2.4: A loop correction to the photon propagator.

$$\psi_0 = Z_\psi^{\frac{1}{2}}\psi_r = \psi_r - \delta\psi \tag{2.3.74}$$

$$A_0^\mu = Z_A^{\frac{1}{2}}A_r^\mu = A_r^\mu - \delta A^\mu \tag{2.3.75}$$

and the diagram in Figure 2.5 has a divergence we must remove by renormalising the charge

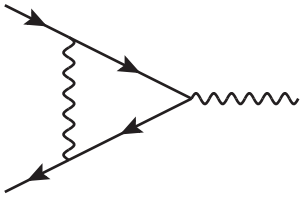

Figure 2.5: A loop correction to the QED vertex.

$$e_0 = Z_e e_r = \frac{Z_1}{Z_\psi\sqrt{Z_A}}e_r = e_r - \delta e, \tag{2.3.76}$$

where the form of this is chosen to minimise the clutter in the next step.

Our Lagrangian (2.2.37) becomes

$$\mathcal{L}_{QED} = Z_\psi i\bar{\psi}_r\gamma^\mu\partial_\mu\psi_r - Z_1 e_r\bar{\psi}_r\gamma^\mu A_{r,\mu}\psi_r - Z_\psi Z_m m_r\bar{\psi}_r\psi_r - Z_A\frac{1}{4}F_r^{\mu\nu}F_{r,\mu\nu}. \tag{2.3.77}$$

In this new Lagrangian, we still wish to respect gauge invariance. The fermion mass term and field-strength tensor terms do so automatically, but as in Section 2.2, the first two terms must do so in combination. We see that we need $Z_1 = Z_\psi$ for this to hold. This is the simplest case of the *Slavnov-Taylor identities* [38,39], which use gauge invariance to impose conditions on the counterterms. Now let us substitute the Zs out of the Lagrangian:

$$\mathcal{L}_{QED} = i\bar{\psi}_r\gamma^\mu\partial_\mu\psi_r - e_r\bar{\psi}_r\gamma^\mu A_{r,\mu}\psi - m_r\bar{\psi}_r\psi_r - \frac{1}{4}F_r^{\mu\nu}F_{r,\mu\nu} + (\delta\text{-containing terms}). \tag{2.3.78}$$

So we have recovered a form that resembles the original Lagrangian but contains the renormalised quantities and some additional counter terms, which act to cancel the UV divergences of the theory.

2.3.7 Running of Parameters

Let us consider a QED cross-section σ, which will be described by a perturbation series in α, dependent upon the set of input momenta P, and after renormalisation also on μ_{Reg}:

$$\sigma(P, \mu_{Reg}) = \sum_{j}^{N} a_j(P, \mu_{Reg})\alpha^{(j+l)}, \tag{2.3.79}$$

where l is the power of α in the LO for this process, and N will be infinite for a perfect calculation, but any practical calculation will be performing an approximation with N a small integer. This equation seems to imply that the (physically measurable) cross-section σ depends upon an unphysical scale that we introduced by hand, which cannot be the case.

Instead, if we can measure σ, taking μ_{Reg} to have any value we choose, we can see this as a measurement of α at this scale – and α will vary with this scale, or *run*. Because in principle the scale we introduced to keep α dimensionless and this scale at which we are measuring α are different, we will call the latter the renormalisation scale μ_R, but we will take them to be equal throughout this thesis.

The fact that σ must be independent of μ_R gives us a further relation:

$$\frac{d\sigma(P, \alpha(\mu_R^2), \mu_R)}{d\mu_R^2} = 0. \tag{2.3.80}$$

Now let us simplify the problem, by saying the cross-section only depends on a single physical scale Q^2. Because cross sections are of mass dimension -2, and because before renormalisation we only had the scale Q^2, we know that

$$\sigma = \frac{1}{Q^2}\bar{\sigma}, \tag{2.3.81}$$

where $\bar{\sigma}$ is dimensionless. This means that in the higher order corrections, which will involve μ_R, it will only appear as $t \equiv \log\left(\frac{Q^2}{\mu_R^2}\right)$, and so from (2.3.80):

$$\frac{\partial\sigma}{\partial t} - \beta(\alpha)\frac{\partial\sigma}{\partial\alpha} = 0 \tag{2.3.82}$$

where
$$\beta(\alpha) \equiv \mu_R^2\frac{\partial\alpha(\mu_R^2)}{\partial\mu_R^2} = \frac{\partial\alpha(t)}{\partial t}. \tag{2.3.83}$$

This β-function can in principle be calculated to any order[24] and written:

$$\beta(\alpha) = -\alpha\left(\beta_0\left(\frac{\alpha}{4\pi}\right) + \beta_1\left(\frac{\alpha}{4\pi}\right)^2 + ...\right), \tag{2.3.84}$$

so to first order, the running of α is:

$$\mu_R^2\frac{\partial\alpha(\mu_R^2)}{\partial\mu_R^2} = -\beta_0\left(\frac{\alpha^2}{4\pi}\right) \tag{2.3.85}$$

$$\int_{\alpha(\mu_R^2)}^{\alpha(Q^2)}\alpha^{-2}d\alpha = -\frac{\beta_0}{4\pi}\int_{\mu_R^2}^{Q^2}(d\log(\mu^2)) \tag{2.3.86}$$

$$\alpha(Q^2) = \frac{\alpha(\mu_R^2)}{1+\alpha(\mu_R^2)\frac{\beta_0}{4\pi}\log\frac{Q^2}{\mu_R^2}}, \tag{2.3.87}$$

so we can evolve any one measurement of α to any other scale at which it is well-defined.

In QED, $\beta_0 = -\frac{4}{3}$, so the coupling strength increases with increasing energy. This increase is sufficiently slow not to cause concern at LHC energies. In QCD (see Section 2.5), the analogous α_s runs with

$$\beta_0 = \frac{11N_C - 2n_f}{3}, \tag{2.3.88}$$

where $N_C = 3$ is the number of colours and n_f is the number of *active* quarks: those with mass well below the scale in question. β_0 is positive, and so the QCD β-function is negative, at all energies in the SM, so the coupling strength of QCD decreases with increasing energy. The corollary is that it will increase with decreasing energy until it hits the *Landau pole*, where $\alpha_s(\mu_R^2)\frac{\beta_0}{4\pi}\log\frac{Q^2}{\mu_R^2} = -1$, at $Q_{pole} \equiv \Lambda_{QCD} \sim 0.2\,\text{GeV}$. This fact, *asymptotic freedom*, is what allows us to take perturbative QCD results seriously at high energies.

We can also expand this analysis to cover other model parameters, and (within the $\overline{\text{MS}}$-scheme, see Section 2.3.8) they will also run with the renormalisation scale.

2.3.8 Renormalisation Schemes

When performing our renormalisation, we have to remove the UV poles exactly. However, we have an additional choice regarding the finite subtraction that we

[24] For QCD, it has been calculated up to fourth order [40, 41].

include as part of our scheme. In this thesis, we work in the $\overline{\text{MS}}$ scheme, which means that we subtract the object:

$$\frac{1}{\bar{\epsilon}} \equiv \frac{1}{\epsilon} - \gamma_E + \log(4\pi). \tag{2.3.89}$$

Another option is the MS scheme, in which only the $\frac{1}{\epsilon}$ is subtracted.

For theories in which there are asymptotic fundamental particles, such as QED, it is possible to measure masses in the low-energy limit, giving them single, defined values, and not to have them run. The scheme in which this is performed is called the on-shell scheme (see for example, Chapters 26-27 of [25]).

2.4 Gauge Fields

In the rest of this chapter, we will extend the theory by expanding to a different type of gauge interaction. In order to do this, we must develop the machinery of the group SU(N).

Where in Section 2.2 we had one electron field, we now have an N-plet of fermion fields, with a gauge transformation

$$\psi_i \to U_{ij}(x)\psi_j, \tag{2.4.90}$$

with U_{ij} being an $N \times N$ unitary matrix with unit determinant. We restrict the discussion to the SU(N), in which we are interested, by excluding U(1) factors, which are phase factors $e^{i\theta}$. For small transformations, can write this matrix in terms of the group generators[25] t^a (we adopt the convention that the generator index is raised, and the component indices of a generator lowered):

$$U_{ij} = \delta_{ij} + \theta^a t^a_{ij} + \mathcal{O}(\theta^2). \tag{2.4.91}$$

The generators are hermitian and traceless and satisfy

$$[t^a, t^b] = if^{abc}t^c, \tag{2.4.92}$$

[25] We will see that the mathematics works in a very similar way to U(1), and that the "generators" in Section 2.2 were hidden as there was only one and it was the identity.

with f^{abc} called the structure constants of the group. Unless all these constants are zero, we have a *non-Abelian* group, which in particle physics terms means that the force-carrying particles have a self-interaction. Notably, in the U(1) case we have an Abelian group, and indeed there is no photon-photon interaction. We have a choice of normalisation:

$$\mathrm{Tr}(t^a, t^b) = T_R \delta^{ab} \tag{2.4.93}$$

and we take $T_R = \frac{1}{2}$.

The gauge field A^a_μ is in the adjoint representation, and similarly to (2.2.30):

$$A_\mu \to U A_\mu U^{-1} + \frac{i}{g} (\partial_\mu U) U^{-1}, \tag{2.4.94}$$

where we have introduced the shorthand $A_\mu = A^a_\mu t^a$, g is the coupling constant, and component indices are suppressed where they are clear from context.

Then the covariant derivative will be:

$$D_\mu = (\partial_\mu + igA^a_\mu t^a) \tag{2.4.95}$$

and we can check the transformation property analogous to (2.2.39):

$$\begin{aligned} D_\mu \psi &= (\partial_\mu + igA_\mu)\psi && (2.4.96)\\ &\to \partial_\mu (U\psi) + ig(UA_\mu U^{-1} + \frac{i}{g}(\partial_\mu U) U^{-1}) U\psi && (2.4.97)\\ &\to U\partial_\mu \psi + (\partial_\mu U)\psi + igUA_\mu \psi - (\partial_\mu U)\psi && (2.4.98)\\ &\to U D_\mu \psi, && (2.4.99) \end{aligned}$$

so indeed $D_\mu \psi$ does transform as ψ does.

We now define the field-strength tensor:

$$F^{\mu\nu} = F^{a,\mu\nu} t^a = \frac{-i}{g} [D^\mu, D^\nu] \tag{2.4.100}$$

so

$$\begin{aligned} F^{a,\mu\nu} t^a &= \partial^\mu A^{a,\nu} t^a - \partial^\nu A^{a,\mu} t^a + igA^{b,\mu} A^{c,\nu} \left[t^b, t^c\right] && (2.4.101)\\ F^{a,\mu\nu} &= \partial^\mu A^{a,\nu} - \partial^\nu A^{a,\mu} - g f^{abc} A^{b,\mu} A^{c,\nu} && (2.4.102) \end{aligned}$$

and we can see that, unlike for the U(1) case, $F^{\mu\nu}$ is not gauge-invariant alone[26], but the combination $\mathrm{Tr}(F^{\mu\nu} F_{\mu\nu}) = F^{a,\mu\nu} F^a_{\mu\nu}$, which we will use in the Lagrangian, is.

[26] Rather, $F^{\mu\nu} \to U F^{\mu\nu} U^{-1}$

Examples

We will need two examples for the Standard Model. The first is the SU(2) of the weak interaction, for which the three generators $\tau^j = \frac{i}{2}\sigma^j$, where

$$\sigma^1 = \begin{pmatrix} 0 & 1 \\ 1 & 0 \end{pmatrix} \qquad \sigma^2 = \begin{pmatrix} 0 & -i \\ i & 0 \end{pmatrix} \qquad \sigma^3 = \begin{pmatrix} 1 & 0 \\ 0 & -1 \end{pmatrix} \tag{2.4.103}$$

are the *Pauli matrices*, and the structure constants are the Levi-Civita tensor ϵ^{ijk}. The second is the SU(3) of the strong interaction, for which the generators $t^a = \frac{\lambda^a}{2}$, where λ^a are the eight *Gell-Mann matrices* :

$$\begin{aligned}
\lambda^1 &= \begin{pmatrix} 0 & 1 & 0 \\ 1 & 0 & 0 \\ 0 & 0 & 0 \end{pmatrix} \quad \lambda^2 = \begin{pmatrix} 0 & -i & 0 \\ i & 0 & 0 \\ 0 & 0 & 0 \end{pmatrix} \quad \lambda^3 = \begin{pmatrix} 1 & 0 & 0 \\ 0 & -1 & 0 \\ 0 & 0 & 0 \end{pmatrix} \\
\lambda^4 &= \begin{pmatrix} 0 & 0 & 1 \\ 0 & 0 & 0 \\ 1 & 0 & 0 \end{pmatrix} \quad \lambda^5 = \begin{pmatrix} 0 & 0 & -i \\ 0 & 0 & 0 \\ i & 0 & 0 \end{pmatrix} \\
\lambda^6 &= \begin{pmatrix} 0 & 0 & 0 \\ 0 & 0 & 1 \\ 0 & 1 & 0 \end{pmatrix} \quad \lambda^7 = \begin{pmatrix} 0 & 0 & 0 \\ 0 & 0 & -i \\ 0 & i & 0 \end{pmatrix} \quad \lambda^8 = \begin{pmatrix} \frac{1}{\sqrt{3}} & 0 & 0 \\ 0 & \frac{1}{\sqrt{3}} & 0 \\ 0 & 0 & \frac{-2}{\sqrt{3}} \end{pmatrix}
\end{aligned} \tag{2.4.104}$$

and the structure constants are f^{abc}, with:

$$f^{123} = 1, \quad f^{147} = f^{165} = f^{246} = f^{257} = f^{345} = f^{378} = \frac{1}{2}, \quad f^{458} = f^{678} = \frac{\sqrt{3}}{2}, \tag{2.4.105}$$

and all other entries being either deduced from the antisymmetry, or zero.

2.5 Quantum Chromodynamics

We can now describe Quantum Chromodynamics (QCD)[27], as a theory of six flavours of quark, each of which is in a colour triplet (index i), interacting with eight gluons.

[27] An excellent introduction is given in [22].

The Lagrangian (in an R_ξ gauge) is[28]:

$$\mathcal{L}_{QCD} = \sum_q \left(i\bar{\psi}_{q,i}\gamma^\mu D_\mu \psi_{q,i} - m_q \bar{\psi}_{q,i}\psi_{q,i} \right) - \frac{1}{4}F^{\mu\nu}F_{\mu\nu} - \frac{(\partial_\mu A^\mu)^2}{2\xi}. \tag{2.5.106}$$

Normalisations

In QCD, we have a normalisation choice for:

$$\mathrm{Tr}\{t^a t^b\} = T_R \delta^{ab} \tag{2.5.107}$$

$$t^a_{ij} t^a_{jk} = C_F \delta_{ik} \tag{2.5.108}$$

$$f^{acd} f^{bcd} = C_A \delta^{ab} \tag{2.5.109}$$

and we take $T_R = \frac{1}{2}$, which gives $C_F = \frac{4}{3}$ and $C_A = N_C = 3$.

2.5.1 Feynman Rules for QCD

Let us list Feynman rules[29] for QCD:

Outgoing fermion	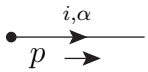	$\bar{u}_{i,\alpha}(s,p)$
Incoming fermion	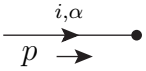	$u_{i,\alpha}(s,p)$
Outgoing antifermion	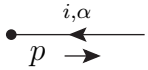	$v_{i,\alpha}(s,p)$
Incoming antifermion	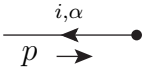	$\bar{v}_{i,\alpha}(s,p)$
Outgoing gluon	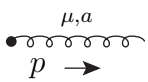	$\epsilon^{*\mu,a}(\lambda,p)$
Incoming gluon	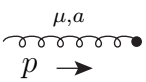	$\epsilon^{\mu,a}(\lambda,p)$

[28] In this thesis, we do not consider *ghost fields* [42], which are unphysical fields arising from gauge fixing. A full explanation of the mechanism is given in, for example, Chapter 16 of [21], but need not concern us here.

[29] The quarks will also, similarly to the leptons, interact with the photon. The charges are fractional, and there is a multiplicative δ_{ij} of colour at the vertex.

Internal gluon line	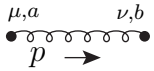	$\frac{-i\delta^{ab}}{p^2+i\lambda}\left(g^{\mu\nu}-(1-\xi)\frac{p^\mu p^\nu}{p^2}\right)$
Internal fermion line	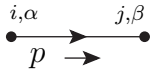	$\frac{i(\not{p}+m)_{\beta\alpha}}{p^2-m^2+i\lambda}\delta_{ij}$
Quark-gluon Vertex	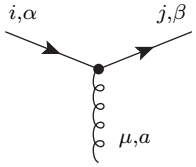	$ig\gamma^\mu_{\beta\alpha}t^a_{ij}$
Three-gluon Vertex	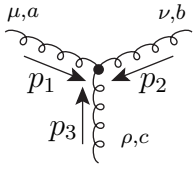	$gf^{abc}(g^{\mu\nu}(p_1-p_2)^\rho + g^{\nu\rho}(p_2-p_3)^\mu + g^{\rho\mu}(p_3-p_1)^\nu)$
Four-gluon Vertex	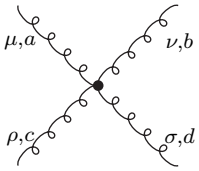	$-ig^2\left(f^{abe}f^{cde}(g^{\mu\rho}g^{\nu\sigma}-g^{\mu\sigma}g^{\nu\rho}) + f^{ace}f^{bde}(g^{\mu\nu}g^{\rho\sigma}-g^{\mu\sigma}g^{\nu\rho}) + f^{ade}f^{bce}(g^{\mu\nu}g^{\rho\sigma}-g^{\mu\rho}g^{\nu\sigma})\right)$

and we define $\alpha_s = \frac{g^2}{4\pi}$, similarly to the QED case.

2.5.2 Colour Confinement and Hadronisation

In Section 2.3.7, we noted that the QCD coupling rises as we decrease the energy scale, diverging at Λ_{QCD}. That is to say that at low energy scales, the strong force is non-perturbative, and indeed we have colour-singlet bound states – hadrons – in that regime. We must also consider, however, that long distance scales are equivalent to low energies, so the strong force must grow with distance r: if we consider it as a potential, there will be both the $\frac{1}{r}$ Coulomb-like term, and a linear r-term. This second term grows without limit, and so it would take an infinite amount of energy to separate two colour-connected objects entirely (*colour confinement*). Instead, as two such particles separate, the energy contained in the field between them rises until there is enough to create two or more coloured particles and break the colour-connection. This proliferation of new hadrons is called *hadronisation*, and due to it, any hard coloured particles produced in a collider are seen as jets of hadrons.

2.6 Hadron Colliders and the LHC

The LHC, like its predecessor as the world's highest-energy particle collider the Tevatron, is a hadron collider. It collides not pointlike particles with well-defined single-particle asymptotic states, but protons, which are extended clusters of quarks and gluons.

Because the proton is a complicated object, one might expect that all aspects of the modelling of their collisions would have to be very phenomenological, and that QFT calculations, like the ones laid out in this chapter, would be of too small a (length) scale to have any bearing on experimental results. Fortunately, it is exactly this scale which saves us, through the concept of factorisation.

2.6.1 Factorisation

We model a hadron as an extended object containing pointlike particles ("partons"), with a range of momenta. In a collision, an incident particle (usually another hadron) strikes one of these partons, and scattering takes place. We have two different scales: the low-energy behaviour of the hadron, and the high-energy collision. Factorisation [43] states that we can separate these processes, with the dividing line being the factorisation scale μ_F, and so we have:

Parton Distribution Functions $f_i^{(a)}(x_i, \mu_F)$, specific to each hadron a but otherwise process-independent, which give the distribution of momentum fractions x_i for different possible partons i; and

A Partonic Cross Section $\hat{\sigma}(x_i, x_j, \mu_R, \mu_F)$, constructed from the above QFT, which is specific for that process, and takes the parton momenta as inputs, but does not depend directly on the identity of the hadrons.

In addition, if we have final-state coloured particles, they will hadronise (see Section 2.5.2).

Now that the situation is well-defined, we can construct a total cross-section σ (or any other observable) from our partonic cross section $\hat{\sigma}$ by summing over possible

partons i and j and integrating over the momentum fractions[30]:

$$\sigma(\mu_R^2, \mu_F^2) = \sum_{i,j} \int dx_i dx_j f_i^{(a)}(x_i, \mu_F^2) f_j^{(b)}(x_j, \mu_F^2) \hat{\sigma}(x_i, x_j, \mu_R^2, \mu_F^2). \tag{2.6.110}$$

We can use this new scale, along with the renormalisation scale of Section 2.3.7, to provide an estimate of the uncertainty in a calculation: because (as we also stated there) they are arbitrarily introduced, an exact physical result (i.e. not one calculated in perturbation theory) cannot depend on them. However, because any calculation that we can currently do is a truncated approximation[31], we do have a residual dependence on these scales. The strength of that dependence gives an indication of the size of the terms which are missing. Because the $\mu_{F,R}$-dependence of these terms will arise in the form of logarithms of the ratio of $\mu_{F,R}$ and the scales of the problem, we take a typical scale of our process to be our central scale choice for $\mu_{F,R}$, in order that these logarithms will not be large, with the conventional limits on the uncertainty estimate being the values of the observable using twice and half the central scale.

A typical scale for the LHC might be the mass of the Z-boson M_Z. Values for the fine structure constants vary according to definitions and methodology, but as a guide, $\alpha_s(M_Z) \sim 0.12$ whereas $\alpha(M_Z) \sim \frac{1}{130} = 0.008$, and so unless there is a reason for the electroweak corrections to be enhanced, for example, by large logarithms $\log^2(s/m_W^2)$ for $s \gg m_W^2$, the QCD corrections are usually much more important for a given order.

[30] The programmes performing this function, event generators, are described in Section 7.3.

[31] Usually, a truncated series in α, α_s or both, but sometimes truncated in one of these parameters multiplied by a logarithm of two scales.

Chapter 3

Next to Leading Order Calculations

Although designed as a discovery machine, rather than a precision machine (Lepton colliders are better suited to high precision), the LHC, which is the most important particle collider for this generation, can measure differential and integrated cross sections to accuracies of a few percent. However, a leading order (LO) result can often have an uncertainty (estimated using the scale variation: see Section 2.6.1.) on the ten-percent level, requiring next-to-leading order (NLO) calculations to match the experimental accuracy.

In particular, early studies at the LHC have had to do with rediscovery of the Standard Model, but if we wish to discover New Physics, then we must often isolate a small New Physics interaction rate on a large Standard Model background: therefore, in order for the New Physics signal to be visible, the Standard Model result must have errors which are as small as possible.

3.1 Structure of the NLO Calculation

In the rest of the chapter, we lay out a sketch of the structure of an NLO calculation. To find the NLO matrix element $\mathcal{M}_{NLO}$ for (a given phase space point of) a given process, we start with the leading order piece, i.e. the piece with the lowest possible order in the coupling (which might be QED, QCD or a combination), which usually

consists of the "tree-level", or "Born" piece [1] – in this part of the calculation, there are no loops or additional final- or initial-state particles. Two examples of tree-level Feynman diagrams are given in Figure 3.1. To increase to NLO accuracy, we need

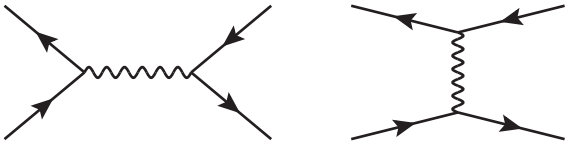

Figure 3.1: Two leading order diagrams.

two pieces, which are the two possible ways of increasing the order in the coupling:

- adding a loop ("virtual correction"), such as in Figure 3.2, which gives us an undertermined momentum running around the loop.

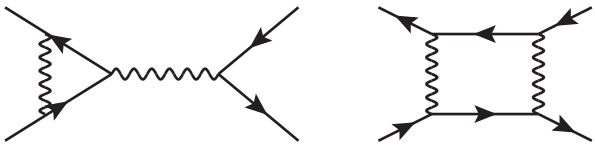

Figure 3.2: Two one-loop diagrams.

- adding a real emission, i.e. a new particle which appears in the final state, such as in Figure 3.3. Note that if we have a programme producing generic Born-level calculations, it will automatically be able to calculate the real part (apart from the subtraction, see Section 3.1.1).

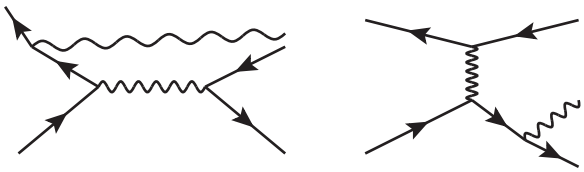

Figure 3.3: Two real emission diagrams.

So naïvely we then have:

$$\text{“}\mathcal{M}_{NLO} = \mathcal{M}_{Born} + \mathcal{M}_{1loop} + \mathcal{M}_{Real}\text{”}, \tag{3.1.1}$$

[1] In some cases (e.g. the $gg \to ZZ$ of Section 7.4.2), there are no tree-level diagrams, and the lowest-order matrix element has one loop.

although illustrative, this is not strictly meaningful, as $\mathcal{M}_{Real}$ has a different phase space, having an extra particle in the final state.

Now if we wish to find the NLO cross section we must interfere the matrix element with itself and integrate it over phase space. On squaring, we have the LO cross-section, the real cross-section, and then the loop contribution comes from the Born-loop cross term. The square of the virtual contribution is another order higher, and is therefore neglected in a strict NLO calculation[2]. Schematically, the NLO cross-section can be written:

$$\sigma_{NLO} = \int_N |\mathcal{M}_{Born}|^2 + \int_N 2\mathrm{Re}\left(\mathcal{M}_{Born}\mathcal{M}^*_{1loop}\right) + \int_{N+1} |\mathcal{M}_{Real}|^2 , \tag{3.1.2}$$

where the subscript on the integral indicates the number of particles in the phase space. We saw in Section 2.3 that both the second and third terms are (usually) formally infinite, having divergences that must be cancelled against each other. In addition, the real matrix element is too complicated to be integrated analytically, so we cannot simply write it as a Laurent expansion in ϵ. We deal with these problems using subtraction, explained in the next section.

3.1.1 Subtraction

We have in (3.1.2) two terms which are separately divergent, but whose divergences cancel for a sufficiently inclusive physical observable (by the Kinoshita-Lee-Nauenberg theorem [44, 45]). The complication comes about because the loop and real contributions have different phase spaces, so this cancellation of divergences is not trivial. To solve this, we use a subtraction method (of which there are several versions, such as dipole [46, 47], antenna [48, 49] and FKS [50, 51]) in which we add and subtract a well-chosen function F. The function is used to subtract out the divergences from the real emission part in the $(N + 1)$-particle phase space, and is added to the loop part, integrated over the one particle phase space. Our NLO

[2]But see Section 7.4.2 for a case in which it is necessary to include it.

cross-section

$$\begin{aligned}\sigma_{NLO} = &\int_N |\mathcal{M}_{Born}|^2 \\ &+ \int_N \left(2\mathrm{Re}\left(\mathcal{M}_{Born}\mathcal{M}^*_{1loop}\right) + \int_1 F\right) \\ &+ \int_{N+1} \left(|\mathcal{M}_{Real}|^2 - F\right)\end{aligned} \tag{3.1.3}$$

now has three lines, each of which is individually finite, and so they can be calculated separately by Monte Carlo integration (see Section 7.3).

3.2 Loop Diagram Example

An example of the calculation of the first term of (3.1.3) was given for $e^+e^- \to \mu^+\mu^-$ in Section 2.2.4. Now let us pick one contribution to the second term, coming from the loop diagram in Figure 3.4, to illustrate the appearance of tensor integrals. We have

$$\begin{aligned}i\mathcal{M}_{1loop} =&\bar{v}_2(-i(-1)e\gamma^\mu)u_1\frac{-ig_{\nu\mu}}{q^2+i\lambda} \\ &\times \bar{u}_3\int\frac{d^dk}{(2\pi)^d}(ie\gamma^\sigma)\frac{i\not{k}}{k^2+i\lambda}(ie\gamma^\nu)\frac{i(\not{k}+\not{p_3}+\not{p_4})}{(k+p_3+p_4)^2+i\lambda}\frac{-ig_{\sigma\rho}}{(k+p_3)^2+i\lambda}(ie\gamma^\rho)v_4\end{aligned} \tag{3.2.4}$$

and so (for one phase-space point), the contributing term after spin summation and averaging will be

$$\begin{aligned}\left(\mathcal{M}_{Born}\mathcal{M}^*_{1loop}\right) = &-\frac{ie^6}{4q^4}\not{p_2}\gamma^\nu\not{p_1}\gamma^\mu\not{p_3}\gamma_\nu\not{p_4} \\ &\times\int\frac{d^dk}{(2\pi)^d}\frac{\not{k}+\not{p_3}+\not{p_4}}{(k+p_3+p_4)^2+i\lambda}\gamma^\rho\frac{1}{(k+p_3)^2+i\lambda}\gamma_\rho\frac{\not{k}}{k^2+i\lambda}\gamma_\mu\end{aligned} \tag{3.2.5}$$

For this type of integral, we will separate out the terms in the numerator, and then refer to those components with r instances of the loop momenta in the numerators as *rank-r tensor* integrals, and those without a loop momentum in the numerator as *scalar* integrals. The higher the rank of a tensor integral, the more difficult is its computation, so of the integrals which we will have to perform here,

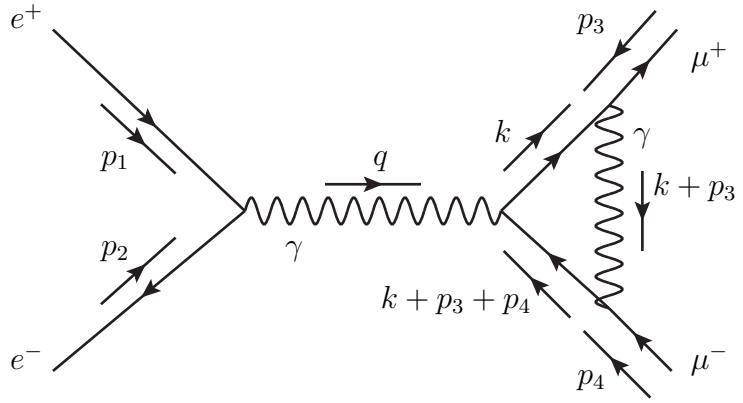

Figure 3.4: An example of a loop diagram for $e^+e^- \to \mu^+\mu^-$ (using a convention of all momenta incoming).

the hardest is the rank-2 tensor integral

$$\mathcal{I} = \int \frac{d^d k}{(2\pi)^d} \frac{k^\lambda k^\tau}{(k^2 + i\lambda)((k+p_3)^2 + i\lambda)((k+p_3+p_4)^2 + i\lambda)} \tag{3.2.6}$$

the evaluation of terms of this type will be the theme of Chapter 4.

3.3 Loop Calculation Methods

So far we have demonstrated the flow of a one-loop calculation, and shown that tensor integrals appear in loop calculations. The evaluation of these tensor integrals is a major thrust of this thesis, and has historically been a major bottleneck in this class of NLO calculations. We would prefer to do simpler, scalar, integrals, which are much less time consuming, even at the cost of evaluating more terms.

The conventional method for achieving this, tensor reduction [52–54], consists of forming the squared matrix element, as in the previous section, and then passing the tensor integrals through an algorithm which reduces the rank, often to a standard scalar integral, as described in Chapter 4. This is the method used in `golem95` [55][3]. It is explained in Section 4.3.1 that this method can suffer numerical instabilities for exceptional kinematic conditions, due to the choice of the scalar integrals as a basis, and that `golem95` has an alternative method to avoid these instabilities.

[3]Although now it also includes tensorial reconstruction, explained in the following section.

In 2006, an alternative method was introduced by Ossola, Papadopoulos and Pittau (OPP) [56, 57], in which the reduction is performed at the integrand level. This is explained in the following section.

3.3.1 Integrand-level Reduction

In this technique, the integrand I of an expression for an N-point amplitude is written with its maximal denominator [58]:

$$I = \frac{\mathcal{N}(k)}{D_1 ... D_{(N-1)}} \tag{3.3.7}$$

with
$$D_i = (k + r_i)^2 - m_i^2 \tag{3.3.8}$$

and the numerator $\mathcal{N}(k)$ is seen as a polynomial in the loop momentum k, and expanded in terms of the possible D_i in the numerator:

$$\begin{aligned}\mathcal{N}(k) = &\sum_{i<j<l<m}^{(N-1)} (d_{ijlm} + \tilde{d}_{ijlm}(k)) \prod_{\lambda \neq i,j,l,m}^{(N-1)} D_\lambda \\ &+ \sum_{i<j<l}^{(N-1)} (c_{ijl} + \tilde{c}_{ijl}(k)) \prod_{\lambda \neq i,j,l}^{(N-1)} D_\lambda \\ &+ \sum_{i<j}^{(N-1)} (b_{ij} + \tilde{b}_{ij}(k)) \prod_{\lambda \neq i,j}^{(N-1)} D_\lambda \\ &+ \sum_{i}^{(N-1)} (a_i + \tilde{a}_i(k)) \prod_{\lambda \neq i}^{(N-1)} D_\lambda \\ &+ \tilde{P}(k) \prod_{\lambda}^{(N-1)} D_\lambda \end{aligned} \tag{3.3.9}$$

where the tilded terms are defined by the fact that they disappear when the n-dimensional k-integration is performed, and all depend on k. They are referred to as the *spurious* terms. If we are dealing in a renormalisable theory and gauge, then $\tilde{P} = 0$.

Before the important untilded terms can be calculated, the k-dependence of the vanishing part of the amplitude must be constructed, and this is performed sequentially from $\tilde{d}$ to $\tilde{a}$ by working in terms of an explicit decomposition of k in a basis of massless four-momenta, and proving that certain combinations of momenta vanish upon integration. Explicit forms are given in [56].

Once the spurious terms have been extracted, this polynomial can be then sampled for different values of k, in order to fit for the coefficients.

The (loop) expressions on which this method operates can be obtained from Feynman diagrams, as is performed by Samurai [59], or by the technique of unitarity cuts [60], in which factorisation properties of the amplitude, including the optical theorem (see Section 6.1), are used to build up an expression for the one-loop matrix element from tree-level diagrams. This method has the general implementations BlackHat [61] and Rocket [62].

Tensorial Reconstruction at the Integrand Level

Because the basis choice of scalar integrals is also made in the OPP method, it suffers from the same numerical instabilities for exceptional kinematic conditions as the conventional method. In [63], an approach avoiding these instabilities is presented. In this case the expression is written out as a sum of tensor integrals, and the system of equations at the integrand level is solved. This different choice of basis avoids the numerical instability.

Chapter 4

Tensor Integrals

In this chapter we describe the process for the calculation of tensor integrals followed by `golem95` [55,64–68]. This is based on Passarino-Veltman reduction [53], but with modifications for the avoidance of numerical instabilities.

4.1 Tensor Reduction and `golem95`

In the `golem95` method, we start with a general one-loop N-point graph.

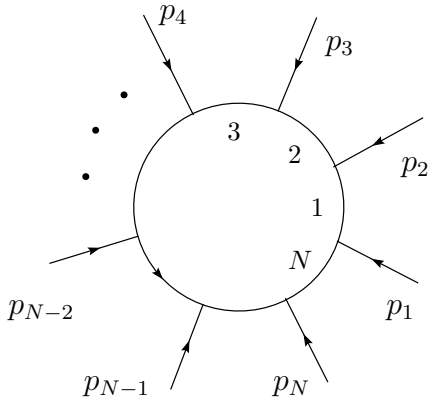

Figure 4.1: General N-point one-loop graph with momenta labelled p_i and propagators labelled with their numbers.

The momenta p_i are all defined as incoming, and so

$$\sum_{i=1}^{N} p_i = 0. \tag{4.1.1}$$

We will consider the tensor integrals that may occur. We allow the numerator to contain not only the loop momentum k but any combination of the loop momentum and the external momenta $q_a = k + r_a$ where[1] $r_a = \sum_{i=1}^{a} p_i$. For this reason, the golem95 method has an additional set of labels on its integrals, the a_i, which other formalisms all effectively set to N:

$$\mathcal{I}_N^{d,\mu_1\mu_2\ldots\mu_r}(a_1,a_2,\ldots,a_r) = \int \frac{d^d k}{i\pi^{d/2}} \frac{q_{a_1}^{\mu_1} q_{a_2}^{\mu_2} \ldots q_{a_r}^{\mu_r}}{(q_1^2 - m_1^2 + i\lambda)(q_2^2 - m_2^2 + i\lambda)\ldots(q_N^2 - m_N^2 + i\lambda)}, \tag{4.1.2}$$

where r is the rank of the tensor integral.

4.1.1 Feynman Parameters

To aid in the solving of these integrals, we use the technique of Feynman parameters. The aim is to change the form of the denominator so that, rather than a product of several terms, we have a sum of such terms, raised to a power.

In order to understand the method, let us first consider the integral (for constants A and B)

$$\begin{aligned}\mathcal{J} &= \int_0^1 dxdy\delta(1-x-y)\frac{1}{(xA+yB)^2} \\ &= \int_0^1 dx \frac{1}{(xA+(1-x)B)^2}\end{aligned}$$

substitute $X = x(A-B)+B$

$$\begin{aligned}&= \int_B^A dX \frac{1}{A-B}\frac{1}{X^2} \\ &= \frac{1}{AB},\end{aligned} \tag{4.1.3}$$

i.e. we can write the reciprocal of a product of terms as the reciprocal of their sum, at the expense of including new parameters that must be integrated over. In

[1]Because of (4.1.1), we could take $r_N = 0$, but we do not so that we have a shift invariant formulation, see Section 4.1.3.

Appendix C.1, we show how this can be extended to

$$\frac{1}{A_1 A_2 \dots A_n} = \int_0^1 dx_1 dx_2 \dots dx_n \delta\left(\sum_{i=1}^{n} x_i - 1\right) \frac{(n-1)!}{[x_1 A_1 + x_2 A_2 + \dots + x_n A_n]^n}. \tag{4.1.4}$$

4.1.2 The Set S

Later in this thesis, we will need to consider integrals in which some of the propagators have been removed, or *pinched*. In order to do this efficiently, we introduce the set S, which is the set giving the numerical labels of the propagators in an integral. We term the maximal such set S_0.

For example, we can write the scalar box integral, using the set $S_0 = \{1, 2, 3, 4\}$

$$\mathcal{I}_4^d(S_0) = \int \frac{d^d k}{i\pi^{d/2}} \frac{1}{(q_1^2 - m_1^2 + i\lambda)(q_2^2 - m_2^2 + i\lambda)(q_3^2 - m_3^2 + i\lambda)(q_4^2 - m_4^2 + i\lambda)}, \tag{4.1.5}$$

and it will be useful to be able to denote the integrals which are obtained by pinching certain propagators. Let us pinch the first and third propagators, obtaining a bubble, with the set becoming $S_0 \backslash \{1, 3\} = \{2, 4\}$, where the backslash represents the removal of the set that follows it:

$$\mathcal{I}_2^d(S_0 \backslash \{1, 3\}) = \int \frac{d^d k}{i\pi^{d/2}} \frac{1}{(q_2^2 - m_2^2 + i\lambda)(q_4^2 - m_4^2 + i\lambda)}. \tag{4.1.6}$$

4.1.3 Shift Invariance

At the start of Section 4.1, we discussed integrals of the form (4.1.2), in which not only the loop momentum k but also combinations of external momenta with it, $q_a = k + r_a$, were permitted to be in the numerator of our tensor integrals. Although adding the complication of requiring additional momentum labels a_i, this system is beneficial as it makes the formulation invariant under shifts of the loop momentum $k \to k + r_a$.

During reduction, it is very common to move between integrals with different momenta in the numerator, requiring a loop momentum shift to return to the original form (an example is given in Appendix C.2). This creates additional terms (2^r for

a rank-r integral). If instead a shift-invariant formulation is used, these additional terms are avoided, improving the speed of calculation.

We can therefore think about our integrals in terms of vectors

$$\Delta_{ij}^{\mu} = r_i^{\mu} - r_j^{\mu} = q_i^{\mu} - q_j^{\mu} \tag{4.1.7}$$

which are invariant under shifts of the loop momentum.

4.1.4 The Modified Cayley Matrix $\mathcal{S}$

The kinematic information is entered into the calculation using the modified Cayley matrix [52], which we represent with a calligraphic $\mathcal{S}$:

$$\mathcal{S}_{ij} = (q_i - q_j)^2 - m_i^2 - m_j^2 \tag{4.1.8}$$

$$= (r_i - r_j)^2 - m_i^2 - m_j^2. \tag{4.1.9}$$

The range of i and j will be the maximum set S_0, and for any pinched propagators, the entries for that row and column will be set to zero, so for the example of Section 4.1.2, we have:

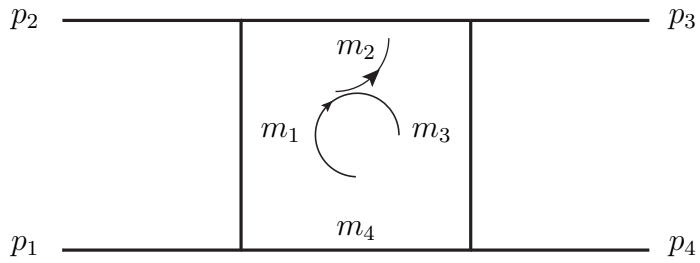

Figure 4.2: A four-point (box) diagram.

$$\mathcal{S}(S_0) = \begin{pmatrix} -2m_1^2 & (r_1-r_2)^2 - m_1^2 - m_2^2 & (r_1-r_3)^2 - m_1^2 - m_3^2 & (r_1-r_4)^2 - m_1^2 - m_3^2 \\ (r_1-r_2)^2 - m_1^2 - m_2^2 & -2m_2^2 & (r_2-r_3)^2 - m_2^2 - m_3^2 & (r_2-r_4)^2 - m_2^2 - m_4^2 \\ (r_1-r_3)^2 - m_1^2 - m_3^2 & (r_2-r_3)^2 - m_2^2 - m_3^2 & -2m_3^2 & (r_3-r_4)^2 - m_3^2 - m_4^2 \\ (r_1-r_4)^2 - m_1^2 - m_4^2 & (r_2-r_4)^2 - m_2^2 - m_4^2 & (r_3-r_4)^2 - m_3^2 - m_4^2 & -2m_4^2 \end{pmatrix} \tag{4.1.10}$$

and

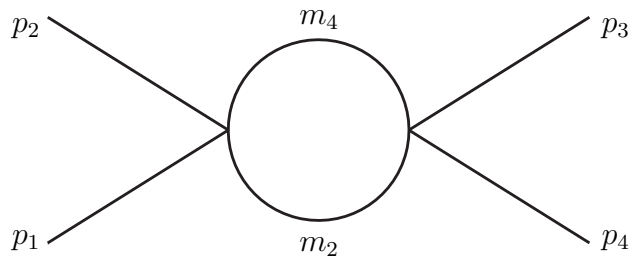

Figure 4.3: A four-point diagram with two legs pinched, making a bubble.

$$\mathcal{S}(S_0\backslash\{1,3\}) = \begin{pmatrix} 0 & 0 & 0 & 0 \\ 0 & -2m_2^2 & 0 & (r_2-r_4)^2 - m_2^2 - m_4^2 \\ 0 & 0 & 0 & 0 \\ 0 & (r_2-r_4)^2 - m_2^2 - m_4^2 & 0 & -2m_4^2 \end{pmatrix}. \quad (4.1.11)$$

In this calculation, the inverse of $\mathcal{S}$ is also needed. However, if there are any pinches, this is not defined, so we use instead the Moore-Penrose pseudo-inverse[2], and refer to it simply as $\mathcal{S}^{-1}$. This is formed by taking the inverse of the smaller matrix with the zero rows and columns omitted, and then replacing the zero entries.

$$\mathcal{S}^{-1}(S_0\backslash\{1,3\}) = \frac{1}{\kappa((r_2-r_4)^2, m_2^2, m_4^2)} \begin{pmatrix} 0 & 0 & 0 & 0 \\ 0 & 2m_4^2 & 0 & (r_2-r_4)^2 - m_2^2 - m_4^2 \\ 0 & 0 & 0 & 0 \\ 0 & (r_2-r_4)^2 - m_2^2 - m_4^2 & 0 & 2m_2^2 \end{pmatrix}, \quad (4.1.12)$$

where $\kappa(x,y,z) = x^2 + y^2 + z^2 - 2xy - 2yz - 2zx$ is called the Källén function [71]. We will see in Section 6.2 that $\det \mathcal{S} \to 0$ can lead to *Landau singularities* [72], and there we discuss how to deal with them.

4.1.5 Gram Matrix

A second, related matrix carrying kinematic information is the Gram matrix, defined as a matrix of dimension one lower than the $\mathcal{S}$-matrix, with a particular row and column with index A having been removed. If the shift invariance (see Section 4.1.3)

[2] A matrix $\mathcal{P}$ defined by [69,70]: $\mathcal{PSP} = \mathcal{P}, \mathcal{SPS} = \mathcal{S}, \mathcal{PS} = \mathcal{SP}$.

is broken by setting a particular $r_i = 0$, this $i = A$ should be taken. If the shift invariance is unbroken, it is not important which A is chosen.

$$\mathcal{G}_{ij}^{(A)} = 2\Delta_{iA} \cdot \Delta_{jA} \tag{4.1.13}$$

As shown in Section 4.3.1, the inverse of the Gram matrix, and therefore the reciprocal of its determinant, can appear in the tensor reduction process. This determinant approaches zero as the r_j become linearly dependent, and so numerical instabilities can occur around this limit. In tensor reduction, these singularities can be non-integrable (inverse power greater than $\frac{1}{2}$): in this case, the singularity is certainly spurious, and is dependent on our choice of reduction basis.

4.1.6 The Scalar N-Point Integral

Let us consider a scalar N-point integral[3]:

$$\mathcal{I}_N^d(S) = \int \frac{d^d k}{i\pi^{d/2}} \frac{1}{\prod_{i=1}^N (q_i^2 - m_i^2 + i\lambda)} \tag{4.1.14}$$

in which the integration measure is chosen for convenience: we will see that the $i\pi^{d/2}$ cancels later. Let us substitute (4.1.4):

$$\mathcal{I}_N^d(S) = \int \frac{d^d k}{i\pi^{d/2}} \int_0^1 \prod_{i=1}^N (dx_i) \delta\left(\sum_{i=1}^N x_i - 1\right) \frac{(N-1)!}{\left[\sum x_i (q_i^2 - m_i^2 + i\lambda)\right]^N}, \tag{4.1.15}$$

and examine the sum in the denominator:

$$\mathcal{D} = \sum x_i (q_i^2 - m_i^2 + i\lambda) \tag{4.1.16}$$

$$= k^2 \sum x_i + \sum x_i (2k \cdot r_i) + \sum x_i r_i^2 - \sum x_i m_i^2 + \sum x_i i\lambda, \tag{4.1.17}$$

then perform a shift

$$k \to k' = k + \sum x_i r_i \tag{4.1.18}$$

so that

$$\mathcal{D} = k'^2 - \left(\sum x_i r_i\right)^2 + \sum x_i r_i^2 - \sum x_i m_i^2 + i\lambda \tag{4.1.19}$$

[3]In this derivation, and in the rest of this chapter, the Einstein convention is not used, and sums are shown explicitly.

where in the first term, we have used the δ-functional in (4.1.15) to set $\sum x_i = 1$, and for the last term, as all the x_i are positive, we have rescaled $\sum(x_i\lambda) \to \lambda$

Now we can investigate the terms with neither a λ nor a k'-dependence

$$J = -\left(\sum x_i r_i\right)^2 + \sum x_i r_i^2 - \sum x_i m_i^2 \tag{4.1.20}$$

and insert $\sum x_i = 1$

$$J = -\sum_{i,j=1}^{N} x_i r_i x_j r_j + \sum_{i=1}^{N} x_i(r_i^2 - m_i^2)\sum_{j=1}^{N} x_j, \tag{4.1.21}$$

then split the second term into two equal parts

$$J = -\sum_{i,j=1}^{N} x_i x_j r_i \cdot r_j + \frac{1}{2}\sum_{i=1}^{N} x_i(r_i^2 - m_i^2)\sum_{j=1}^{N} x_j + \frac{1}{2}\sum_{j=1}^{N} x_j(r_j^2 - m_j^2)\sum_{i=1}^{N} x_i \tag{4.1.22}$$

$$J = \frac{1}{2}\sum_{i,j=1}^{N} x_i x_j(r_i^2 + r_j^2 - 2r_i \cdot r_j - m_i^2 - m_j^2) \tag{4.1.23}$$

$$J = \frac{1}{2}\sum_{i,j=1}^{N} x_i x_j \mathcal{S}_{ij}, \tag{4.1.24}$$

and we see we are now dealing with the modified Cayley matrix $\mathcal{S}_{ij} = (r_i - r_j)^2 - m_i^2 - m_j^2$ of Section 4.1.4.

We have now arrived at (dropping the primes on k, and writing $(N-1)!$ as $\Gamma(N)$):

$$\mathcal{I}_N^d(S) = \int_{-\infty}^{\infty} \frac{d^d k}{i\pi^{d/2}} \int_0^1 \prod_{i=1}^{N}(dx_i)\delta\left(\sum_{i=1}^{N} x_i - 1\right) \frac{\Gamma(N)}{\left[k^2 + \frac{1}{2}x \cdot \mathcal{S} \cdot x + i\lambda\right]^N}, \tag{4.1.25}$$

and we want to do the momentum integration. Let us first examine the poles in the denominator, remembering that $k^2 = k_0^2 - |\underline{k}|^2$. Poles will occur at:

$$k_0^2 - |\underline{k}|^2 + \frac{1}{2}x \cdot \mathcal{S} \cdot x + i\lambda = 0 \tag{4.1.26}$$

$$k_0 = \pm\sqrt{|\underline{k}|^2 - \frac{1}{2}x \cdot \mathcal{S} \cdot x \mp i\lambda}, \tag{4.1.27}$$

where again we have rescaled λ.

We must first deal with the fact that we have one temporal component, which is not treated like the spatial components: $k^2 = k_0^2 - |\underline{k}|^2$. To do this, we use

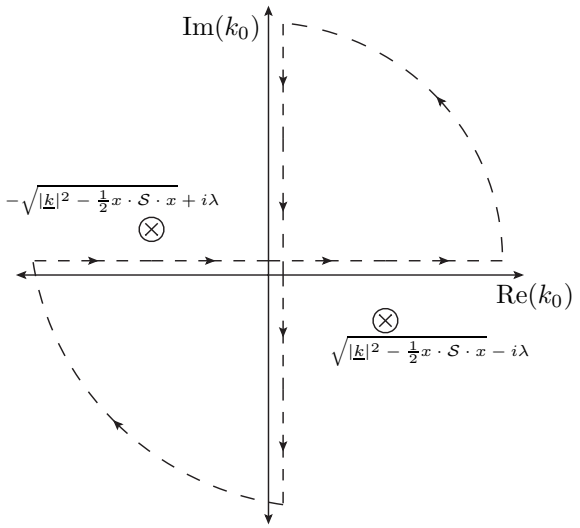

Figure 4.4: Wick rotation: the poles are shown as crossed circles, and the integration contour is given as a dashed line. The contour is shown displaced from the axes for clarity, but would in reality be along them.

Wick rotation to move (from Minkowski) to a Euclidean space. Let us write our integral $\int_{-\infty}^{\infty} dk_0 f(k_0, |\underline{k}|)$, with the integration contour along the real axis. Then let us consider the dashed integration contour in Figure 4.4. The path encloses no poles, so the integral along it must be zero by the residue theorem. We also assume that $f(k_0, |\underline{k}|)$ falls off sufficiently quickly at infinity for the integrals along the two quarter-circle paths to be zero. Then:

$$\int_{-\infty}^{\infty} dk_0 f(k_0, |\underline{k}|) + \int_{i\infty}^{-i\infty} dk_0 f(k_0, |\underline{k}|) = 0 \tag{4.1.28}$$

so

$$\int_{-\infty}^{\infty} dk_0 f(k_0, |\underline{k}|) = \int_{k_0=-i\infty}^{k_0=i\infty} dk_0 f(k_0, |\underline{k}|)) \tag{4.1.29}$$

$$= i \int_{k_4=-\infty}^{k_4=+\infty} dk_4 f(k_E), \tag{4.1.30}$$

where we have taken $k_0 = ik_4$ and $k_E = (ik_4, |\underline{k}|)$, so

$$k_E^2 = -k_4^2 - |\underline{k}|^2 = -\sum_{i=1}^{d} k_i^2 \tag{4.1.31}$$

and we have a four-dimensional Euclidean integration:

$$\mathcal{I}_N^d(S) = i \int_0^1 \prod_{i=1}^{N} (dx_i) \delta \left(\sum_{i=1}^{N} x_i - 1 \right) \Gamma(N) \int_{-\infty}^{\infty} \frac{d^d k_E}{i\pi^{d/2}} \frac{(-1)^N}{\left[k_E^2 - \frac{1}{2} x \cdot \mathcal{S} \cdot x - i\lambda \right]^N}. \tag{4.1.32}$$

We can evaluate the momentum integral using a d-dimensional sphere:

$$\int_{-\infty}^{\infty} d^d k_E = \int_0^{\infty} dk_r k_r^{d-1} \int d\Omega_{d-1}, \tag{4.1.33}$$

where $k_r = \sqrt{k_E^2}$ is the radius of the d-dimensional sphere, and $d\Omega_{d-1}$ is its surface element:

$$\int d\Omega_{d-1} = \frac{2\pi^{d/2}}{\Gamma(\frac{d}{2})} \tag{4.1.34}$$

which is demonstrated in Appendix C.4.

So then

$$\mathcal{I}_N^d(S) = i \int_0^1 \prod_{i=1}^N (dx_i)\delta\left(\sum_{i=1}^n x_i - 1\right) \Gamma(N) \frac{2\pi^{d/2}}{\Gamma(\frac{d}{2})} \frac{(-1)^N}{i\pi^{d/2}} \int_0^{\infty} dk_r \frac{k_r^{d-1}}{\left[k_r^2 - \frac{1}{2}x\cdot\mathcal{S}\cdot x - i\lambda\right]^N}, \tag{4.1.35}$$

and we can substitute $K = \frac{k_r^2}{-\frac{1}{2}x\cdot\mathcal{S}\cdot x - i\lambda}$, remembering that $\mathcal{S}$ only contains external momenta, and so has no dependence on the loop momentum:

$$\begin{aligned}\mathcal{I}_N^d(S) = &\int_0^1 \prod_{i=1}^N (dx_i)\delta\left(\sum_{i=1}^N x_i - 1\right) \Gamma(N) \frac{2}{\Gamma(\frac{d}{2})} (-1)^N \frac{1}{2} \\ &\times \left(-\frac{1}{2}x\cdot\mathcal{S}\cdot x - i\lambda\right)^{\frac{d}{2}-N} \int_0^{\infty} dK \frac{K^{\frac{d}{2}-1}}{[K+1]^N}.\end{aligned} \tag{4.1.36}$$

We can identify our remaining K-integral with the Euler Beta function, discussed in Appendix B.4, with $s = \frac{d}{2}$ and $t = N - \frac{d}{2}$, as long as $(N - \frac{d}{2})$ is neither zero nor a negative integer.

$$B(s,t) = \int_0^{\infty} dz \frac{z^{s-1}}{[z+1]^{(s+t)}} = \int_0^1 dy y^{s-1}(1-y)^{t-1} = \frac{\Gamma(s)\Gamma(t)}{\Gamma(s+t)}. \tag{4.1.37}$$

Finally our momentum integration is complete and we have

$$\mathcal{I}_N^d(S) = \int_0^1 \prod_{i=1}^N (dx_i)\delta\left(\sum_{i=1}^N x_i - 1\right) \Gamma(N) \frac{1}{\Gamma(\frac{d}{2})} (-1)^N \left(-\frac{1}{2}x\cdot\mathcal{S}\cdot x - i\lambda\right)^{\frac{d}{2}-N} \frac{\Gamma(\frac{d}{2})\Gamma(N-\frac{d}{2})}{\Gamma(N)} \tag{4.1.38}$$

$$\mathcal{I}_N^d(S) = (-1)^N \Gamma\left(N - \frac{d}{2}\right) \int_0^1 \prod_{i=1}^N (dx_i)\delta\left(\sum_{i=1}^n x_i - 1\right) \left(-\frac{1}{2}x\cdot\mathcal{S}\cdot x - i\lambda\right)^{\frac{d}{2}-N}. \tag{4.1.39}$$

4.2 Form Factors

Starting with a tensor integral of the form (4.1.2), we wish to separate the Lorentz structure from the integrals. The only quantities carrying Lorentz structure are external momenta, in this case in the form of the shift-invariant vectors Δ^{μ}_{ij}, and the metric tensor $g^{\mu\nu}$, so for $N \leq 5$, we can define *Form Factors* $A^{N,r}_{j_1\dots j_r}(S)$, $B^{N,r}_{j_1\dots j_{r-2}}(S)$ and $C^{N,r}_{j_1\dots j_{r-4}}(S)$ by:

$$\begin{aligned}\mathcal{I}^{d,\mu_1\mu_2\dots\mu_r}_N(a_1,a_2,\dots,a_r;S) = &\sum_{j_1\dots j_r\in S}\left[\Delta^{\cdot}_{j_1\cdot}\Delta^{\cdot}_{j_2\cdot}\cdots\Delta^{\cdot}_{j_r\cdot}\right]^{\{\mu_1\mu_2\dots\mu_r\}}_{\{a_1a_2\dots a_r\}} A^{N,r}_{j_1\dots j_r}(S)\\ &+\sum_{j_1\dots j_{r-2}\in S}\left[g^{\cdot\cdot}\Delta^{\cdot}_{j_1\cdot}\Delta^{\cdot}_{j_2\cdot}\cdots\Delta^{\cdot}_{j_{r-2}\cdot}\right]^{\{\mu_1\mu_2\dots\mu_r\}}_{\{a_1a_2\dots a_r\}} B^{N,r}_{j_1\dots j_{r-2}}(S)\\ &+\sum_{j_1\dots j_{r-4}\in S}\left[g^{\cdot\cdot}g^{\cdot\cdot}\Delta^{\cdot}_{j_1\cdot}\Delta^{\cdot}_{j_2\cdot}\cdots\Delta^{\cdot}_{j_{r-4}\cdot}\right]^{\{\mu_1\mu_2\dots\mu_r\}}_{\{a_1a_2\dots a_r\}} C^{N,r}_{j_1\dots j_{r-4}}(S),\end{aligned} \tag{4.2.40}$$

where $[]^{\{\mu_1\mu_2\dots\mu_r\}}_{\{a_1a_2\dots a_r\}}$ signifies the distribution of the Lorentz indices μ_1 to μ_r and the momentum labels a_1 to a_r into the positions indicated by the dots: Lorentz indices going onto metric tensors $g^{\mu_i\mu_j}$ and onto vectors $\Delta^{\mu_i}_{ja_i}$, and momentum labels going only onto the vectors. This means that for the $B^{N,r}_{j_1\dots j_{r-2}}(S)$ and $C^{N,r}_{j_1\dots j_{r-4}}(S)$, each term of the sum will carry only a subset of the momentum labels.

Now let us write equation (4.2.40) specifically for each case with $r \leq 4$:

$$\mathcal{I}^{d}_N(S) = A^{N,0}(S) \tag{4.2.41}$$

$$\mathcal{I}^{d,\mu}_N(a;S) = \sum_{j\in S}\Delta^{\mu}_{ja}A^{N,1}_j(S) \tag{4.2.42}$$

$$\mathcal{I}^{d,\mu\nu}_N(a,b;S) = \sum_{i,j\in S}\Delta^{\mu}_{ia}\Delta^{\nu}_{jb}A^{N,2}_{ij}(S) + g^{\mu\nu}B^{N,2}(S) \tag{4.2.43}$$

$$\begin{aligned}\mathcal{I}^{d,\mu\nu\rho}_N(a,b,c;S) = &\sum_{i,j,k\in S}\Delta^{\mu}_{ia}\Delta^{\nu}_{jb}\Delta^{\rho}_{kc}A^{N,3}_{ijk}(S)\\ &+\sum_{j\in S}\left(g^{\mu\nu}\Delta^{\rho}_{jc}+g^{\mu\rho}\Delta^{\nu}_{jb}+g^{\nu\rho}\Delta^{\mu}_{ja}\right)B^{N,3}_j(S)\end{aligned} \tag{4.2.44}$$

$$\begin{aligned}\mathcal{I}_N^{d,\mu\nu\rho\sigma}(a,b,c,d;S) = &\sum_{i,j,k,l\in S} \Delta_{ia}^{\mu}\Delta_{jb}^{\nu}\Delta_{kc}^{\rho}\Delta_{ld}^{\sigma}A_{ijkl}^{N,4}(S)\\ &+\sum_{i,j\in S}(g^{\mu\nu}\Delta_{ic}^{\rho}\Delta_{jd}^{\sigma}+g^{\mu\rho}\Delta_{ib}^{\nu}\Delta_{jd}^{\sigma}+g^{\mu\sigma}\Delta_{ib}^{\nu}\Delta_{jc}^{\rho}\\ &+g^{\nu\rho}\Delta_{ia}^{\mu}\Delta_{jd}^{\sigma}+g^{\nu\sigma}\Delta_{ia}^{\mu}\Delta_{jc}^{\rho}+g^{\rho\sigma}\Delta_{ia}^{\mu}\Delta_{jb}^{\nu})B_{ij}^{N,2}(S)\\ &+\left(g^{\mu\nu}g^{\rho\sigma}+g^{\mu\rho}g^{\nu\sigma}+g^{\mu\sigma}g^{\nu\rho}\right)C^{N,4}(S). \end{aligned} \tag{4.2.45}$$

There is a general relation between tensor integrals and parameter integrals with Feynman parameters in the numerator [64, 73, 74]:

$$\begin{aligned}\mathcal{I}_N^{d,\mu_1\cdots\mu_r}(a_1,\ldots,a_r\,;S) =&(-1)^r\sum_{m=0}^{\lfloor\frac{r}{2}\rfloor}\left(-\frac{1}{2}\right)^m\\ &\times\sum_{j_1,\cdots j_{r-2m}=1}^{N}\left[(g^{\cdot\cdot})^{\otimes m}\,\Delta_{j_1\cdot}^{\cdot}\cdots\Delta_{j_r\cdot}^{\cdot}\right]_{\{a_1\cdots a_r\}}^{\{\mu_1\cdots\mu_r\}}\,\mathcal{I}_N^{d+2m}(j_1\ldots,j_{r-2m}\,;S)\,,\end{aligned} \tag{4.2.46}$$

where $\mathcal{I}$ with a_i as arguments is understood to have momenta q_{a_i} in the numerator, and with j_i as arguments it is understood to have Feynman parameters z_{j_i} in the numerator; $\lfloor\frac{r}{2}\rfloor$ stands for the nearest integer less or equal to $\frac{r}{2}$; and the symbol $\otimes m$ indicates that m instances of the metric tensor are present in the square bracket.

From this relation, we can see very clearly that the presence of the metric tensor in (4.2.43) to (4.2.45), and the form factors B and C that accompany it, is related to integrals in higher numbers of dimensions.

4.3 Separation of Divergences by Subtraction

In our reduction procedure, we wish to separate the infrared divergent and finite parts of our expressions, and to do so in a way that avoids spurious Gram determinants, following the procedure of [65]. Let us take a scalar N-point integral

$$\mathcal{I}_N^d(S) = \int \frac{d^dk}{i\pi^{d/2}}\frac{1}{\prod_{i=1}^N(q_i^2-m_i^2+i\lambda)}, \tag{4.3.47}$$

and make an ansatz that the IR divergence, if present, can be split off into a simpler integral I_{div}, which has one propagator pinched, and leaving an IR finite part of the

original rank:

$$\mathcal{I}_N^d(S) = \mathcal{I}_{div}(S) + \mathcal{I}_{fin}(S) \tag{4.3.48}$$

$$= \sum_{i\in S} b_i(S) \int \frac{d^dk}{i\pi^{d/2}} \frac{(q_i^2 - m_i^2 + i\lambda)}{\prod_{j\in S}(q_j^2 - m_j^2 + i\lambda)} + \int \frac{d^dk}{i\pi^{d/2}} \frac{1 - \sum_{i\in S} b_i(S)(q_i^2 - m_i^2 + i\lambda)}{\prod_{j\in S}(q_j^2 - m_j^2 + i\lambda)}, \tag{4.3.49}$$

where the b_i are at this stage not fixed. Clearly $I_{div}(S) = \sum_i b_i \mathcal{I}_{N-1}^d(S\backslash\{i\})$. Let us examine the second integral (which we will show is finite), and introduce N Feynman parameters x_i as explained in Section 4.1.1. As in (4.1.18), we shift

$$k = k' - \sum_{i\in S} x_i r_i \tag{4.3.50}$$

to gain a quadratic form in the denominator

$$\prod_{j\in S}(q_j^2 - m_j^2 + i\lambda) = k'^2 + \frac{1}{2} x \cdot \mathcal{S} \cdot x \tag{4.3.51}$$

Now let us write out the numerator of the finite integral in two steps. First, using

$$\left(\sum_{i\in S} x_i \Delta_{ji}\right)^2 = -\frac{1}{2} x \cdot \mathcal{S} \cdot x + \sum_{i\in S} x_i \mathcal{S}_{ij} + m_j^2, \tag{4.3.52}$$

we perform the shift (4.3.50) on a single term in i:

$$q_i^2 - m_i^2 = k'^2 - \frac{1}{2} x \cdot \mathcal{S} \cdot x + \sum_{j\in S} x_j \left(\mathcal{S}_{ij} + 2k'\Delta_{ij}\right) \tag{4.3.53}$$

Now let us write out the full numerator $\mathcal{N}$:

$$\mathcal{N} = 1 - \sum_{i\in S} b_i(S)(q_i^2 - m_i^2 + i\lambda) \tag{4.3.54}$$

$$= \sum_{j\in S} x_j - \sum_{i\in S} b_i(S)(q_i^2 - m_i^2 + i\lambda) \tag{4.3.55}$$

$$= -\left(k'^2 - \frac{1}{2} x \cdot \mathcal{S} \cdot x\right) \sum_{i\in S} b_i(S) + \sum_{j\in S} x_j \left(1 - \sum_{i\in S} b_i(S) \left(\mathcal{S}_{ij} + 2k'\Delta_{ij}\right)\right). \tag{4.3.56}$$

Here, the k'-dependent term is an odd function being integrated over a symmetric region, and so will give zero, so the whole second term will give zero if the following condition is satisfied for all $j \in S$:

$$\sum_{i\in S} b_i(S)\mathcal{S}_{ij} = 1. \tag{4.3.57}$$

Let us take this to be true, and define

$$\mathcal{B}(S) = \sum_{i \in S} b_i(S). \tag{4.3.58}$$

The relation

$$\mathcal{B} = (-1)^{N+1} \frac{\det \mathcal{G}}{\det \mathcal{S}} \tag{4.3.59}$$

is shown in [74], and will be important in Section 5.1.2.

Then we have (dropping the primes on k):

$$\mathcal{I}_{fin}(S) = -\mathcal{B}(S)\Gamma(N) \int \frac{d^{\not d}k}{i\pi^{\not d/2}} \int_0^1 \prod_{i \in S} (dx_i) \delta\left(\sum_{i \in S} x_i - 1\right) \frac{k^2 - \frac{1}{2} x \cdot \mathcal{S} \cdot x}{\left(k^2 + \frac{1}{2} x \cdot \mathcal{S} \cdot x + i\lambda\right)^N}. \tag{4.3.60}$$

We can now follow through the derivation from (4.1.25) to (4.1.35), with the additional powers of the loop momentum having had as yet no impact:

$$\mathcal{I}_{fin}(S) = -\mathcal{B}(S) \int_0^1 \prod_{i=1}^N (dx_i) \delta\left(\sum_{i=1}^n x_i - 1\right) \Gamma(N) \frac{2(-1)^N}{\Gamma(\frac{\not d}{2})} \int_0^\infty dk_r \frac{-k_r^{\not d+1} + (-\frac{1}{2} x \cdot \mathcal{S} \cdot x) k_r^{\not d-1}}{\left[k_r^2 - \frac{1}{2} x \cdot \mathcal{S} \cdot x - i\lambda\right]^N}, \tag{4.3.61}$$

and on doing the same substitution $K = \frac{k_r^2}{-\frac{1}{2} x \cdot \mathcal{S} \cdot x - i\lambda}$, we have:

$$\begin{aligned}
\mathcal{I}_{fin}(S) = &- \mathcal{B}(S) \int_0^1 \prod_{i=1}^N (dx_i) \delta\left(\sum_{i=1}^N x_i - 1\right) \Gamma(N) \frac{2(-1)^N}{\Gamma(\frac{\not d}{2})} \frac{1}{2} \left(-\frac{1}{2} x \cdot \mathcal{S} \cdot x - i\lambda\right)^{-N+1} \\
&\times \int_0^\infty dK \frac{-(-\frac{1}{2} x \cdot \mathcal{S} \cdot x)^{\frac{\not d}{2}} K^{\frac{\not d}{2}} + (-\frac{1}{2} x \cdot \mathcal{S} \cdot x)(-\frac{1}{2} x \cdot \mathcal{S} \cdot x)^{\frac{\not d-2}{2}} K^{\frac{\not d-2}{2}}}{[K+1]^N}
\end{aligned} \tag{4.3.62}$$

$$\begin{aligned}
= &- \mathcal{B}(S) \int_0^1 \prod_{i=1}^N (dx_i) \delta\left(\sum_{i=1}^N x_i - 1\right) \Gamma(N) \frac{2(-1)^N}{\Gamma(\frac{\not d}{2})} \frac{1}{2} \left(-\frac{1}{2} x \cdot \mathcal{S} \cdot x - i\lambda\right)^{\frac{\not d}{2}-N+1} \\
&\times \left(-\frac{\Gamma\left(\frac{\not d}{2}+1\right) \Gamma\left(N - \frac{\not d}{2} - 1\right)}{\Gamma(N)} + \frac{\Gamma\left(\frac{\not d}{2}\right) \Gamma\left(N - \frac{\not d}{2}\right)}{\Gamma(N)} \right)
\end{aligned} \tag{4.3.63}$$

$$\begin{aligned}
= &- \mathcal{B}(S) \int_0^1 \prod_{i=1}^N (dx_i) \delta\left(\sum_{i=1}^N x_i - 1\right) (-1)^N \left(-\frac{1}{2} x \cdot \mathcal{S} \cdot x - i\lambda\right)^{\frac{\not d}{2}-N+1} \\
&\times \Gamma\left(N - \frac{\not d}{2} - 1\right) (N - \not d - 1),
\end{aligned} \tag{4.3.64}$$

where we have used the property of the Γ function (B.3.15). Now let us compare this equation with our expression for the general case after momentum integra-

tion (4.1.39), written in $\not{d}+2$ dimensions

$$\mathcal{I}_N^{\not{d}+2}(S) = (-1)^N \Gamma\left(N - \frac{\not{d}}{2} - 1\right) \int_0^1 \prod_{i=1}^N (dx_i)\delta\left(\sum_{i=1}^N x_i - 1\right)\left(-\frac{1}{2}x\cdot\mathcal{S}\cdot x - i\lambda\right)^{\frac{\not{d}}{2}+1-N}. \tag{4.3.65}$$

We see that the part we want to be finite can be expressed as a higher dimensional integral, and so does not have an IR divergence[4]:

$$\mathcal{I}_{fin}(S) = -\mathcal{B}(S)(N - \not{d} - 1)\mathcal{I}_N^{\not{d}+2}(S). \tag{4.3.66}$$

This means we have indeed separated the divergent part off into a set of $(N-1)$-point integrals, leaving a $(\not{d}+2)$-dimensional N-point integral:

$$\mathcal{I}_N^{\not{d}}(S) = \sum_i b_i I_{N-1}^{\not{d}}(S\backslash\{i\}) - \mathcal{B}(S)(N - \not{d} - 1)\mathcal{I}_N^{\not{d}+2}(S). \tag{4.3.67}$$

This process can of course be iterated from high N, and indeed there is an additional convenience that for $N \geq 6$, $\mathcal{B} = 0$ (as there can only be four independent momenta in 4 dimensions, so $\det \mathcal{G} = 0$). For $N = 5$, we also have $\mathcal{I}_{fin} \to 0$, because $(N - \not{d} - 1) = 2\epsilon$, and $\mathcal{I}_5^{\not{d}+2}(S)$ is finite, so the whole term is $\mathcal{O}(\epsilon)$ and can be neglected for our purposes.

4.3.1 Tensor Reduction

Reduction of tensor integrals proceeds in a similar way, shown in [65], with N-leg tensor integrals of rank r being reduced to possibly-divergent $(N-1)$-leg tensor integrals of rank $(r-1)$, and an IR finite part. Although our formalism avoids inverse Gram determinants where possible, they are inevitable in relations which reduce from tensor integrals with $N \leq 4$. It is for this reason that `golem95` does not automatically reduce all integrals as far as scalars.

Example: Rank 1 Triangle Integral

To illustrate the appearance of Gram determinants in reduction from tensor integrals, let us take the example of the rank 1 triangle integral. Let us break the shift

[4] This can be shown by *IR power counting*: see for example Chapter 2 of [75].

invariance by taking $r_3 = 0$, and so express the two independent external momenta as $r_1 = p_1$ and $r_2 = p_1 + p_2$. We only have two form factors $A_1^{3,1}$ and $A_2^{3,1}$ (see Section 4.2):

$$\mathcal{I}_3^{d,\mu}(a=3) = \int \frac{d^d k}{i\pi^{\frac{d}{2}}} \frac{k^\mu}{((k+r_1)^2 - m_1^2)((k+r_2)^2 - m_2^2)(k^2 - m_3^2)} \equiv A_1^{3,1} r_1^\mu + A_2^{3,1} r_2^\mu. \tag{4.3.68}$$

Now we can multiply in $r_{1,\mu}$ and use $r_1 \cdot k = \frac{1}{2}\left([(k-r_1)^2 - m_1^2] - [k^2 - m_3^2] - r_1^2 + m_1^2 - m_3^2\right)$:

$$A_1^{3,1} r_1 \cdot r_1 + A_2^{3,1} r_1 \cdot r_2 = \int \frac{d^d k}{i\pi^{\frac{d}{2}}} \frac{k^\mu}{((k+r_1)^2 - m_1^2)((k+r_2)^2 - m_2^2)(k^2 - m_3^2)} \tag{4.3.69}$$

$$\begin{aligned} =& \frac{1}{2} \int \frac{d^d k}{i\pi^{\frac{d}{2}}} \frac{1}{((k+r_2)^2 - m_2^2)(k^2 - m_3^2)} \\ & - \frac{1}{2} \int \frac{d^d k}{i\pi^{\frac{d}{2}}} \frac{1}{((k+r_1)^2 - m_1^2)((k+r_2)^2 - m_2^2)} \\ & - \frac{1}{2} \int \frac{d^d k}{i\pi^{\frac{d}{2}}} \frac{r_1^2 - m_1^2 + m_3^2}{((k+r_1)^2 - m_1^2)((k+r_2)^2 - m_2^2)(k^2 - m_3^2)} \end{aligned} \tag{4.3.70}$$

$$= \frac{1}{2}\mathcal{I}_2^d(S\backslash\{1\}) - \frac{1}{2}\mathcal{I}_2^d(S\backslash\{3\}) - \frac{1}{2}(r_1^2 - m_1^2 + m_3^2)\mathcal{I}_3^d. \tag{4.3.71}$$

When we do the same for r_2, we have:

$$\begin{pmatrix} r_1 \cdot r_1 & r_1 \cdot r_2 \\ r_2 \cdot r_1 & r_2 \cdot r_2 \end{pmatrix} \begin{pmatrix} A_1^{3,1} \\ A_2^{3,1} \end{pmatrix} = \begin{pmatrix} \frac{1}{2}\mathcal{I}_2^d(S\backslash\{1\}) - \frac{1}{2}\mathcal{I}_2^d(S\backslash\{3\}) - \frac{1}{2}(r_1^2 - m_1^2 + m_3^2)\mathcal{I}_3^d \\ \frac{1}{2}\mathcal{I}_2^d(S\backslash\{2\}) - \frac{1}{2}\mathcal{I}_2^d(S\backslash\{3\}) - \frac{1}{2}(r_2^2 - m_2^2 + m_3^2)\mathcal{I}_3^d \end{pmatrix}, \tag{4.3.72}$$

we see that the Gram matrix $\mathcal{G}^{(3)}$ has appeared on the left-hand side, and so to find $A_1^{3,1}$ and $A_2^{3,1}$, we will have to invert it, which involves multiplication by $\frac{1}{\det \mathcal{G}^{(3)}}$.

Tensor Integral Basis

In `golem95`, we take as our primary basis[5] the set of integrals to which all relevant integrals can be reduced without introducing inverse Gram determinants, which is

[5] The endpoints of the first set of reductions, rather than a mathematical basis.

the scalar integrals $\mathcal{I}_1^{\mathcal{d}}$, $\mathcal{I}_2^{\mathcal{d}}$, $\mathcal{I}_2^{\mathcal{d}+2}$, $\mathcal{I}_3^{\mathcal{d}}$, $\mathcal{I}_3^{\mathcal{d}+2}$, $\mathcal{I}_4^{\mathcal{d}+2}$, $\mathcal{I}_4^{\mathcal{d}+4}$, and

$$\mathcal{I}_2^{\mathcal{d}}(j_1,\ldots,j_r) =\Gamma\left(2-\frac{\mathcal{d}}{2}\right)\int_0^1\prod_{i=1}^{3}dz_i\,\delta(1-\sum_{l=1}^{2}z_l)\,\frac{z_{j_1}\ldots z_{j_r}}{(-\frac{1}{2}\,z\cdot\mathcal{S}\cdot z-i\lambda)^{2-\mathcal{d}/2}} \tag{4.3.73}$$

$$\mathcal{I}_3^{\mathcal{d}}(j_1,\ldots,j_r) =-\,\Gamma\left(3-\frac{\mathcal{d}}{2}\right)\int_0^1\prod_{i=1}^{3}dz_i\,\delta(1-\sum_{l=1}^{3}z_l)\,\frac{z_{j_1}\ldots z_{j_r}}{(-\frac{1}{2}\,z\cdot\mathcal{S}\cdot z-i\lambda)^{3-\mathcal{d}/2}} \tag{4.3.74}$$

$$\mathcal{I}_3^{\mathcal{d}+2}(j_1) =-\,\Gamma\left(2-\frac{\mathcal{d}}{2}\right)\int_0^1\prod_{i=1}^{3}dz_i\,\delta(1-\sum_{l=1}^{3}z_l)\,\frac{z_{j_1}}{(-\frac{1}{2}\,z\cdot\mathcal{S}\cdot z-i\lambda)^{2-\mathcal{d}/2}} \tag{4.3.75}$$

$$\mathcal{I}_4^{\mathcal{d}+2}(j_1,\ldots,j_r) =\Gamma\left(3-\frac{\mathcal{d}}{2}\right)\int_0^1\prod_{i=1}^{4}dz_i\,\delta(1-\sum_{l=1}^{4}z_l)\,\frac{z_{j_1}\ldots z_{j_r}}{(-\frac{1}{2}\,z\cdot\mathcal{S}\cdot z-i\lambda)^{3-\mathcal{d}/2}} \tag{4.3.76}$$

$$\mathcal{I}_4^{\mathcal{d}+4}(j_1) =\Gamma\left(2-\frac{\mathcal{d}}{2}\right)\int_0^1\prod_{i=1}^{4}dz_i\,\delta(1-\sum_{l=1}^{4}z_l)\,\frac{z_{j_1}}{(-\frac{1}{2}\,z\cdot\mathcal{S}\cdot z-i\lambda)^{2-\mathcal{d}/2}}\ , \tag{4.3.77}$$

where the bubbles can be up to rank 2 and the triangles and boxes up to rank 3. Of this set of integrals, the n-dimensional triangles can be IR divergent[6] (see Section 4.4 for the IR divergence conditions), and the one- and two-point functions, $\mathcal{I}_3^{\mathcal{d}+2}$, $\mathcal{I}_3^{\mathcal{d}+2}$, $\mathcal{I}_4^{\mathcal{d}+4}$ and $\mathcal{I}_4^{\mathcal{d}+4}(j_1)$ are UV divergent[7], but otherwise the integrals are finite. This gives a convenient separation of the divergences. It is shown in Section 5 of [65] that, in the Feynman gauge[8] only this set of basis functions is required for all the form factors ((4.2.41) to (4.2.45), and also $N \geq 5$).

For the case with massive internal lines, we additionally use analytic expressions for the scalar integral $\mathcal{I}_4^{\mathcal{d}}$, for the pragmatic reason that the expressions were already present in the literature: we have our own implementation of the divergent boxes from [78], and call the finite boxes from an external programme (OneLOop [79] by

[6]Two similar methods, [76] and [77], exist to separate the IR divergences into the triangles.

[7]These UV divergences are, in practical calculations, cancelled by each other or by the counterterms.

[8]The restriction is that the maximum r is equal to N, so any cases in which the Feynman rules allow $r > N$, such as models with particles of spin 2, are also excluded.

default, also LoopTools [80] is possible).

4.3.2 Reduction to Scalar Integrals and Numerical Rescue System

Once we have our integrals written out in terms of the primary basis (4.3.73)-(4.3.77), we can consider the additional reduction steps of Section 5 of [65], for example:

$$\mathcal{I}_3^n(l;S) = \frac{b_l}{\mathcal{B}}\left[\mathcal{I}_3^n(S) - \sum_{j\in S} b_j \mathcal{I}_2^n(S\backslash\{j\})\right] + \sum_{j\in S} \mathcal{S}_{lj}^{-1}\mathcal{I}_2^n(S\backslash\{j\}), \tag{4.3.78}$$

which can reduce our integrals further to a set of scalars, at the cost of introducing inverse Gram determinants. Where possible, the integral terms are grouped in such a way that those sums of integrals which go to zero for small Gram determinant are performed before the Gram determinant is divided out, which reduces the numerical instability for moderately small Gram determinant. It is for this reason that the square bracket of (4.3.78) is important.

The crucial aspect of the `golem95` method is that we test before each step of these secondary reductions whether it would result in a small inverse Gram determinant as a prefactor, and if it would, do not perform that step. Because $\mathcal{B}$ is a dimensionful parameter, we use the parameter $\mathcal{B}' \equiv \mathcal{B}\mathcal{S}_{max}$, where $\mathcal{S}_{max}$ is the largest entry of the $\mathcal{S}$-matrix, to define the boundary value. We use $\mathcal{B}' = 0.005$ as a default.

At the end of our reduction we will have a set of scalar integrals which are calculated using analytic expressions (using expressions from [78, 81], or from the programmes [79, 80][9], although using the methods of Chapter 5 for difficult limits), and possibly some tensor integrals, which we will calculate numerically[10].

[9] The user may choose at the compilation stage.

[10] There is an alternative technique to deal with the case of small Gram determinant [33,77,82,83], which is to use as an approximation the expansion around $\det \mathcal{G} = 0$. This can be a very efficient method in that region. In `golem95`, we prefer exact methods to approximate ones, as the formulae concerned remain valid on both sides of the value at which the switch is made, making the system more robust for different choices of this value.

An efficient formulation[11] in one dimension, with the other integrations being performed analytically, has been developed for the numerical evaluations of tensor integrals. It is described in Appendix A.2 of [55].

We can illustrate the utility of this rescue system with an example. In Figure 4.5, a plot is given showing a limit with $\mathcal{B}' \to 0$ for the modulus of the $(d+2)$-dimensional four-point integral with three Feynman parameters in the numerator (z_1, z_2, z_2), for the case with two external masses and no internal masses. It demonstrates that without the rescue system, the integral becomes unstable at approximately $\mathcal{B}' = 0.003$. We also note that there is no discontinuity visible at the switch point.

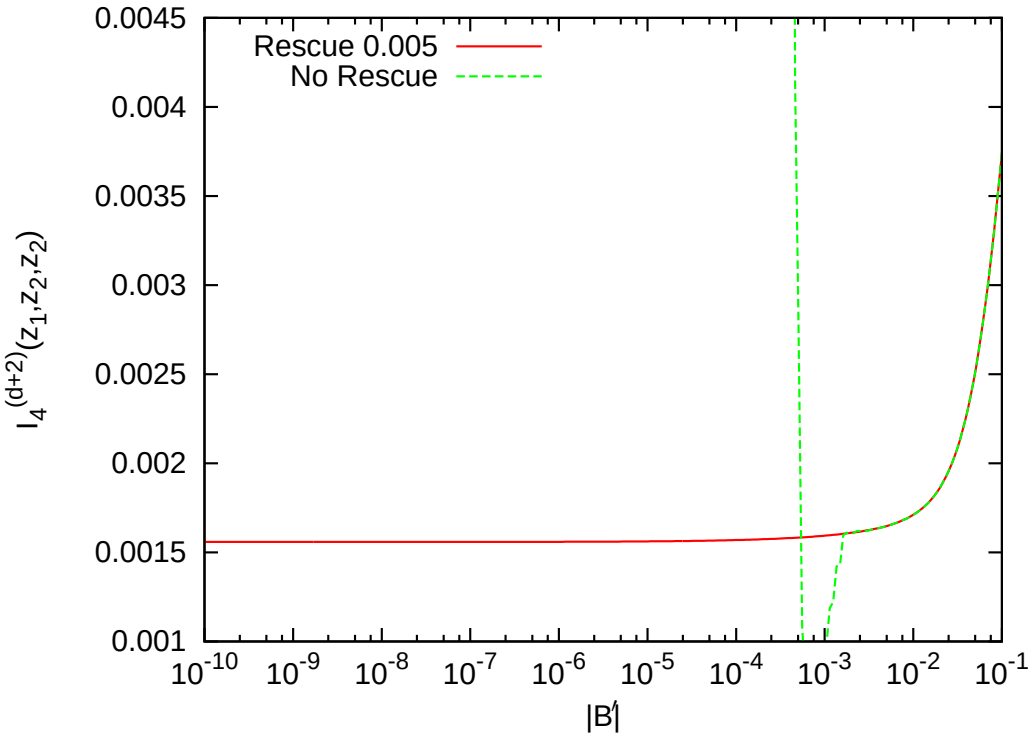

Figure 4.5: The behaviour of the tensor integral $I_4^{(d+2)}(z_1, z_2, z_2)$ as $|\mathcal{B}'| \to 0$, with the numerical rescue system for $|\mathcal{B}'| < 0.005$ (red, solid line), and without it (green, dashed line).

At the time of writing, this method has been implemented for all three- and four-point tensor integrals without internal masses, with the exception of the four-

[11] A deterministic, adaptive Gauss-Kronrod [84] method is used.

point integral with four external masses, and also for the triangle with two external masses and one internal mass (including the complex-mass case).

4.4 Landau Conditions

In [72, 78, 85] the Landau conditions are defined and explored (see Section 6.2 for more details). These are the necessary conditions for a divergence to occur in the one-loop integral. They are:

$$x \cdot \mathcal{S} \cdot x = 0, \tag{4.4.79}$$

and for each x_i, either

$$x_i = 0 \tag{4.4.80}$$

or

$$\frac{\partial (x \cdot \mathcal{S} \cdot x)}{\partial x_i} = 0. \tag{4.4.81}$$

There are two classes of solution to these equations:

Infrared divergences

The equations can be solved with fixed (relative) values for some or all internal masses m_i (at least one zero) and external virtualities s_i, with any unfixed quantities, including both s_{ij} in the case of boxes, varying freely. These are the configurations which give the soft and collinear IR divergences[12] for loop integrals, which cancel against the IR divergences in the real radiation part to give a finite physical answer.

In [44], it is shown that we can extract necessary conditions for (4.4.81) to be satisfied, remembering that the conditions can wrap around the top, bottom and sides of the matrix:

Soft Divergence[13]: $\mathcal{S}_{i+1,i+1} = \mathcal{S}_{i+1,i+2} = \mathcal{S}_{i+1,i} = 0$

$$\text{e.g. } \mathcal{S} = \begin{pmatrix} \dots & 0 & \dots & \dots \\ 0 & 0 & 0 & \dots \\ \dots & 0 & \dots & \dots \\ \dots & \dots & \dots & \dots \end{pmatrix}$$

[12] Some authors use *infrared divergences* to refer only to what we call *soft divergences*, and refer to (our) *collinear divergences* as *mass singularities*.

[13] Kinoshita's λ singularity

Collinear Divergence[14]: $\mathcal{S}_{i+1,i+1} = \mathcal{S}_{i+1,i+2} = \mathcal{S}_{i+1,i} = 0$

$$\text{e.g. } \mathcal{S} = \begin{pmatrix} \dots & \dots & \dots & \dots \\ \dots & 0 & 0 & \dots \\ \dots & 0 & 0 & \dots \\ \dots & \dots & \dots & \dots \end{pmatrix} .$$

Threshold divergences

These are solutions of the Landau conditions which occur for specific values of the invariants of the problem, and so arise only at individual points in phase space. They are explored in Section 6.2.

[14]Kinoshita's m singularity

Chapter 5

Limits in Integration Libraries

The latest public version of `golem95` [86] had all the divergent cases and all massless cases for the three- and four-point scalar integrals implemented, but called the finite massive cases from an external program (OneLOop [79] by default, or LoopTools [80] if the user wishes).

An important advantage of `golem95` over its competitors is its numerical rescue system, which greatly reduces the numerical instability of its integrals. In the previous chapter, we described the rescue system which replaces tensor reduction, in cases where it would be unstable, by numerical integration of the tensor integrals. The computational cost of these numerical integrations is justified by the gain in stability, which can reduce the number of points that a phase-space integrator requires to produce a given accuracy.

We would also like to have a rescue system available for the scalar integrals because, as we demonstrate in this chapter, there are cases in which the analytic result is not stable. For this reason, we decided to implement our own finite three-point function[1] in `golem95`, and to examine the unstable limits that occur[2]. The discussion of one such limit, the Landau singularity, is postponed until Chapter 6, as the technique used (implementation of complex masses) is separate from those of this chapter.

In this chapter, we begin by giving the derivation of the analytic formula for the

[1] And also the four-point integrals, which will be performed for a future version.

[2] Either clearly from the form of the expressions, or those which arise during testing.

scalar three-point function [65, 81, 87], and continue by giving the limits which are examined. All of these limits of scalar integrals have been implemented in `golem95`, although that of Section 5.2.3, as explained in that section, has not been optimised. We follow this with a discussion of the scalar two-point function, and those limits for which it requires a reexpression.

5.1 Scalar Three-point Function

Let us first study the finite scalar three-point function: the function where the IR divergence is not present, as none of the IR conditions in Section 4.4 apply. We can take $\epsilon \to 0$, so the integral is $\mathcal{I}_3^4$, and the power of the integrand $\frac{d}{2} - N \to -1$:

$$\mathcal{I}_3^4 = -\int_0^1 \prod_{i=1}^{3} dz_i \delta\left(1 - \sum_i^3 z_i\right) \left(-\frac{1}{2} z^T \cdot \mathcal{S} \cdot z - i\lambda\right)^{-1} \tag{5.1.1}$$

and let us eliminate one z, say z_3, using $z_3 = 1 - \sum_{i\neq 3} z_i$, and break the shift-invariance by taking $r_3 = 0$:

$$\begin{aligned} z^T \cdot \mathcal{S} \cdot z = &\sum_{i,j\neq 3} z_i \mathcal{S}_{ij} z_j + \sum_{i\neq 3} z_i \mathcal{S}_{i3} \left(1 - \sum_{j\neq 3} z_j\right) + \sum_{j\neq 3} \left(1 - \sum_{i\neq 3} z_i\right) \mathcal{S}_{3j} z_j \\ &+ \left(1 - \sum_{i\neq 3} z_i\right) \mathcal{S}_{33} \left(1 - \sum_{j\neq 3} z_j\right) \qquad (5.1.2) \\ = &\sum_{i,j\neq 3} z_i z_j \left(\mathcal{S}_{ij} - \mathcal{S}_{i3} - \mathcal{S}_{3j} + \mathcal{S}_{33}\right) + 2 \sum_{i\neq 3} z_i \left(\mathcal{S}_{i3} - \mathcal{S}_{33}\right) + \mathcal{S}_{33}. \qquad (5.1.3) \end{aligned}$$

Now if we multiply out the sums and substitute $z_1 = 1 - x$ and $z_2 = y$ we have

$$\begin{aligned} z^T \cdot \mathcal{S} \cdot z = &x^2(\mathcal{S}_{11} - 2\mathcal{S}_{13} + \mathcal{S}_{33}) + y^2(\mathcal{S}_{22} - 2\mathcal{S}_{23} + \mathcal{S}_{33}) \\ &+ xy(-2)(\mathcal{S}_{12} - \mathcal{S}_{13} - \mathcal{S}_{32} + \mathcal{S}_{33}) \\ &+ x(-2)(\mathcal{S}_{11} - \mathcal{S}_{13}) + y(-2)(\mathcal{S}_{13} - \mathcal{S}_{12}) + \mathcal{S}_{11}. \end{aligned} \tag{5.1.4}$$

So, remembering the factor of $-\frac{1}{2}$, we can write our integral as:

$$\mathcal{I}_3^4 = -\int_0^1 dx \int_0^x dy \left(ax^2 + by^2 + cxy + dx + ey + f - i\lambda\right)^{-1}, \tag{5.1.5}$$

with (remembering that $\mathcal{S}$ is symmetric)

$$\begin{aligned} a =& -\frac{1}{2}(\mathcal{S}_{11} - 2\mathcal{S}_{13} + \mathcal{S}_{33}) = s_1 & b =& -\frac{1}{2}(\mathcal{S}_{22} - 2\mathcal{S}_{23} + \mathcal{S}_{33}) = s_3 \\ c =& \mathcal{S}_{12} - \mathcal{S}_{13} - \mathcal{S}_{23} + \mathcal{S}_{33} = s_2 - s_1 - s_3 & d =& \mathcal{S}_{11} - \mathcal{S}_{13} = -s_1 - m_1^2 + m_3^2 \\ e =& \mathcal{S}_{13} - \mathcal{S}_{12} = s_1 - s_2 - m_3^2 + m_2^2 & f =& -\frac{1}{2}\mathcal{S}_{11} = m_1^2. \end{aligned} \tag{5.1.6}$$

We can write out $\det \mathcal{S}$ as:

$$\det \mathcal{S} = \mathcal{S}_{11}(\mathcal{S}_{22}\mathcal{S}_{33} - \mathcal{S}_{23}^2) + \mathcal{S}_{12}(\mathcal{S}_{23}\mathcal{S}_{13} - \mathcal{S}_{12}\mathcal{S}_{33}) + \mathcal{S}_{13}(\mathcal{S}_{12}\mathcal{S}_{23} - \mathcal{S}_{22}\mathcal{S}_{13}) \tag{5.1.7}$$

$$= 2bd^2 - 2cde + 2ae^2 - 8abf + 2c^2 f. \tag{5.1.8}$$

There is also a very instructive form in terms of the kinematic parameters, which shows clearly the invariance under cyclic permutations:

$$\begin{aligned} \det \mathcal{S} =& 2[s_1 s_2 s_3 + s_1^2 m_2^2 + s_2^2 m_3^2 + s_3^2 m_1^2 \\ & - s_1 s_2 (m_2^2 + m_3^2) - s_1 s_3 (m_1^2 + m_2^2) - s_2 s_3 (m_1^2 + m_3^2) \\ & + s_1 (m_1^2 - m_2^2)(m_3^2 - m_2^2) + s_2 (m_2^2 - m_3^2)(m_1^2 - m_3^2) + s_3 (m_3^2 - m_1^2)(m_2^2 - m_1^2)]. \end{aligned} \tag{5.1.9}$$

5.1.1 Gram Matrix

Because we have broken the shift invariance by singling out the third row and column, the Gram matrix (see Section 4.1.5) here is $\mathcal{G}^{(3)}_{ij} = 2r_i \cdot r_j$, so its determinant in this case is

$$\det \mathcal{G}^{(3)} = 4((r_1 \cdot r_1)(r_2 \cdot r_2) - (r_1 \cdot r_2)^2) \tag{5.1.10}$$

$$= (\mathcal{S}_{11} - 2\mathcal{S}_{13} + \mathcal{S}_{33})(\mathcal{S}_{22} - 2\mathcal{S}_{23} + \mathcal{S}_{33}) - (\mathcal{S}_{12} - \mathcal{S}_{13} - \mathcal{S}_{23} + \mathcal{S}_{33})^2 \tag{5.1.11}$$

$$= -(c^2 - 4ab), \tag{5.1.12}$$

and in terms of kinematic parameters:

$$\det \mathcal{G}^{(3)}_{ij} = -(s_1^2 + s_2^2 + s_3^2 - 2s_1 s_2 - 2s_1 s_3 - 2s_2 s_3) \tag{5.1.13}$$

$$= -\kappa(s_1, s_2, s_3), \tag{5.1.14}$$

with $\kappa(x, y, z)$ again the Källén function [71]. From this form, we can see that the condition for $\det \mathcal{G}$ to be zero is that one $s_i = 0$ and the other two are equal (this of course includes the trivial case where all three s_i are zero).

5.1.2 The Second Integration

Now we wish to simplify and perform the x-integration, so we aim to make the integrand the reciprocal of a linear expression in x. We start by shifting $y \to y - \zeta x$, and choosing ζ such that[3]:

$$b\zeta^2 + c\zeta + a = 0, \tag{5.1.15}$$

so that

$$\mathcal{I}_3^4 = -\int_0^1 dx \int_{-\zeta x}^{x(1-\zeta)} dy \left(x^2(b\zeta^2 + c\zeta + a) + by^2 + xy(2b\zeta + c) + x(d + e\zeta) + ey + f - i\lambda\right)^{-1}. \tag{5.1.16}$$

Now we split the y-integral at zero:

$$\int_0^1 dx \int_{-\zeta x}^{x(1-\zeta)} dy = \int_0^1 dx \int_0^{x(1-\zeta)} dy - \int_0^1 dx \int_0^{-\zeta x} dy, \tag{5.1.17}$$

and reverse the order of the integrations:

$$\int_0^1 dx \int_{-\zeta x}^{x(1-\zeta)} dy = \int_0^{1-\zeta} dy \int_{\frac{y}{1-\zeta}}^1 dx - \int_0^{-\zeta} dy \int_{\frac{y}{-\zeta}}^1 dx, \tag{5.1.18}$$

giving

$$\begin{aligned}\mathcal{I}_3^4 = &-\int_0^{1-\zeta} dy \int_{\frac{y}{1-\zeta}}^1 dx \left(x(y(2b\zeta + c) + d + e\zeta) + by^2 + ey + f - i\lambda\right)^{-1} \\ &+ \int_0^{-\zeta} dy \int_{\frac{y}{-\zeta}}^1 dx \left(x(y(2b\zeta + c) + d + e\zeta) + by^2 + ey + f - i\lambda\right)^{-1},\end{aligned} \tag{5.1.19}$$

and as required the x-integral is standard, as the overall bracket is linear in x, and so introducing a new symbol for the coefficient of x in the above integrals,

$$\mathcal{N} = y(2b\zeta + c) + d + e\zeta, \tag{5.1.20}$$

we can use

$$\int_{x_0}^{x_1} dx \frac{1}{Ax + B} = \frac{1}{A}\left(\log\left(Ax_1 + B\right) - \log\left(Ax_0 + B\right)\right) \tag{5.1.21}$$

[3]This equation will in general have two solutions, and we will use the freedom to choose later.

and combine the two terms with logarithms of the same argument:

$$\begin{aligned}\mathcal{I} = &-\int_{-\zeta}^{1-\zeta} dy \frac{1}{\mathcal{N}} \log\left(\mathcal{N} + by^2 + ey + f - i\lambda\right) \\ &+ \int_{0}^{1-\zeta} dy \frac{1}{\mathcal{N}} \log\left(\frac{\mathcal{N}y}{1-\zeta} + by^2 + ey + f - i\lambda\right) \\ &- \int_{0}^{-\zeta} dy \frac{1}{\mathcal{N}} \log\left(\frac{\mathcal{N}y}{-\zeta} + by^2 + ey + f - i\lambda\right).\end{aligned} \tag{5.1.22}$$

For $\mathcal{N} = 0$, we have a pole. Let us call the value of y at which this occurs

$$y_0 = -\frac{d + e\zeta}{2b\zeta + c}, \tag{5.1.23}$$

and let us then use the (trivial) fact that

$$\begin{aligned}-\int_{-\zeta}^{1-\zeta} dy \frac{-1}{\mathcal{N}} \log\left(by_0^2 + ey_0 + f - i\lambda\right) + \int_{0}^{1-\zeta} dy \frac{-1}{\mathcal{N}} \log\left(by_0^2 + ey_0 + f - i\lambda\right) \\ - \int_{0}^{-\zeta} dy \frac{-1}{\mathcal{N}} \log\left(by_0^2 + ey_0 + f - i\lambda\right) = 0\end{aligned} \tag{5.1.24}$$

to subtract the pole. For convenience, we name the constant $\mathcal{C} = by_0^2 + ey_0 + f - i\lambda$

$$\begin{aligned}\mathcal{I} = &-\int_{-\zeta}^{1-\zeta} dy \frac{1}{\mathcal{N}} \left(\log\left(\mathcal{N} + by^2 + ey + f - i\lambda\right) - \log\left(\mathcal{C}\right)\right) \\ &+ \int_{0}^{1-\zeta} dy \frac{1}{\mathcal{N}} \left(\log\left(\frac{\mathcal{N}y}{1-\zeta} + by^2 + ey + f - i\lambda\right) - \log\left(\mathcal{C}\right)\right) \\ &- \int_{0}^{-\zeta} dy \frac{1}{\mathcal{N}} \left(\log\left(\frac{\mathcal{N}y}{-\zeta} + by^2 + ey + f - i\lambda\right) - \log\left(\mathcal{C}\right)\right)\end{aligned} \tag{5.1.25}$$

Note that the arguments of the y-dependent logarithms differ from the quadratic $by^2 + ey + f - i\lambda$ only by multiples of $\mathcal{N}$, and so $\mathcal{C}$ will be equivalent to the value of the arguments of all of the y-dependent logarithms taken at y_0.

Let us investigate $\mathcal{C} = by_0^2 + ey_0 + f - i\lambda$, remembering the value of y_0 (5.1.23), and the quadratic in ζ (5.1.15). First let us use the definition of ζ to write the denominator as:

$$(2b\zeta + c)(2b\zeta + c) = 4b(b\zeta^2 + c\zeta) + c^2 = -4ba + c^2 = -\det \mathcal{G}, \tag{5.1.26}$$

then[4]

$$\mathcal{C} = -\frac{b(d+e\zeta)(d+e\zeta) - e(d+e\zeta)(2b\zeta+c) + f(c^2-4ab)}{\det\mathcal{G}} - i\lambda \tag{5.1.27}$$

$$= -\frac{bd^2 - cde + e^2a + c^2f - 4abf}{\det\mathcal{G}} - i\lambda \tag{5.1.28}$$

$$= -\frac{1}{2}\frac{\det\mathcal{S}}{\det\mathcal{G}} \tag{5.1.29}$$

$$= -\frac{1}{2\mathcal{B}} \tag{5.1.30}$$

where $\mathcal{B}$ is as defined in Section 4.3. It is important to note that the ζ-dependence has cancelled, as later we will use both possible ζ values (i.e. two distinct values for which $\mathcal{N}$) is zero, and this will not affect $\mathcal{C}$.

Now let us perform three different transformations on the three integrals, so as to have each one being an integral between 0 and 1. Specifically, we write $y = z - \zeta$ for the first integral, $y = (1-\zeta)z$ for the second, and $y = -\zeta z$ for the third. Many terms cancel, particularly if we remember $b\zeta^2 + c\zeta + a = 0$:

$$\begin{aligned}\mathcal{I} = &-\int_0^1 dz \frac{1}{(2b\zeta+c)z + (c+e)\zeta + 2a + d}\left(\log(bz^2 + (c+e)z + a + d + f - i\lambda) - \log(\mathcal{C})\right)\\ &+\int_0^1 dz \frac{(1-\zeta)}{(1-\zeta)(2b\zeta+c)z + d + e\zeta}\left(\log((a+b+c)z^2 + (d+e)z + f - i\lambda) - \log(\mathcal{C})\right)\\ &+\int_0^1 dz \frac{\zeta}{(c\zeta+2a)z + d + e\zeta}\left(\log(az^2 + dz + f - i\lambda) - \log(\mathcal{C})\right).\end{aligned} \tag{5.1.31}$$

Now all the ζ-dependence has dropped out of the arguments of the logarithms. We recall from Section 4.3 that $b_i = \sum_k \mathcal{S}^{-1}_{ki}$, so in this case

$$\begin{aligned} b_1 =& \frac{4ab + 2bd - c^2 - ce}{2bd^2 - 2cde + 2ae^2 - 8abf + 2c^2f} = \frac{4ab + 2bd - c^2 - ce}{\det\mathcal{S}}\\ =& \frac{2s_3(s_1 - m_1^2 + m_3^2) + (-s_3 + m_2^2 - m_3^2)(s_1 - s_3 + s_2)}{\det\mathcal{S}}\end{aligned} \tag{5.1.32}$$

$$\begin{aligned} b_2 =& \frac{cd - 2ae}{2bd^2 - 2cde + 2ae^2 - 8abf + 2c^2f} = \frac{cd - 2ae}{\det\mathcal{S}}\\ =& \frac{2s_1(s_2 - s_1 + m_3^2 - m_2^2) + (-s_1 + m_3^2 - m_1^2)(s_2 - s_1 - s_3)}{\det\mathcal{S}}\end{aligned} \tag{5.1.33}$$

$$\begin{aligned} b_3 =& \frac{-2bd - cd + 2ae + ce}{2bd^2 - 2cde + 2ae^2 - 8abf + 2c^2f} = \frac{-2bd - cd + 2ae + ce}{\det\mathcal{S}}\\ =& \frac{2s_2(s_1 - m_3^2 + m_1^2) + (-s_2 + m_2^2 - m_1^2)(s_1 + s_2 - s_3)}{\det\mathcal{S}}\end{aligned} \tag{5.1.34}$$

[4] The absorption of the $i\lambda$ into $\det\mathcal{S}$ is explained in Appendix C.6.

and as we expect, their sum is equal to $\mathcal{B}$. The significance of the formulation in terms of kinematic parameters will become apparent in Section 5.2.6.

We wish to eliminate the remaining ζ-dependence, and to do so we will use the freedom that we have to use either root and we will use both, i.e. writing our functions $F(\zeta) = \frac{1}{2}\left(F(\zeta_+) + F(\zeta_-)\right)$, and also $\zeta_\pm = \frac{1}{2}\left(-c \pm \sqrt{c^2 - 4ab}\right)$, so $\zeta_+\zeta_- = \frac{a}{b}$ and $\zeta_+ + \zeta_- = -\frac{c}{b}$

Let us consider only the first integral, using L as a shorthand for the logarithms:

$$\mathcal{I}_1 = -\frac{1}{2}\int_0^1 dz \left(\frac{1}{(2b\zeta_+ + c)z + (c+e)\zeta_+ + 2a + d} + \frac{1}{(2b\zeta_- + c)z + (c+e)\zeta_- + 2a + d}\right) L$$

$$\mathcal{I}_1 = -\frac{1}{2}\int_0^1 dz \left(\frac{-ce - c^2 + 2bd + 4ab}{bz^2(4ab - c^2) + z(4ab - c^2)(e + c) + ae^2 - ced + d^2b + (4ab - c^2)(a + d)}\right) L$$

$$\mathcal{I}_1 = -\frac{1}{2}\int_0^1 dz \left(\frac{b_1 \det \mathcal{S}}{\det \mathcal{G}(bz^2 + (e+c)z + a + d + f) + \frac{\det \mathcal{S}}{2}}\right) L, \tag{5.1.35}$$

so we have all the z-dependence of this first term, both in the denominator and the logarithm, being contained within a function $g_1(z) = bz^2 + (c+e)z + a + d + f - i\lambda$. The other two terms also reduce in this way, so that we have the neat result

$$\begin{aligned}\mathcal{I} = -\Bigg(& b_1 \int_0^1 dz \frac{\log(g_1(z)) - \log\left(\frac{-1}{2\mathcal{B}}\right)}{2\mathcal{B}g_1 + 1} \\ &+ b_2 \int_0^1 dz \frac{\log(g_2(z)) - \log\left(\frac{-1}{2\mathcal{B}}\right)}{2\mathcal{B}g_2 + 1} \\ &+ b_3 \int_0^1 dz \frac{\log(g_3(z)) - \log\left(\frac{-1}{2\mathcal{B}}\right)}{2\mathcal{B}g_3 + 1}\Bigg)\end{aligned} \tag{5.1.36}$$

with
$$g_1(z) = bz^2 + (c+e)z + a + d + f - i\lambda \tag{5.1.37}$$
$$g_2(z) = az^2 + dz + f - i\lambda \tag{5.1.38}$$
$$g_3(z) = (a+b+c)z^2 + (d+e)z + f - i\lambda \tag{5.1.39}$$

or
$$g_1(z) = s_3 z^2 + (-s_3 + m_2^2 - m_3^2)z + m_3^2 - i\lambda \tag{5.1.40}$$
$$g_2(z) = s_1 z^2 + (-s_1 + m_3^2 - m_1^2)z + m_1^2 - i\lambda \tag{5.1.41}$$
$$g_3(z) = s_2 z^2 + (-s_2 + m_2^2 - m_1^2)z + m_1^2 - i\lambda. \tag{5.1.42}$$

For the rest of this chapter, we will consider a generic one of the three terms in the bracket of (5.1.36), $\mathcal{I}_i$, with the argument of its z-dependent logarithm written $g_i = \alpha_i z^2 + \beta_i z + \gamma_i$.

5.1.3 The Third Integration

We can now perform the remaining integration of the three integrands, writing the solution in terms of dilogarithms (or *Spence functions*). First, we require an identity which we will use to simplify the roots, which can be shown by looking at the three cases (5.1.33)–(5.1.34)[5] individually:

$$(b_i \det \mathcal{S})^2 = 2\alpha_i \det \mathcal{S} - \det \mathcal{G} \left(\beta_i^2 - 4\alpha_i\gamma_i\right). \tag{5.1.43}$$

We can then start with an integral from (5.1.36), slightly modified:

$$\mathcal{I}_i = \frac{b_1}{2\mathcal{B}} \int_0^1 dz \frac{\log(g_1(z)) - \log\left(\frac{-1}{2\mathcal{B}}\right)}{\alpha_i z^2 + \beta_i z + \gamma_i + \frac{1}{2\mathcal{B}}} \tag{5.1.44}$$

and rewrite the denominator in terms of its roots $d_{i,\pm}$

$$d_{i,\pm} = -\frac{\beta_i}{2\alpha_i} \pm \frac{1}{2\alpha_i}\sqrt{\beta_i^2 - 4\alpha_i\gamma_i - \frac{2\alpha_i}{\mathcal{B}}} \tag{5.1.45}$$

$$= -\frac{\beta_i}{2\alpha_i} \pm \frac{1}{2\alpha_i}\sqrt{-(b_i \det \mathcal{S})^2 \frac{1}{\det \mathcal{G}}} \tag{5.1.46}$$

$$= -\frac{\beta_i}{2\alpha_i} \pm \frac{|b_i \det \mathcal{S}|}{2\alpha_i} \frac{1}{\sqrt{-\det \mathcal{G}}}, \tag{5.1.47}$$

So as $\det \mathcal{G} \to 0$, the poles move ever further from zero, one positive and one negative. The difference of the values will be

$$d_{i,+} - d_{i,-} = \frac{|b_i \det \mathcal{S}|}{\alpha_i} \frac{1}{\sqrt{-\det \mathcal{G}}}. \tag{5.1.48}$$

We will also write the z-dependent logarithm in terms of its own roots

$$l_{i,\pm} = -\frac{\beta_i}{2\alpha_i} \pm \frac{1}{2\alpha_i}\sqrt{\beta_i^2 - 4\alpha_i\gamma_i} \tag{5.1.49}$$

$$= -\frac{\beta_i}{2\alpha_i} \pm \frac{1}{2\alpha_i}\sqrt{\frac{2\alpha_i \det \mathcal{S}}{\det \mathcal{G}} - \frac{(b_i \det \mathcal{S})^2}{\det \mathcal{G}}} \tag{5.1.50}$$

$$= -\frac{\beta_i}{2\alpha_i} \pm \frac{|b_i \det \mathcal{S}|}{2\alpha_i} \frac{1}{\sqrt{-\det \mathcal{G}}} \sqrt{1 - \frac{2\alpha_i}{b_i^2 \det \mathcal{S}}} \tag{5.1.51}$$

[5] This is performed in more detail in Appendix C.5.

Let us take partial fractions to split the denominator of the integral:

$$\begin{aligned}\mathcal{I}_i =& \frac{b_i}{2\mathcal{B}\alpha_i}\left(\frac{|b_i \det \mathcal{S}|}{\alpha_i}\frac{1}{\sqrt{-\det \mathcal{G}}}\right)^{-1} \\ & \times \int_0^1 dz \left(\log(\alpha_i(z-l_{i,+})(z-l_{i,-})) - \log\left(\frac{-1}{2\mathcal{B}}\right)\right)\left(\frac{1}{z-d_{i,+}} - \frac{1}{z-d_{i,-}}\right) \qquad (5.1.52)\end{aligned}$$

$$= \frac{\sigma(b_i \det \mathcal{S})}{\sqrt{-\det \mathcal{G}}}\int_0^1 dz \left(\log(\alpha_i(z-l_{i,+})(z-l_{i,-})) - \log\left(-\frac{1}{2\mathcal{B}}\right)\right)\left(\frac{1}{z-d_{i,+}} - \frac{1}{z-d_{i,-}}\right) \qquad (5.1.53)$$

where $\sigma(x)$ denotes the sign of a variable x.

Let us examine the term with the first denominator, rewriting[6] $\frac{-1}{2\mathcal{B}}$ as

$$\alpha_i d_{i,+}^2 + \beta_i d_{i,+} + \gamma_i = \alpha_i(d_{i,+} - l_{i,+})(d_{i,+} - l_{i,-}), \qquad (5.1.54)$$

so that

$$\begin{aligned}\mathcal{I}_{i,1} = \frac{\sigma(b_i \det \mathcal{S})}{\sqrt{-\det \mathcal{G}}}\int_0^1 dz \left(\frac{1}{z-d_{i,+}}\right) & \\ \times \left[\log(\alpha_i(z-l_{i,+})(z-l_{i,-})) - \log\left(\alpha_i(d_{i,+}-l_{i,+})(d_{i,+}-l_{i,-})\right)\right] & \qquad (5.1.55)\end{aligned}$$

We now wish to split and recombine the logarithms, remembering the η-functions (see Appendix C.3):

$$\begin{aligned}\mathcal{I}_{i,1} =& \frac{\sigma(b_i \det \mathcal{S})}{\sqrt{-\det \mathcal{G}}}\left(\int_0^1 dz \left[\log\left(\frac{z-l_{i,+}}{d_{i,+}-l_{i,+}}\right) + \log\left(\frac{z-l_{i,-}}{d_{i,+}-l_{i,-}}\right)\right.\right. \\ & - \eta\left(z-l_{i,+}, \frac{1}{d_{i,+}-l_{i,+}}\right) - \eta\left(z-l_{i,-}, \frac{1}{d_{i,+}-l_{i,-}}\right) - \eta\left(\alpha_i - i\epsilon_l, \frac{1}{\alpha_i - i\epsilon_d}\right) \\ & \left.\left. + \eta\left(z-l_{i,+}, z-l_{i,-}\right) - \eta(d_{i,+}-l_{i,+}, d_{i,+}-l_{i,-})\right]\left(\frac{1}{z-d_{i,+}}\right)\right), \qquad (5.1.56)\end{aligned}$$

where ϵ_l and ϵ_d are small quantities with sign opposite to that of the imaginary part of the arguments of the first and second logarithm respectively[7].

[6] We know from the end of section 5.1.2 that we can choose to use the ith polynomial, and from section 5.1.2 that we can choose which root of the denominator to use.

[7] The origin of these terms is given in Appendix C.3.

For the integrals of logarithms, we can obtain the standard form of the dilogarithm

$$\mathrm{Li}_2(x) = -\int_0^x \frac{\log(1-t)}{t} \tag{5.1.57}$$

by substituting $t = -\frac{z-d_{i,+}}{d_{i,+}-l_{i,+}}$ in the first case and $t = -\frac{z-d_{i,-}}{d_{i,+}-l_{i,-}}$ in the second.

So finally, we have, as in Appendix B of [81] or Section 3 of [87]:

$$\begin{aligned}
\mathcal{I}_i =& \frac{\sigma(b_i \det \mathcal{S})}{\sqrt{-\det \mathcal{G}}} \Bigg(\underbrace{\mathrm{Li}_2\left(\frac{d_{i,+}}{d_{i,+}-l_{i,+}}\right)}_{W} - \underbrace{\mathrm{Li}_2\left(\frac{d_{i,+}-1}{d_{i,+}-l_{i,+}}\right)}_{X} \\
&- \log\left(\frac{d_{i,+}-1}{d_{i,+}-l_{i,+}}\right)\eta\left(1-l_{i,+}, \frac{1}{d_{i,+}-l_{i,+}}\right) + \log\left(\frac{d_{i,+}}{d_{i,+}-l_{i,+}}\right)\eta\left(-l_{i,+}, \frac{1}{d_{i,+}-l_{i,+}}\right) \\
&+ \underbrace{\mathrm{Li}_2\left(\frac{d_{i,+}}{d_{i,+}-l_{i,-}}\right)}_{Y} - \underbrace{\mathrm{Li}_2\left(\frac{d_{i,+}-1}{d_{i,+}-l_{i,-}}\right)}_{Z} \\
&- \log\left(\frac{d_{i,+}-1}{d_{i,+}-l_{i,-}}\right)\eta\left(1-l_{i,-}, \frac{1}{d_{i,+}-l_{i,-}}\right) + \log\left(\frac{d_{i,+}}{d_{i,+}-l_{i,-}}\right)\eta\left(-l_{i,-}, \frac{1}{d_{i,+}-l_{i,-}}\right) \\
&+ \log\left(\frac{d_{i,+}-1}{d_{i,+}}\right)\left[\eta\left(-l_{i,+}, -l_{i,-}\right) - \eta(d_{i,+}-l_{i,+}, d_{i,+}-l_{i,-}) - \eta\left(\alpha_i - i\epsilon_l, \frac{1}{\alpha_i - i\epsilon_d}\right)\right] \\
&- (d_{i,+} \to d_{i,-})\Bigg),
\end{aligned} \tag{5.1.58}$$

and the complete result comes from a sum of three such terms.

We can see, using (5.1.47) and (5.1.51), that there are problematic limits with this formula:

- For small $\mathcal{B}$, we know that $|d_{i,\pm}|, |l_{i,\pm}| \gg 1$, and so we have a large cancellation between the terms W and X, and another between Y and Z.
- For small α_i we have $d_{i,\pm} \to l_{i,\pm}$, so we have similar large cancellations.
- $\det \mathcal{S} \to 0$ is also a problematic limit, but is dealt with separately, with the methods of Section 6.3 (except in the case where also $\det \mathcal{G} \to 0$).

The resultant loss of precision is not acceptable for the quality of results we need, and so we need an alternative approach, which is explored in the next section.

5.2 Limits

We can now explore some limits of this equation. Where the formulation in terms of dilogarithms is not numerically acceptable, we can choose instead to do the integral numerically.

5.2.1 $\det \mathcal{G} \to 0$ only

We have stated that for small $\det \mathcal{G}$, the formula (5.1.58) is not well-behaved numerically. However, we can alternatively integrate (5.1.36) numerically, and in doing so, avoid the differences between roots that cause the problems. We know for this case that the $d_{i,\pm}$ and $l_{i,\pm}$ lie far from zero: i.e. for small enough $\det \mathcal{G}$ they will always lie outside the range $[0, 1]$. Now we remember that we introduced the term that became $-\log\left(-\frac{1}{2\mathcal{B}}\right)$ into the three integrals in such a way that their sum was zero, in order to cope with the behaviour at $z \to d_{i,\pm}$. So if this limit never arises in any of the integrals, as it will not, we can leave this term out from all three.

5.2.2 $\det \mathcal{S} \to 0$ only

In contrast to $\det \mathcal{G} \to 0$, the case $\det \mathcal{S} \to 0$ can be a true anomalous threshold: this situation, and the method for avoiding it, is discussed in Section 6.2. It is also possible that, for the cases away from the Landau singularity, there are numerically difficult cases. In our testing, we have found only one, which is detailed in the following section.

5.2.3 $\det \mathcal{G}, \det \mathcal{S} \to 0$ simultaneously

As we saw in Section 5.1.1, $\det \mathcal{G} \to 0$ requires one of the $s_i \to 0$ and the other two to be close in value. For concreteness, let us take the example $s_2 = s_1 + \delta$ and imagine small s_3. Then (5.1.14) becomes:

$$\det \mathcal{G}^{(3)}_{ij} = -(\delta^2 + s_3(s_3 - 4s_1 - 2\delta)), \tag{5.2.59}$$

and (5.1.9) becomes

$$\begin{aligned}\det\mathcal{S} =& 2\Big(s_3\big[s_1^2+s_1\delta+m_1^2-s_1(m_1^2+m_2^2)-s_1(m_1^2+m_3^2)\\ &-\delta(m_1^2+m_3^2)+(m_3^2-m_1^2)(m_2^2-m_1^2)\big]\\ &+s_1[\delta(m_3^2-m_2^2)+(m_3^2-m_2^2)^2]+\delta(m_2^2-m_3^2)(m_1^2-m_3^2)+\delta^2m_3^2\Big),\end{aligned} \tag{5.2.60}$$

so, ignoring the $\mathcal{O}(\delta^2)$ term, for $\det\mathcal{S}\to 0$, we require also $m_2^2\to m_3^2$ (unless we have $s_1=s_2=s_3\to 0$, which we discount: this is a different case, and is kinematically forbidden.).

In the Standard Model, there are no pairs of particles whose masses[8] are very close, say within 10^{-3}, but not equal. For this reason, in the following we consider only the case where the two relevant masses are equal.

Under these conditions, there is a different class of numerical problems which arises. It is more explicit in the unintegrated form (5.1.36), which we repeat below for ease of reference, and indeed we will do a numerical integration in this case, rather than use (5.1.58), due to the low $\det\mathcal{G}$. Note that in this case, we do not know whether the roots of the denominator will be within [0,1] or not, so we leave the second logarithms in each of the integrals.

$$\begin{aligned}\mathcal{I}=-\Bigg(&b_1\int_0^1 dz\frac{\log(g_1(z))-\log\left(\frac{-1}{2\mathcal{B}}\right)}{2\mathcal{B}g_1+1}\\ &+b_2\int_0^1 dz\frac{\log(g_2(z))-\log\left(\frac{-1}{2\mathcal{B}}\right)}{2\mathcal{B}g_2+1}\\ &+b_3\int_0^1 dz\frac{\log(g_3(z))-\log\left(\frac{-1}{2\mathcal{B}}\right)}{2\mathcal{B}g_3+1}\Bigg).\end{aligned} \tag{5.2.61}$$

[8]In modern collider experiments, we consider everything lighter than a b-quark to be massless unless stated.

In our case, with $s_2 = s_1 + \delta$, small s_3 and $m_2^2 = m_3^2$:

$$g_2(z) = s_1 z^2 + (-s_1 + m_2^2 - m_1^2)z + m_1^2 \tag{5.2.62}$$

$$g_3(z) = (s_1 + \delta)z^2 + (-s_1 - \delta + m_2^2 - m_1^2)z + m_1^2 \to g_2(z) \tag{5.2.63}$$

$$b_2 \det \mathcal{S} = (m_1^2 - m_2^2)(s_3 - \delta) + s_1(s_3 + \delta) \tag{5.2.64}$$

$$b_3 \det \mathcal{S} = (m_1^2 - m_2^2)(s_3 + \delta) + s_1(s_3 - \delta) + \delta(s_3 - \delta) \tag{5.2.65}$$

$$\det \mathcal{S} = 2\Big[s_3(s_1^2 + s_1\delta + m_1^2 - 2s_1(m_1^2 + m_2^2) - \delta(m_1^2 + m_2^2) + (m_2^2 - m_1^2)^2) + \delta^2 m_3^2\Big]. \tag{5.2.66}$$

We can see that b_2 and b_3 are small numbers divided by $\det \mathcal{S}$, which is also small, and so we would like to reformulate the integrals in a careful way to improve the numerical stability. We also have the potential, in the limit $s_3 \ll \delta$, for large cancellations between the second and third terms, with the integrals having similar values and the prefactors becoming equal and opposite.

To solve the numerical problem in the bad limit, let us explore the effect of reexpressing the two cancelling terms. Let us define:

$$\mathcal{I}_2 = b_2 \mathcal{J}_2 \qquad \text{and} \qquad \mathcal{I}_3 = b_3 \mathcal{J}_3, \tag{5.2.67}$$

and we will wish to use the formula

$$b_2\mathcal{J}_2 + b_3\mathcal{J}_3 = \frac{1}{2}(b_2 + b_3)(\mathcal{J}_2 + \mathcal{J}_3) + \frac{1}{2}(b_2 - b_3)(\mathcal{J}_2 - \mathcal{J}_3) \tag{5.2.68}$$

to separate the terms in such a way that the large cancellations do not occur.

We have

$$(b_2 + b_3)\det \mathcal{S} = 2(m_1^2 - m_2^2)s_3 + 2s_1 s_3 + \delta(\delta + s_3) \tag{5.2.69}$$

$$(b_2 - b_3)\det \mathcal{S} = -2(m_1^2 - m_2^2)\delta + 2s_1\delta - \delta(\delta + s_3), \tag{5.2.70}$$

and we can then calculate the difference between the integrals, for which we will need a formula similar to (5.2.68)

$$\frac{A}{\alpha} - \frac{B}{\beta} = \frac{1}{2}\left(\frac{1}{\alpha} - \frac{1}{\beta}\right)(A + B) + \frac{1}{2}\left(\frac{1}{\alpha} + \frac{1}{\beta}\right)(A - B), \tag{5.2.71}$$

to give

$$\mathcal{J}_2 - \mathcal{J}_3 = \int_0^1 dz \frac{\log(g_2) - \log\left(\frac{-1}{2\mathcal{B}}\right)}{2\mathcal{B}g_2 + 1} - \frac{\log(g_3) - \log\left(\frac{-1}{2\mathcal{B}}\right)}{2\mathcal{B}g_3 + 1} \tag{5.2.72}$$

$$= \frac{1}{2}\int_0^1 dz \Bigg(\left(-\frac{2\mathcal{B}}{(2\mathcal{B}g_2+1)(2\mathcal{B}g_3+1)}\right)(g_2 - g_3)\left(\log(g_2) + \log(g_3) - 2\log\left(\frac{-1}{2\mathcal{B}}\right)\right)$$

$$- \left(\frac{1}{2\mathcal{B}g_2+1} + \frac{1}{2\mathcal{B}g_3+1}\right)(\log(g_2) - \log(g_3))\Bigg). \tag{5.2.73}$$

In this formulation, both of the terms in the integral carry a small quantity, the first $(g_2 - g_3)$ and the second $(\log(g_2) - \log(g_3))$, and therefore $\mathcal{J}_2 - \mathcal{J}_3 \to 0$.

The case with b_2 and b_3 of the same order

The most difficult case in this problem has b_2 and b_3 of the same order[9], in which case their difference might go to zero or might still diverge. For this case, we start by introducing the variable $u = \frac{|\delta|}{\sqrt{|s_3|}}$, giving $\delta = \sigma(\delta)u\sqrt{|s_3|}$. Note that as of yet, we do not know anything about the size of u. In terms of u:

$$(b_2 + b_3)\det\mathcal{S} = s_3\left(2(m_1^2 - m_2^2) + 2s_1 + \sigma(s_3)u^2 + \sigma(\delta)u\sqrt{|s_3|}\right) \tag{5.2.74}$$

$$(b_2 - b_3)\det\mathcal{S} = u\sqrt{|s_3|}\left(-2(m_1^2 - m_2^2)\sigma(\delta) + 2s_1\sigma(\delta) - u\sqrt{|s_3|} - \sigma(\delta)s_3\right) \tag{5.2.75}$$

$$\det\mathcal{S} = 2s_3\Big[s_1^2 + s_1\sigma(\delta)u\sqrt{|s_3|} + m_1^2 - 2s_1(m_1^2 + m_2^2)$$

$$- \sigma(\delta)u\sqrt{|s_3|}(m_1^2 + m_2^2) + (m_2^2 - m_1^2)^2 + \sigma(s_3)u^2m_3^2\Big]. \tag{5.2.76}$$

In this formulation, the limits $u \to 0$ and $u \to \infty$ are unproblematic. In the limit $s_3 \to 0$, $(b_2 + b_3)$ will be well-behaved, but $(b_2 - b_3)$ will diverge as $s_3^{-\frac{1}{2}}$. However, we note that

$$g_2 - g_3 = -\delta z(z-1) = \sigma(\delta)u\sqrt{|s_3|}z(z-1) \tag{5.2.77}$$

$$\log(g_2) - \log(g_3) = \log\left(1 - \frac{\delta z(z-1)}{g_3}\right) \tag{5.2.78}$$

[9] In `golem95`, this is taken to be $0.1 < \frac{b_2}{b_3} < 10$.

and so the term $(b_2 - b_3)(\mathcal{J}_2 - \mathcal{J}_3)$ can be made to converge numerically:

$$\begin{aligned}(b_2 - b_3)(\mathcal{J}_2 - \mathcal{J}_3) =& \sigma(\delta) u \sqrt{|s_3|}(b_2 - b_3)\frac{1}{2}\int_0^1 dz \Bigg[\left(\frac{2\mathcal{B}z(z-1)}{(2\mathcal{B}g_2+1)(2\mathcal{B}g_3+1)} \right) \\ & \times \left(\log(g_2) + \log(g_3) - 2\log\left(\frac{-1}{2\mathcal{B}}\right)\right) \\ & - \left(\frac{1}{2\mathcal{B}g_2+1} + \frac{1}{2\mathcal{B}g_3+1} \right) \frac{1}{\delta}\big(\log(g_2) - \log(g_3)\big) \Bigg], \end{aligned} \tag{5.2.79}$$

where we have made use of the fact that the final term is of the form $\frac{\log(1-x)}{x}$ (implemented as $q(1,x)$ in `golem95`), which is numerically well-behaved as $x \to 0$.[10] Now we have only well-behaved terms inside the integral. The prefactor, taken as a single unit, behaves as:

$$u\sqrt{|s_3|}(b_2 - b_3) \sim u^2 s_3^0 \tag{5.2.80}$$

and so we have removed the divergent behaviour. Neither the first integral of (5.2.61), nor the term $(b_2 + b_3)(\mathcal{J}_2 + \mathcal{J}_3)$ is numerically difficult in this limit, so they remain as they are, and the formula used is:

$$\begin{aligned}\mathcal{I} =& -\Bigg(b_1 \int_0^1 dz \frac{\log(g_1(z)) - \log\left(\frac{-1}{2\mathcal{B}}\right)}{2\mathcal{B}g_1+1} \\ & + \frac{1}{2}(b_2+b_3)\int_0^1 dz \left(\frac{\log(g_2(z)) - \log\left(\frac{-1}{2\mathcal{B}}\right)}{2\mathcal{B}g_2+1} + \frac{\log(g_3(z)) - \log\left(\frac{-1}{2\mathcal{B}}\right)}{2\mathcal{B}g_3+1} \right) \\ & + \frac{1}{4}\sigma(\delta) u\sqrt{|s_3|}(b_2 - b_3) \\ & \times \int_0^1 dz \Bigg[\left(\frac{2\mathcal{B}z(z-1)}{(2\mathcal{B}g_2+1)(2\mathcal{B}g_3+1)} \right) \left(\log(g_2) + \log(g_3) - 2\log\left(\frac{-1}{2\mathcal{B}}\right)\right) \\ & - \left(\frac{1}{2\mathcal{B}g_2+1} + \frac{1}{2\mathcal{B}g_3+1} \right) \frac{1}{\delta} \left(\log(g_2) - \log(g_3) \right) \Bigg] \Bigg). \end{aligned} \tag{5.2.81}$$

where the last term is implemented as

$$\frac{1}{\delta}\left(\log(g_2) - \log(g_3) \right) = \frac{z(z-1)}{g_3}\frac{1}{\xi}\log(1-\xi) \tag{5.2.82}$$

with

$$\xi = \frac{\delta z(z-1)}{g_3} \tag{5.2.83}$$

[10] For small z, it is implemented as $q(1,z) = \left(1 + \sum_{j=2}^{\infty} \frac{x^{j-1}}{j}\right)$, with terms evaluated up to the desired accuracy (2×10^{-16}).

The case with b_2 and b_3 not of the same order

If b_2 and b_3 are not of the same order, we will not have the problem that causes us to have to recombine the logarithms. In order to obtain convenient expressions, in which cancellations between small quantities can be made explicit, we use $v = \frac{|\delta|}{|s_3|}$, giving:

$$(b_2 + b_3)\det\mathcal{S} = s_3\left[2m_1^2 - 2m_2^2 + 2s_1 + vs_3(v + \sigma(\delta)\sigma(s_3))\right] \tag{5.2.84}$$

$$(b_2 - b_3)\det\mathcal{S} = s_3\sigma(\delta)\sigma(s_3)v\left[-2m_1^2 + 2m_3^2 + s_1 + s_3(\sigma(\delta)\sigma(s_3)v + 1)\right] \tag{5.2.85}$$

$$\det\mathcal{S} = 2s_3\big(s_1^2 + m_1^2 - 2s_1(m_1^2 + m_2^2) + (m_2^2 - m_1^2)^2 \tag{5.2.86}$$

$$+ s_3v\sigma(\delta)\sigma(s_3)(s_1 - m_1^2 - m_2^2) + s_3^2v^2m_3^2\big) \tag{5.2.87}$$

Now we see that all the quantities are stable for all limits with one exception: $(b_2 - b_3)$ diverges as s_3^{-1} where v is large and s_3 is small. However, this is the limit addressed in the previous section. This means that for all other regions, this is a stable formulation, and it does not require a reexpression of the logarithms, so this formulation is used as the default case.

Entry into this limit

The values of $\det\mathcal{G}$ and $\det\mathcal{S}$ for which this limb should be entered have not yet been optimised: this will be done before this limit forms part of the public version. Currently, we are using the restrictions that two masses must be equal, $\mathcal{B} < 0.5$ and $|\det\mathcal{G} - \det\mathcal{S}| < 10$.

Other cases of cancellation

It is of course in principle possible that there are other circumstances, completely separate from this limit, in which pairs of the $\mathcal{I}_i$ cancel against each other, however no such situations have been revealed by our testing.

5.2.4 Leading Coefficient $\alpha_i \to 0$ only

We now consider the limits when parameters in the arguments of the logarithms in (5.1.40)–(5.1.42), $g_i = \alpha_i z^2 + \beta_i z + \gamma_i$, become small. As $\alpha_i \to 0$, the character of

the calculation changes. The $l_{i,\pm}$ roots become

$$l_{i,\pm} = -\frac{\beta_i}{2\alpha_i}\left[1 \mp \frac{|\beta_i|}{\beta_i}\sqrt{1 - \frac{4\alpha_i^2}{\beta_i^2}\frac{\gamma_i}{\alpha_i}}\right] \tag{5.2.88}$$

$$= -\frac{\beta_i}{2\alpha_i}\left[1 \mp \sigma(\beta_i)(1 - \frac{2\alpha_i\gamma_i}{\beta_i^2} + \mathcal{O}(\alpha_i^2))\right], \tag{5.2.89}$$

so up to $\mathcal{O}(\alpha_i^0)$, we have:

$$\sigma(\beta_i) = 1 \qquad \begin{cases} l_{i,+} & = -\frac{\gamma_i}{\beta_i} \\ l_{i,-} & = -\frac{\beta_i}{\alpha_i} + \frac{\gamma_i}{\beta_i} \to -\sigma(\alpha_i)\infty \end{cases} \tag{5.2.90}$$

$$\sigma(\beta_i) = -1 \qquad \begin{cases} l_{i,+} & = -\frac{\beta_i}{\alpha_i} + \frac{\gamma_i}{\beta_i} \to +\sigma(\alpha_i)\infty \\ l_{i,-} & = -\frac{\gamma_i}{\beta_i}. \end{cases} \tag{5.2.91}$$

Similarly, the $d_{i,\pm}$ roots become

$$d_{i,\pm} = -\frac{\beta_i}{2\alpha_i}\left[1 \mp \sigma(\beta_i)(1 - \frac{2\alpha_i\gamma_i}{\beta_i^2} - \frac{\alpha_i}{\mathcal{B}\beta_i^2} + \mathcal{O}(\alpha_i^2))\right], \tag{5.2.92}$$

so up to $\mathcal{O}(\alpha_i^0)$, we have:

$$\sigma(\beta_i) = 1 \qquad \begin{cases} d_{i,+} & = -\frac{\gamma_i}{\beta_i} - \frac{1}{2\mathcal{B}\beta_i} \\ d_{i,-} & = -\frac{\beta_i}{\alpha_i} + \frac{\gamma_i}{\beta_i} + \frac{1}{2\mathcal{B}\beta_i} \to -\sigma(\alpha_i)\infty \end{cases} \tag{5.2.93}$$

$$\sigma(\beta_i) = -1 \qquad \begin{cases} d_{i,+} & = -\frac{\beta_i}{\alpha_i} + \frac{\gamma_i}{\beta_i} + \frac{1}{2\mathcal{B}\beta_i} \to +\sigma(\alpha_i)\infty \\ d_{i,-} & = -\frac{\gamma_i}{\beta_i} - \frac{1}{2\mathcal{B}\beta_i}. \end{cases} \tag{5.2.94}$$

Let us now take $\sigma(\beta_i) = 1$ for concreteness (the other case will be similar), for which the +-labelled roots are stable, and examine the behaviour of the individual parts of the full expression in terms of logarithms, dilogarithms and η-functions (5.1.58).

First let us examine the logarithms. Their arguments:

$$\frac{d_{i,+}-1}{d_{i,+}} \to 1 \tag{5.2.95}$$

$$\frac{d_{i,+}}{d_{i,+}-l_{i,+}} \to 2\mathcal{B}\gamma+1 \tag{5.2.96}$$

$$\frac{d_{i,+}}{d_{i,+}-l_{i,-}} \to 0 \tag{5.2.97}$$

$$\frac{d_{i,-}}{d_{i,-}-l_{i,+}} \to 1 \tag{5.2.98}$$

$$\frac{d_{i,-}}{d_{i,-}-l_{i,-}} \to \infty \tag{5.2.99}$$

and the corresponding cases with an additional (-1) in the numerator act similarly. This means that, in order to avoid unstable numerical behaviour, we will have to find reexpressions of the four terms involving the logarithms

$$\frac{d_{i,+}}{d_{i,+}-l_{i,-}} \qquad \frac{d_{i,+}-1}{d_{i,+}-l_{i,-}} \qquad \frac{d_{i,-}}{d_{i,-}-l_{i,-}} \qquad \frac{d_{i,-}-1}{d_{i,-}-l_{i,-}} \tag{5.2.100}$$

Let us examine the terms involving the first pair of logarithms, and use the fact that in this limit, $l_{i,-} \gg 1$, to find a numerically stable formulation:

$$\mathcal{P}_l = -\log\left(\frac{d_{i,+}-1}{d_{i,+}-l_{i,-}}\right)\eta\left(1-l_{i,-},\frac{1}{d_{i,+}-l_{i,-}}\right)+\log\left(\frac{d_{i,+}}{d_{i,+}-l_{i,-}}\right)\eta\left(-l_{i,-},\frac{1}{d_{i,+}-l_{i,-}}\right) \tag{5.2.101}$$

$$\sim \eta\left(-l_{i,-},\frac{1}{d_{i,+}-l_{i,-}}\right)\left[\log\left(\frac{d_{i,+}}{d_{i,+}-1}\right)+\eta\left(d_{i,+},\frac{1}{d_{i,+}-l_{i,-}}\right)-\eta\left(d_{i,+}-1,\frac{1}{d_{i,+}-l_{i,-}}\right)\right]. \tag{5.2.102}$$

The same reexpression can be applied to the other pair of terms, and so we have a stable formulation for the logarithms.

The dilogarithms have the same set of arguments, excluding (5.2.95). Of the four cases, only the last causes numerical difficulty. To solve this problem, we first notice that $d_{i,-}-l_{i,-}$ is algebraically finite for all small α_i

$$d_{i,-}-l_{i,-} = -\frac{\beta_i}{\alpha_i}+\frac{\gamma_i}{\beta_i}+\frac{1}{2\mathcal{B}\beta_i}+\frac{\beta_i}{\alpha_i}-\frac{\gamma_i}{\beta_i}+\mathcal{O}(\alpha_i) \to \frac{1}{2\mathcal{B}\beta_i} \tag{5.2.103}$$

and so if a case of small α_i arises, we must calculate this difference algebraically.

We can then use the identity:

$$\mathrm{Li}_2\left(\frac{1}{z}\right) = -\mathrm{Li}_2(z)-\frac{1}{2}\log^2(-z)-\frac{\pi^2}{6} \tag{5.2.104}$$

on the pair of dilogarithms

$$\begin{aligned}\mathcal{P}_d =&\mathrm{Li}_2\left(\frac{d_{i,-}}{d_{i,-}-l_{i,-}}\right)-\mathrm{Li}_2\left(\frac{d_{i,-}-1}{d_{i,-}-l_{i,-}}\right)\\ =&-\mathrm{Li}_2\left(\frac{d_{i,-}-l_{i,-}}{d_{i,-}}\right)+\mathrm{Li}_2\left(\frac{d_{i,-}-l_{i,-}}{d_{i,-}-1}\right)-\frac{1}{2}\log^2\left(-\frac{d_{i,-}-l_{i,-}}{d_{i,-}}\right)+\frac{1}{2}\log^2\left(-\frac{d_{i,-}-l_{i,-}}{d_{i,-}-1}\right)\\ =&-\mathrm{Li}_2\left(\frac{d_{i,-}-l_{i,-}}{d_{i,-}}\right)+\mathrm{Li}_2\left(\frac{d_{i,-}-l_{i,-}}{d_{i,-}-1}\right)\\ &+\frac{1}{2}\left(\log\left(\frac{d_{i,-}}{l_{i,-}-d_{i,-}}\right)+\log\left(\frac{d_{i,-}-1}{l_{i,-}-d_{i,-}}\right)\right)\left[\log\left(\frac{d_{i,-}-1}{d_{i,-}}\right)-\eta\left((d_{i,-}-1),\frac{1}{d_{i,-}}\right)\right.\\ &\left.+\eta\left((l_{i,-}-d_{i,-}),\frac{1}{d_{i,-}}\right)-\eta\left((l_{i,-}-d_{i,-}),\frac{1}{d_{i,-}-1}\right)\right],\end{aligned}\tag{5.2.105}$$

where we have expanded out the difference of two squares, and expanded and recombined the logarithms in the difference term.

In fact, the first η-function is zero, because the imaginary parts of its arguments are of opposite sign, and the other two cancel in the limit of large $d_{i,-}$. Let us multiply and divide the last term by $\frac{1}{d_{i,-}}$:

$$\begin{aligned}\mathcal{P}_d =&-\mathrm{Li}_2\left(\frac{d_{i,-}-l_{i,-}}{d_{i,-}}\right)+\mathrm{Li}_2\left(\frac{d_{i,-}-l_{i,-}}{d_{i,-}-1}\right)\\ &+\frac{1}{2}\frac{1}{d_{i,-}}\left(\log\left(\frac{d_{i,-}}{l_{i,-}-d_{i,-}}\right)+\log\left(\frac{d_{i,-}-1}{l_{i,-}-d_{i,-}}\right)\right)\left(\frac{\log\left(\frac{d_{i,-}-1}{d_{i,-}}\right)}{\frac{1}{d_{i,-}}}\right),\end{aligned}\tag{5.2.106}$$

so now we have two terms of the form $\frac{\log(d_{i,-})}{d_{i,-}}$, and a term $q(1,\frac{1}{d_{i,-}})$ (as in Section 5.2.3, below (5.2.79)), so all terms are now unproblematic as $d_{i,-}\to\infty$.

In `golem95`, the default value for which the programme switches to this regime is $\frac{\alpha_i}{\mathcal{S}_{max}}=10^{-10}$, where $\mathcal{S}_{max}$ is the largest entry of the $\mathcal{S}$-matrix.

5.2.5 Subleading Coefficient $\beta_i\to 0$ only

As $\beta_i\to 0$, the roots

$$l_{i,\pm}\to\pm\sigma(\alpha_i)\sqrt{-\frac{\gamma_i}{\alpha_i}}\tag{5.2.107}$$

and

$$d_{i,\pm}\to\pm\sigma(\alpha_i)\sqrt{-\frac{\gamma_i}{\alpha_i}-\frac{1}{2\mathcal{B}\alpha_i}}\tag{5.2.108}$$

and there are no numerical problems.

5.2.6 Coefficients $\alpha_i, \beta_i \to 0$ simultaneously

From (5.1.40)–(5.1.42), we recall that

$$g_i = s_a z^2 + (-s_a + m_b^2 - m_c^2)z + m_d^2 - i\lambda \qquad \text{for some} \qquad a, b, c, d \in \{1, 2, 3\}.$$

We also recall the argument of Section 5.2.3, that in the Standard Model there is no possibility for masses to be very close to each other, and yet not equal. Therefore, if we have $s_a = \alpha_i \to 0$, in order also to have $\beta_i \to 0$, we need to have $m_b = m_c$, and $s_a = \alpha_i = -\beta_i$.

So we have:

$$d_{i,\pm} \to \frac{1}{2} \pm \sqrt{\frac{1}{4} - \frac{\gamma_i}{\alpha_i} - \frac{1}{2\mathcal{B}\alpha_i}} \tag{5.2.109}$$

and

$$l_{i,\pm} \to \frac{1}{2} \pm \sqrt{\frac{1}{4} - \frac{\gamma_i}{\alpha_i}} \tag{5.2.110}$$

and so all the roots are divergent as $\alpha_i, \beta_i \to 0$.

However, if we look at an example dilogarithm argument, and expand the square roots just to zeroth order in α_i:

$$\frac{d_{i,+}}{d_{i,+} - l_{i,+}} \simeq \frac{\frac{1}{2} + \sqrt{\frac{\gamma_i + \frac{1}{2\mathcal{B}}}{-\alpha_i}}}{\sqrt{\frac{\gamma_i + \frac{1}{2\mathcal{B}}}{-\alpha_i}} - \sqrt{\frac{\gamma_i}{-\alpha_i}}} \tag{5.2.111}$$

$$\simeq \frac{\sqrt{\gamma_i + \frac{1}{2\mathcal{B}}}}{\sqrt{\gamma_i + \frac{1}{2\mathcal{B}}} - \sqrt{\gamma_i}}. \tag{5.2.112}$$

We can now see that this combination of roots is finite, as indeed are all the others. This suggests that we can continue to use (5.1.58), as long as we find a more numerically stable representation of the combinations of the roots.

Let us define

$$\tilde{d}_{i,\pm} = |\alpha_i| d_{i,\pm} = -\sigma(\alpha_i)\frac{\beta_i}{2} \pm \sigma(\alpha_i)\sqrt{\frac{\beta_i^2}{4} - \alpha_i\gamma_i - \frac{\alpha_i}{2\mathcal{B}}} \tag{5.2.113}$$

and

$$\tilde{l}_{i,\pm} = |\alpha_i| l_{i,\pm} = -\sigma(\alpha_i)\frac{\beta_i}{2} \pm \sigma(\alpha_i)\sqrt{\frac{\beta_i^2}{4} - \alpha_i\gamma_i}. \tag{5.2.114}$$

Now the roots will converge (indeed they will go to zero as $\sqrt{\alpha_i}$), and we will have to rewrite (5.1.58) for the tilded quantities:

$$\begin{aligned}\mathcal{I}_i =&\frac{\sigma(b_i \det \mathcal{S})}{\sqrt{-\det \mathcal{G}}}\Bigg(\mathrm{Li}_2\left(\frac{\tilde{d}_{i,+}}{\tilde{d}_{i,+}-\tilde{l}_{i,+}}\right)-\mathrm{Li}_2\left(\frac{\tilde{d}_{i,+}-|\alpha_i|}{\tilde{d}_{i,+}-\tilde{l}_{i,+}}\right)\\
&-\log\left(\frac{\tilde{d}_{i,+}-|\alpha_i|}{\tilde{d}_{i,+}-\tilde{l}_{i,+}}\right)\eta\left(|\alpha_i|-\tilde{l}_{i,+},\frac{1}{\tilde{d}_{i,+}-\tilde{l}_{i,+}}\right)+\log\left(\frac{\tilde{d}_{i,+}}{\tilde{d}_{i,+}-\tilde{l}_{i,+}}\right)\eta\left(-\tilde{l}_{i,+},\frac{1}{\tilde{d}_{i,+}-\tilde{l}_{i,+}}\right)\\
&+\mathrm{Li}_2\left(\frac{\tilde{d}_{i,+}}{\tilde{d}_{i,+}-\tilde{l}_{i,-}}\right)-\mathrm{Li}_2\left(\frac{\tilde{d}_{i,+}-|\alpha_i|}{\tilde{d}_{i,+}-\tilde{l}_{i,-}}\right)\\
&-\log\left(\frac{\tilde{d}_{i,+}-|\alpha_i|}{\tilde{d}_{i,+}-\tilde{l}_{i,-}}\right)\eta\left(|\alpha_i|-\tilde{l}_{i,-},\frac{1}{\tilde{d}_{i,+}-\tilde{l}_{i,-}}\right)+\log\left(\frac{\tilde{d}_{i,+}}{\tilde{d}_{i,+}-\tilde{l}_{i,-}}\right)\eta\left(-\tilde{l}_{i,-},\frac{1}{\tilde{d}_{i,+}-\tilde{l}_{i,-}}\right)\\
&+\log\left(\frac{\tilde{d}_{i,+}-|\alpha_i|}{\tilde{d}_{i,+}}\right)\left[\eta\left(-\tilde{l}_{i,+},-\tilde{l}_{i,-}\right)-\eta(\tilde{d}_{i,+}-\tilde{l}_{i,+},\tilde{d}_{i,+}-\tilde{l}_{i,-})-\eta\left(\alpha_i-i\epsilon_l,\frac{1}{\alpha_i-i\epsilon_d}\right)\right]\\
&-(\tilde{d}_{i,+}\to\tilde{d}_{i,-})\Bigg),\end{aligned}\tag{5.2.115}$$

In `golem95`, the default value for which the programme switches to this regime is[11] $\frac{\alpha_i}{S_{max}}, \frac{\beta_i}{S_{max}} = 10^{-10}$.

Because the modified roots go to zero for very small α_i, we could in principle have further numerical problems if we are very close to this limit. However, when $\alpha_i, \beta_i \to 0$, the corresponding b_i also goes to zero[12]: this can be seen in the equations (5.1.33)–(5.1.34), in which numerator of each b_i is given as a sum of a term with a factor α_i and a term with a factor β_i. In this limit, the integrand loses all z-dependence, as $g_i(z) \to \gamma_i$. So we can see that if this constant integrand

$$\frac{\log\gamma_i - \log\left(\frac{-1}{2\mathcal{B}}\right)}{2\mathcal{B}\gamma_i+1}\tag{5.2.116}$$

remains finite, then $\mathcal{I}_i \to 0$, and we need not do any calculation for it. Fortunately the integrand does remain finite, by the same argument as in Section 5.2.1: if $\mathcal{B}$ is not small, all the terms are well-behaved, and if it is small, the poles will not be in the integration region and we can cancel the second logarithm it from the

[11] As before, $\mathcal{S}_{max}$ is the largest entry of the $\mathcal{S}$-matrix.

[12] This relies on $\det \mathcal{S}$ not also going to zero.

three integrals. In our implementation, we take the integral $\mathcal{I}_i$ to be zero below $|\alpha_i|, |\beta_i| = 2 \times 10^{-15}$.

5.3 Scalar Two-point Function

The scalar two-point function is a much simpler case, but it also has limits for which the first implementation breaks down, and another formulation must be found. Let us start with the integral $\mathcal{I}_2^d$, for which $\frac{d}{2} - N = \epsilon$ (we will treat only the case with s, m_1 and m_2 neither equal nor zero):

$$\begin{aligned}\mathcal{I}_2^d =&\Gamma(\epsilon) \int_0^1 \prod_{i=1}^{2} dx_i \delta \left(1 - \sum_i^2 x_i\right) \left(-\frac{1}{2} x^T \cdot \mathcal{S} \cdot x - i\lambda\right)^\epsilon \\ =&\frac{1}{\epsilon} - \gamma_E + \int_0^1 \prod_{i=1}^{2} dx_i \delta \left(1 - \sum_i^2 x_i\right) \left(\log(-\frac{1}{2} x^T \cdot \mathcal{S} \cdot x - i\lambda)\right) + \mathcal{O}(\epsilon),\end{aligned} \tag{5.3.117}$$

where we have used (B.3.21): $\Gamma(\epsilon) = \frac{1}{\epsilon} - \gamma_E + \mathcal{O}(\epsilon)$. We can then integrate over x_2 using the δ-functional:

$$\mathcal{I}_2^d = \frac{1}{\epsilon} - \gamma_E - \int_0^1 dx \left(\log(-\frac{1}{2}\left(x^2 \mathcal{S}_{11} + 2x(1-x)\mathcal{S}_{12} + (1-x)^2 \mathcal{S}_{22}\right) - i\lambda)\right) + \mathcal{O}(\epsilon) \tag{5.3.118}$$

and substitute in $\mathcal{S}_{11} = -2m_1^2$, $\mathcal{S}_{12} = s - m_1^2 - m_2^2$ and $\mathcal{S}_{22} = -2m_2^2$:

$$\mathcal{I}_2^d = \frac{1}{\epsilon} - \gamma_E - \int_0^1 dx \left(\log(sx^2 + (-s + m_1^2 - m_2^2)x + m_2^2 - i\lambda)\right). \tag{5.3.119}$$

Let us now name the final, integral, term $\mathcal{I}_{2,I}$ and proceed to solve it. We have

$$\mathcal{I}_{2,I} = \int_0^1 dx \log(sx^2 + (-s + m_1^2 - m_2^2)x + m_2^2 - i\lambda) \tag{5.3.120}$$

and we wish to find a solution by factorising the quadratic form and splitting the logarithm. To do this, we need to remember that s is a real of either sign and that m_1^2 and m_2^2 have positive real part. Then as demonstrated in Appendix C.3, the appropriate way to split for real masses is:

$$\log(sx^2 + (-s + m_1^2 - m_2^2)x + m_2^2 - i\lambda) = \log\left(s(x - x_1)(x - x_2)\right) \tag{5.3.121}$$

$$= \log(s - i\lambda) + \log(x - x_1) + \log(x - x_2), \tag{5.3.122}$$

and if the masses are complex, we gain one additional η-function. The roots of the quadratic form are

$$x_{1,2} = \frac{-(-s + m_1^2 - m_2^2) \pm \sqrt{s^2 + m_1^4 + m_2^4 - 2sm_1^2 - 2sm_2^2 - 2m_1^2m_2^2 + i\lambda s}}{2s}, \tag{5.3.123}$$

where whenever λ has been multiplied by an internal mass, the mass can be omitted as it is the sign of the term which is important.

We can solve the integral directly using $\int dx \log(x) = x\log(x) + x + C$:

$$\begin{aligned}\mathcal{I}_{2,I} = &-2 + \log(s - i\lambda) + (1 - x_1)\log(1 - x_1) + (1 - x_2)\log(1 - x_2) \\ &+ x_1 \log(-x_1) + x_2 \log(-x_2).\end{aligned} \tag{5.3.124}$$

To consider the $s \to 0$ case, let us expand in small s, and keep only terms up to zero order[13]:

$$x_{1,2} = \frac{1}{2s}\left[-(m_1^2 - m_2^2) \pm |m_1^2 - m_2^2|\right] \pm \frac{m_1^2 + m_2^2}{2|m_1^2 - m_2^2|} + \frac{1}{2}. \tag{5.3.125}$$

We see that not only $\log(s - i\lambda)$, but also exactly one of the roots $x_{1,2}$ will cause numerical difficulties for small[14] s. These can be solved by reexpressing the function. The method of rexpression depends whether we are in:

Case 1a	$s \ll m_1^2$ and $(m_1^2 - m_2^2) > 0$;	(5.3.126)
Case 1b	$s \ll m_2^2$ and $(m_1^2 - m_2^2) < 0$; or	(5.3.127)
Case 2	$s, (m_1^2 - m_2^2) \ll m_1^2, m_2^2$.	(5.3.128)

5.3.1 Case 1a: $s \ll m_1^2$ and $(m_1^2 - m_2^2) > 0$

When $s \to 0$, one of the roots will be badly behaved, and, as we see in (5.3.125), which one that is will depend on the sign of $(m_1^2 - m_2^2)$. In the case $(m_1^2 - m_2^2) > 0$, x_2 becomes very large, so we would like to have a reexpression without $\log(s - i\lambda)$, $\log(-x_2)$ or $\log(1 - x_2)$.

[13] We do not make this approximation in the `golem95` programme.

[14] In `golem95`, we use a ratio of 10^{-4} as our dividing line.

First let us multiply out the prefactors $(1 - x_{1,2})$ in Equation (5.3.124) and combine the logarithms[15] with coefficients $x_{1,2}$:

$$\mathcal{I}_{2,I} = -2 + \log(s - i\lambda) + \log(1 - x_1) + \log(1 - x_2) - x_1 \log\left(\frac{1 - x_1}{-x_1}\right) - x_2 \log\left(\frac{1 - x_2}{-x_2}\right). \tag{5.3.129}$$

Now let us rewrite terms 2, 3 and 4 as follows:

$$\begin{aligned}
\mathcal{T}_+ &= \log(s - i\lambda) + \log(1 - x_1) + \log(1 - x_2) && (5.3.130)\\
&= \log(s - i\lambda) + \log\left(\frac{m_1^2 - i\lambda}{s}\right) - \eta(1 - x_1, 1 - x_2) && (5.3.131)\\
&= \log(\sigma(s) - i\lambda) + \log\left(m_1^2\sigma(s) - i\lambda\sigma(s)\right) - \eta(1 - x_1, 1 - x_2), && (5.3.132)
\end{aligned}$$

where $\sigma(s)$ represents the sign of s. We consider the two cases:

$$\begin{aligned}
\sigma(s) = 1 \qquad \mathcal{T}_+ &= \log(1 - i\lambda) + \log\left(m_1^2 - i\lambda\right) - \eta(1 - x_1, 1 - x_2) && (5.3.133)\\
&= \log\left(m_1^2 - i\lambda\right) - \eta(1 - x_1, 1 - x_2) && (5.3.134)\\
\sigma(s) = -1 \qquad \mathcal{T}_+ &= \log(-1 - i\lambda) + \log\left(-m_1^2 + i\lambda\right) - \eta(1 - x_1, 1 - x_2) && (5.3.135)\\
&= -i\pi + \log\left(-m_1^2 + i\lambda\right) - \eta(1 - x_1, 1 - x_2) && (5.3.136)\\
&= -i\pi + \log\left(m_1^2 - i\lambda\right) + i\pi - \eta(1 - x_1, 1 - x_2) && (5.3.137)\\
&= \log\left(m_1^2 - i\lambda\right) - \eta(1 - x_1, 1 - x_2), && (5.3.138)
\end{aligned}$$

so we have for $(m_1^2 - m_2^2) > 0$ a better formulation:

$$\mathcal{I}_{2,I} = -2 + \log\left(m_1^2 - i\lambda\right) - \eta(1 - x_1, 1 - x_2) - x_1 \log\left(\frac{1 - x_1}{-x_1}\right) - x_2 \log\left(1 - \frac{1}{x_2}\right), \tag{5.3.139}$$

the last term of which is well-behaved for all values of m_2^2: it goes to unity as $x_2 \to \infty$, being $q(1, \frac{1}{x_2})$ (as in Section 5.2.3).

5.3.2 Case 1b: $s \ll m_2^2$ and $(m_1^2 - m_2^2) < 0$

For $(m_1^2 - m_2^2) < 0$, we are instead seeking a form with no $\log(s - i\lambda)$, $\log(-x_1)$ or $\log(1 - x_1)$ terms. We start by adding and subtracting two terms in (5.3.124):

[15] There are no η-functions here as $(1 - x_{1,2})$ and $-x_{1,2}$ have imaginary parts of the same sign.

$(1-x_1)\log(-x_1)$ and $(1-x_2)\log(-x_2)$:

$$\begin{aligned}\mathcal{I}_{2,I} =& -2+\log(s-i\lambda)+(1-x_1)\log\left(\frac{1-x_1}{-x_1}\right)+\log(-x_1)\\ &+(1-x_2)\log\left(\frac{1-x_2}{-x_2}\right)+\log(-x_2).\end{aligned} \tag{5.3.140}$$

Now we take a subset of terms and rearrange, using the same pattern of argumentation:

$$\mathcal{T}_- = \log(s-i\lambda)+\log(-x_1)+\log(-x_2) \tag{5.3.141}$$

$$= \log(s-i\lambda)+\log\left(\frac{m_2^2-i\lambda}{s}\right)+\eta(-x_1,-x_2) \tag{5.3.142}$$

$$= \log\left(m_2^2-i\lambda\right)+\eta(-x_1,-x_2), \tag{5.3.143}$$

and also we see that

$$(1-x_1)\log\left(\frac{1-x_1}{-x_1}\right) = -(1-x_1)\log\left(\frac{-x_1}{1-x_1}\right) = -(1-x_1)\log\left(1-\frac{1}{1-x_1}\right), \tag{5.3.144}$$

so we have a convenient form

$$\begin{aligned}\mathcal{I}_{2,I} =& -2+\log\left(m_2^2-i\lambda\right)+\eta(-x_1,-x_2)\\ &-(1-x_1)\log\left(1-\frac{1}{1-x_1}\right)+(1-x_2)\log\left(\frac{1-x_2}{-x_2}\right).\end{aligned} \tag{5.3.145}$$

This equation is unproblematic for all m_1^2.

5.3.3 Case 2: $s, (m_1^2-m_2^2) \ll m_1^2, m_2^2$

In this case, a further variable is instructive: $r = \frac{m_1^2-m_2^2}{s}$. We we can write out the roots as

$$x_{1,2} = \frac{1}{2s}\left[s(r-1)\pm\sqrt{s^2(r-1)^2-4sm_2^2}\right] \tag{5.3.146}$$

$$= \frac{r-1}{2}\pm\left(\frac{r-1}{2}\right)\sqrt{1-\frac{4m_2^2}{s(r-1)}}. \tag{5.3.147}$$

Without subdividing this case, we do not know which root will go to ∞: indeed, both roots will diverge if $s\to 0$ more quickly than $m_1^2-m_2^2$. Fortunately, with a

slight reexpression, we have two formulae that are well-behaved as both $x_{1,2} \to \infty$: we can use (5.3.139)

$$\begin{aligned}\mathcal{I}_{2,I} = &-2 + \log\left(m_1^2 - i\lambda\right) - \eta(1-x_1, 1-x_2) \\ &- x_1 \log\left(1 - \frac{1}{-x_1}\right) - x_2 \log\left(1 - \frac{1}{x_2}\right)\end{aligned} \tag{5.3.148}$$

or (5.3.145)

$$\begin{aligned}\mathcal{I}_{2,I} = &-2 + \log\left(m_2^2 - i\lambda\right) + \eta(-x_1, -x_2) \\ &- (1-x_1) \log\left(1 - \frac{1}{1-x_1}\right) - (1-x_2) \log\left(1 - \frac{1}{1-x_2}\right)\end{aligned} \tag{5.3.149}$$

and we take the former when r is positive and the latter when r is negative, so that the logarithm of the mass is unlikely to be problematic.

Chapter 6

Complex masses

In 1963, Veltman proved [88] for a specific example that the scattering matrix $\mathtt{S}$ of a theory with an unstable particle could be unitary, renormalisable and causal[1]. In the Standard Model, all of the heavier particles[2] can be treated as unstable.

In this chapter, we first introduce, with reference to the *optical theorem*, the existence of particle widths, and discuss the different schemes for treating unstable particles. We then move onto the seemingly unrelated topic of Landau singularities. From both sections, we will conclude that it would be best to have a library including complex masses, and we describe our implementation, `golem95C`, in Section 6.3.

6.1 The Optical Theorem and Particle Widths

The optical theorem (see, for example, Chapter 6 of [89] or Chapter 7 of [21]) is a useful way of finding scattering amplitudes, based on the unitarity of the scattering matrix $\mathtt{S}$. Writing $\mathtt{S} = 1 + i\mathtt{T}$, $\mathtt{S}^\dagger\mathtt{S} = 1$ becomes

$$-i(\mathtt{T} - \mathtt{T}^\dagger) = \mathtt{T}^\dagger\mathtt{T}. \tag{6.1.1}$$

[1]Because he was not considering a theory with gauge bosons, only two scalars, the problem of retaining gauge invariance, discussed in Section 6.1, did not arise.

[2]Heavier than the b-quark: the b-quark's width is usually too small to usefully include.

Now let us have the initial state $|i\rangle$ and the final state $|f\rangle$, and a complete set of states, with the sum running over all possible sets of states s:

$$1 = \sum_s \int \prod_j \left(\frac{d^3 q_j}{(2\pi)^2 2E_{q_j}} \right) |s(q_j)\rangle \langle s(q_j)| \,, \tag{6.1.2}$$

so

$$-i \left(\langle f|\mathtt{T}|i\rangle - \langle f|\mathtt{T}^\dagger|i\rangle \right) = \sum_s \int \prod_j \left(\frac{d^3 q}{(2\pi)^2 2E_q} \right) \langle f|\mathtt{T}|s(q_j)\rangle \langle s(q_j)|\mathtt{T}^\dagger|i\rangle \tag{6.1.3}$$

Now let us consider a specific example. We take the initial and final state to be a single particle, for which the initial and final momenta will of course be the same p, and consider the two-point function:

$$-i \left(\langle p|\mathtt{T}|p\rangle - \langle p|\mathtt{T}^\dagger|p\rangle \right) = \sum_s \int \prod_j \left(\frac{d^3 q}{(2\pi)^2 2E_q} \right) \langle p|\mathtt{T}|s(q_j)\rangle \langle s(q_j)|\mathtt{T}^\dagger|p\rangle \tag{6.1.4}$$

$$-2i\mathrm{Im} \left(\langle p|\mathtt{T}|p\rangle \right) = \sum_s \int \prod_j \left(\frac{d^3 q}{(2\pi)^2 2E_q} \right) \left| \langle p|\mathtt{T}|s(q_j)\rangle \right|^2 , \tag{6.1.5}$$

which is to say that the two-point function will gain an imaginary part if there exist ways in which the initial particle could decay into real particles. In the specific case of a Z-boson, there is sufficient energy in the propagator for decay into a pair of light fermions for $p^2 > 2m_{f_l}$, where f_l is the lightest fermion (which physically will be one of the neutrinos[3]), which will lead to there being an imaginary part in the Z-propagator. However, in t-channel diagrams, the Z-boson has $p^2 < 0$, and so has no opportunities for decay into real particles.

This imaginary part will enter our calculations as a particle width[4], which will only be present in the s-channel, and will give the propagator

$$\frac{1}{p^2 - m^2 + im\Gamma}, \tag{6.1.6}$$

that is to say that, when we have an unstable particle, the pole of the propagator will move off the real axis when we do the renormalising Dyson sum (Section 2.3.6).

[3]The neutrinos are so light that for modern collider experiments, we can treat this bound as effectively zero.

[4]A simpler quantum mechanical argument can also be made, using $\phi(t) = \phi(0)\exp(-iE_0 t - \frac{\Gamma}{2}t)$ for an unstable particle, which in energy space is $\phi(E) \sim \phi(0)\frac{1}{(E-E_0)-i\frac{\Gamma}{2}}$.

The mass of the heavy particle, if defined to be on the real axis, will be scheme dependent. There is, however, one scheme-independent way to define the (real) mass and the width together, and that is as the real and imaginary parts at the position of the pole [90–96].

When performing a practical one-loop calculation, the first approximation we might make would be the *narrow width approximation* (NWA). In this scheme, the squared propagator $\mathcal{P}^2$ for a resonant particle of mass M is approximated:

$$\mathcal{P}^2 \equiv \frac{1}{(q^2 - M^2)^2 + (M\Gamma)^2} \tag{6.1.7}$$

$$\sim \frac{\pi}{M\Gamma}\delta(q^2 - M^2). \tag{6.1.8}$$

The standard error estimate for this approximation is $\mathcal{O}(\frac{\Gamma}{M})$, and therefore we would like to include the width in practical calculations, particularly at NLO, as $\mathcal{O}\left(\frac{\Gamma}{M}\right) = \mathcal{O}(\alpha)$ (with α the relevant coupling for the decay: usually EW). Moreover, it is shown in [97–100] that the effects of finite widths can be enhanced[5], further limiting the applicability of the narrow-width approximation.

It is not trivial to include a width because, as we will see, the most naïve methods violate gauge invariance: the inclusion of the width is a partial inclusion of terms of higher order, which will in general cause a violation of Ward identities. This is no trivial formality: in the absence of gauge invariance, calculations can gain very large theoretical errors [101]. Several schemes have been developed in the literature:

Fixed width

In perhaps the simplest scheme, all propagators have a fixed width added into them at the start of the calculation. It is shown in [102] that this scheme retains U(1) gauge invariance for a specific example. However, this technique has the disadvantage that it breaks SU(2) [103], due to the inconsistency of having complex masses in the propagators and a real θ_W (because $\cos\theta_W = \frac{M_W}{M_Z}$), and also it retains an unphysical width for t-channel bosons, introducing a bias.

[5]The conditions for the NWA's applicability are laid out in [98] as: $\Gamma \ll M$; $m \ll M$, with m the daughter particle mass; $\sqrt{s} \gg M$; little interference from non-resonant processes; and separability of the resonant propagator from the rest of the matrix element.

Step width and Running width

Both of these schemes take the imaginary part of the denominator of the propagator to be zero for spacelike momenta, and therefore avoid giving t-channel bosons an unphysical width. Then for timelike momenta, the step width turns on a constant imaginary part $M\Gamma$, and the running width takes $p^2\frac{\Gamma}{M}$.

These schemes not only violate SU(2), but also U(1) [102], so a further scheme is required to render its results gauge invariant.

Fermion loop

In the fermion loop scheme [102–108], the width of a boson propagator is treated by calculating the contribution of a fermion loop to it in its unrenormalised state, and then renormalising. This has the effect of undoing the gauge breaking from the step width or running width schemes, and so they are used in combination.

This is then consistent in terms of orders, as it includes all of the one-loop effects on the propagator, and so preserves gauge invariance. However, it requires the computation of effects one order higher than the rest of the calculation, and so is difficult for higher-order processes. Also, it cannot currently be implemented for unstable fermions with bosonic corrections.

Overall Factor Scheme

In [101, 109], the *Overall Factor scheme*[6] is developed, in which the calculation is performed without a width, and then all diagrams are multiplied by $\frac{p^2-m^2}{p^2-m^2+im\Gamma}$ (with fixed Γ). This preserves gauge invariance at the cost of adding an $\mathcal{O}(\frac{\Gamma}{m}) = \mathcal{O}(\alpha)$ contribution to the non-resonant terms.

In [101], it is compared to a scheme in which the gauge violation is accepted, but terms are chosen so as to minimise its impact, and both are found to be much more stable than the fixed-width scheme.

As stated in [110], this is the scheme used in MCFM, with which we will compare our results in Section 7.4.4.

[6] This is also called the *preserved gauge scheme* or *factorisation scheme*.

Pole expansion

In this scheme [90,92,111,112], an expansion is made around the complex resonance. The position of the resonance is gauge invariant, and therefore so are the results of this scheme. However, the method breaks down near to the threshold for the production of multiple unstable particles (the example of HZ production is given in [113]).

Unstable particle effective theory

In this method [114–118] the unstable heavy particles are integrated out, in order to organise the calculation as a series in both α and $\frac{\Gamma}{M}$. For example, for W-pair production [118], the Ws can be taken as non-relativistic near their threshold, and the parameters of the effective theory can be determined by matching to a full calculation. This strategy can describe the peak region well, but has more limited applicability away from it.

Complex mass scheme

In the complex mass scheme [119–121][7], the mass is defined throughout the calculation, not only in the propagators, as complex – as in other schemes, the values are taken from the position of the pole in the complex plane – so we have a real bare mass and complex counterterms. We therefore have a consistent treatment which respects gauge invariance. The costs of this scheme are that, like the fixed width scheme, it retains an unphysical width for non-resonant diagrams; and that one must rewrite any algorithms to include complex renormalisation, complex couplings and complex-mass integral libraries. We discuss our implementation of such a library in Section 6.3.

In principle, the widths should still be considered as energy-dependent, and in order to integrate this into the scheme, the complex-pole scheme [123–125] has been developed.

[7] This has also been extended to higher loops in [122, 123].

Comparisons

A comparison of several of these schemes is performed in [126]. The programmes WTO [107], RacoonWW [127] and LUCIFER [128] can also perform such comparisons.

6.2 Landau Singularity

Landau [72] showed that there are certain specific kinematic configurations in which an *anomalous threshold* will occur. If we look at equation (4.1.15), neglecting the λ-prescription:

$$\mathcal{I}_N^d(S) = \int \frac{d^d k}{i\pi^{d/2}} \int_0^1 \prod_{i=1}^{N} (dx_i) \delta \left(\sum_{i=1}^{N} x_i - 1 \right) \frac{(N-1)!}{\left[\sum x_i (q_i^2 - m_i^2) \right]^N} \tag{6.2.9}$$

(where the q_i and the x_i are real) we can see that there will be a potential singularity if:

$$x_i (q_i^2 - m_i^2) = 0 \quad \forall i \tag{6.2.10}$$

An additional condition arises from topological considerations, as shown in Chapter 2 of [85], or Chapter 18 of [129]:

$$\frac{\partial}{\partial k} \left[\sum x_i (q_i^2 - m_i^2) \right] = 0 \tag{6.2.11}$$

or

$$\sum x_i q_i = 0, \tag{6.2.12}$$

where we are only considering the one-loop case, and it will be important to remember that the x_i are non-negative.

The *anomalous threshold*, or *leading Landau singularity*, will occur when these conditions apply and none of the $x_i = 0$: we can see from (6.2.10) that this means that all the propagators go on-shell. *Sub-leading Landau singularities*, occur when some of the $x_i = 0$, which is when all the propagators go on-shell in a pinched diagram. Thresholds involving only a 2×2 $\mathcal{S}$-matrix are termed *normal thresholds*, and arise at the point at which the incident momentum can first produce the two adjoining particles (in the loop) on-shell.

In [130], it is shown that we can recast (6.2.12) into the language of our modified Cayley matrix $\mathcal{S}$: the condition simply becomes

$$\det \mathcal{S} = 0 \tag{6.2.13}$$

and similarly for the subleading case, the determinant which is zero will be that of the sub-matrix $\mathcal{S}(S_0 \backslash \{s_{x0}\})$ formed when the rows and columns $\{s_{x0}\}$ corresponding to the zero x_i have been removed.

In [72, 85], it is shown that with N legs at l loops, where a Landau singularity occurs it will behave as:

$$(\det \mathcal{S})^{2l-\frac{1}{2}(N+1)} \log(\det \mathcal{S}) \tag{6.2.14}$$

in the vicinity of the singularity. Later in this section, we will see the leading Landau singularity behaving as $(\det \mathcal{S})^{-\frac{1}{2}}$, the subleading singularity from the triangle as $\log(\det \mathcal{S})$, and the normal threshold from the bubbles, for which only the derivative is discontinuous.

Let us now take a specific example[8] from a supersymmetric context, namely the production of a heavy neutral Higgs and a pair of massless b-quarks by gluon fusion, via a loop containing two squarks (sbottoms) and two neutralinos.

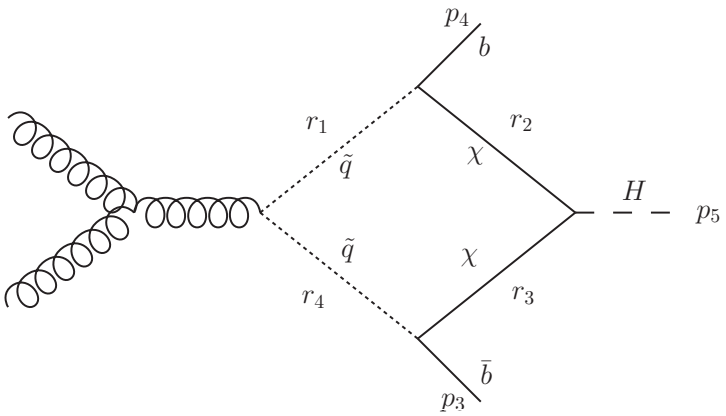

Figure 6.1: A diagram in which all propagators can go simultaneously on-shell to develop a leading Landau singularity which can be regulated by introducing complex masses.

[8] Similar specific examples can be found in [130, 131].

The maximal set $S_0 = \{1, 2, 3, 4\}$. For the box, we will have:

$$\mathcal{S}(S_0) = \begin{pmatrix} -2m_{\tilde{q}}^2 & -m_\chi^2 - m_{\tilde{q}}^2 & s_{45} - m_\chi^2 - m_{\tilde{q}}^2 & s - 2m_{\tilde{q}}^2 \\ -m_\chi^2 - m_{\tilde{q}}^2 & -2m_\chi^2 & m_H^2 - 2m_\chi^2 & s_{35} - m_\chi^2 - m_{\tilde{q}}^2 \\ s_{45} - m_\chi^2 - m_{\tilde{q}}^2 & m_H^2 - 2m_\chi^2 & -2m_\chi^2 & -m_\chi^2 - m_{\tilde{q}}^2 \\ s - 2m_{\tilde{q}}^2 & s_{35} - m_\chi^2 - m_{\tilde{q}}^2 & -m_\chi^2 - m_{\tilde{q}}^2 & -2m_{\tilde{q}}^2 \end{pmatrix}. \tag{6.2.15}$$

We now use the constraint on the physical phase space[9], $\det \mathcal{G}^{(1)} \geq 0$, where:

$$\mathcal{G}^{(1)} = \begin{pmatrix} 0 & s_{35} - m_H^2 & s - s_{35} - s_{45} \\ s_{35} - m_H^2 & 2m_H^2 & s_{45} - m_H^2 \\ s - s_{35} - s_{45} & s_{45} - m_H^2 & 0 \end{pmatrix} \tag{6.2.16}$$

$$\det \mathcal{G}^{(1)} = 2(s_{12} - s_{35} - s_{45} - m_H^2)\left(s_{35}s_{45} - m_H^2 s_{12}\right) \geq 0, \tag{6.2.17}$$

So

$$m_H^2 \frac{s_{12}}{s_{35}} \leq s_{45} \leq m_H^2 + s_{12} - s_{35} \tag{6.2.18}$$

$$m_H^2 \leq s_{35} \leq s_{12}, \tag{6.2.19}$$

where the first pair of constraints comes from requiring both brackets in (6.2.17) to be non-negative for general (positive) s_{35}, and the second pair comes from inserting s_{45}'s minimum value into the first bracket. Following [130], we can write:

$$\det \mathcal{S}(S_0) = \kappa(s_{35}, m_{\tilde{q}}^2, m_\chi^2)(s_{45} - s_{45}^{(0)})^2 + \det \mathcal{S}(S_0 \backslash \{2\}) \det \mathcal{S}(S_0 \backslash \{4\}), \tag{6.2.20}$$

where $s_{45}^{(0)}$ is the solution of

$$\det \mathcal{S}(S_0) - \det \mathcal{S}(S_0 \backslash \{2\}) \det \mathcal{S}(S_0 \backslash \{4\}) = 0. \tag{6.2.21}$$

Now let us choose some values and investigate the behaviour with varying s_{45}. Take:

$$m_H = 450\,\text{GeV} \quad m_{\tilde{q}} = 800\,\text{GeV} \quad m_\chi = 200\,\text{GeV} \quad \sqrt{s} = 1700\,\text{GeV} \tag{6.2.22}$$

and also fix $s_{35} = 2(m_{\tilde{q}} + m_\chi)$. The discontinuities, as shown in Figure 6.2 are:

[9] This is shown, for example, in the appendix of [132], with the difference that they take incoming and outgoing momenta, and ours are all defined as incoming, so there is a minus sign difference.

- A normal threshold at $\sqrt{s_{45}} = (m_{\tilde{q}} + m_{\chi}) = 1000\,\text{GeV}$, where a squark and a neutralino can first be produced on-shell.
- A subleading Landau singularity at $\sqrt{s_{45}} \simeq 1012.7\,\text{GeV}$, corresponding to $\det \mathcal{S}(S_0 \backslash \{2\}) = 0$
- A subleading Landau singularity at $\sqrt{s_{45}} \simeq 1038.1\,\text{GeV}$, corresponding to $\det \mathcal{S}(S_0 \backslash \{4\}) = 0$
- A leading Landau singularity at $\sqrt{s_{45}} \simeq 1078.4\,\text{GeV}$, where $\det \mathcal{S}(S_0) = 0$

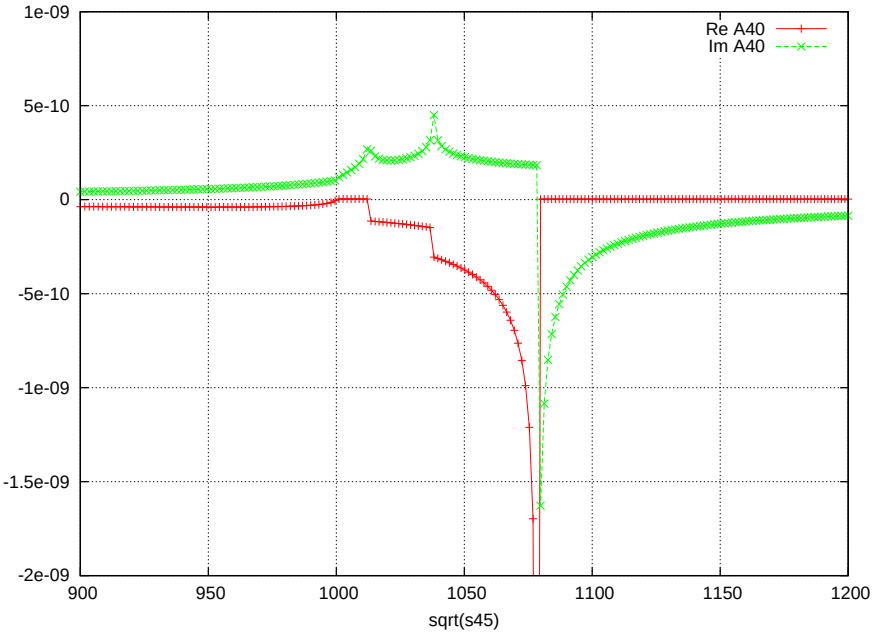

Figure 6.2: Singularity structure of the scalar four-point function $A^{4,0}$ (real masses) contained in the diagram of Figure 6.1 for $900\,\text{GeV} \leq s_{45} \leq 1200\,\text{GeV}$.

6.3 The Complex-mass Library golem95C

In the latest version of our library, golem95C [86], complex masses have been implemented, similarly to [79, 80]. This makes it possible to deal with the schemes of Section 6.1 which require complex propagators, as well as regulating the Landau singularities explained in Section 6.2.

The regulation of the Landau singularities works by moving the poles of the propagators away from the real axis, which is our integration contour. This can be demonstrated in the case of the previous example by sending $m_{\tilde{q}}^2 \to m_{\tilde{q}}^2 - im_{\tilde{q}}\Gamma_{\tilde{q}}$ and $m_\chi^2 \to m_\chi^2 - im_\chi\Gamma_\chi$, where we take $\Gamma_{\tilde{q}} = 3.5\,\text{GeV}$ and $\Gamma_\chi = 1.5\,\text{GeV}$. We show the smoothing of the thresholds in Figure 6.3.

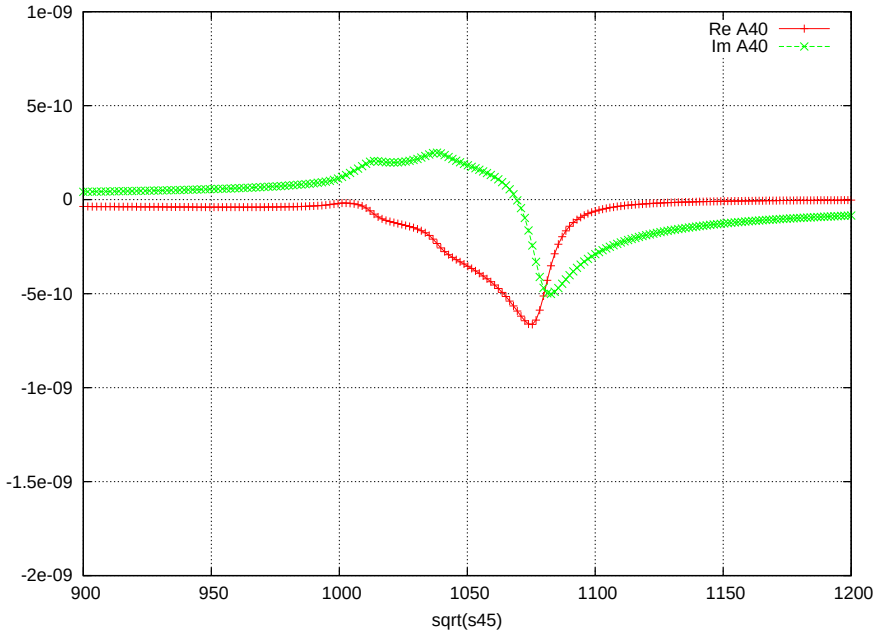

Figure 6.3: Singularity structure of the scalar four-point function $A^{4,0}$ (complex masses) contained in the diagram of Figure 6.1.

We have implemented the analytic forms of all the integrals with complex internal masses which are required, and now have a full library for both scalar integrals and tensor form factors which enter one-loop integrals, up to rank six 6-point functions. It is available at `http://projects.hepforge.org/golem/95`.

Chapter 7

GoSam, Sherpa and $pp \to e^+e^-\mu^+\mu^-$ by diboson production

In this chapter, we will discuss the calculation of $pp \to e^+e^-\mu^+\mu^-$ via two gauge bosons. We include the off-shell photon contribution, as well as the Z-boson, in this NLO calculation. The (formally higher-order) loop-induced gluon-initiated process is also added, as explained in Section 7.4.2.

The matrix elements were calculated using the GoSam project, which is allied to the golem95 project, and Sherpa was linked via the Binoth Les Houches Accord in order to perform all other parts of the calculation. These programmes are described in Sections 7.2 and 7.3.

7.1 Background

The production and decay of a pair of neutral vector bosons is a process which is interesting in its own right, but it also has an important part to play in Higgs searches: the process $H \to ZZ$ has been a major discovery channel for the Higgs, but it is important to see this intermediate Higgs state as part of a full calculation of neutral vector boson pair production, because the interference between it and the process without the Higgs is significant (this was shown in [100], see also Section 7.4.5).

In addition, this final state will also be influenced by certain Beyond the Standard Model scenarios, such as models containing a gZZ or ZZZ-vertex. In order to

observe these processes, we will need to have small uncertainties on the SM background prediction, so that the small signal is visible on top of it.

There has been interest in this process since at least the late 1970s, and the different components of the calculation have been built up over time. Work started with the production of real vector boson pairs at LO [133], and later NLO [110, 134–136], with the gluon-initiated case added in [137–139]. The gluon-initiated case was explored further in [140], and also in the context of Higgs production in [141].

In order to predict results which can be seen in a detector, the decays of the vector bosons must be considered. This work was started, for polarised real Z-bosons, to leading order but including the gluon-initiated channel, in [142, 143].

Full calculations of this process, including the virtual photon and the leptonic decays, have recently been performed to NLO, plus the gluon-initiated channel, by the MCFM group [144], Campbell et al. [145], the aMC@NLO group [146], and gg2VV [100, 147, 148]. However, of these, only the gg2VV results include the $gg \to H \to ZZ$ corrections, and only the aMC@NLO results include parton shower contributions.

At the LHC, both the ATLAS [149] and CMS [150] collaborations realise the importance of this process as a Higgs search channel and its background, and the ZZ-channel, with one Z far off-shell, formed a major part of the discovery of a new particle consistent with the Higgs boson this month [18, 19].

7.2 GoSam

GoSam [151] is an automated programme for the calculation of one-loop amplitudes for processes with up to six external legs. A major strength is its ability to use a variety of methods for the processing of the amplitude, allowing it to combine the best features of different methods for optimum speed and stability. A brief description of the programme follows.

After the user has produced an input file for a specific process, GoSam uses QGRAF [152] to produce FORM [153, 154] code for each diagram. QGRAF provides a number of commands for excluding diagrams from the output[1], and GoSam provides

[1]For example "onshell", a command to produce only amputated diagrams, which is usually

additional such options. The built-in Standard Model model file can be used, or a user-supplied LanHEP [155] or UFO [156] model file. Because currently only tensor integrals with rank equal to or lower than the number of legs are implemented, only the Feynman gauge and particles up to spin 1 are currently supported, although in a forthcoming version tensor integrals with higher ranks will also be available.

At the next stage, Python code is used to set to zero those diagrams with zero colour factor or which have a loop which is zero in dimensional regularisation (because it is scaleless), and also to flag the loop size and maximum rank of any integrals[2].

The diagrams produced are grouped according to the set S of denominators they contain, such that there is a maximal element in each group from which all others are obtained by reduction. In this way, the reduction is made more efficient as in the reduction of the maximal element, much of the computational effort of reducing the other integrals is performed, and need not be repeated.

In GoSam, wavefunctions are represented as sums of massless spinors in the spinor-helicity formalism [157–164]: specifically the implementation in spinney [165] is used. The numerators are then processed using haggies [166], producing optimised Fortran 90 code, in order to prepare the expression for numerical evaluation.

At this point, there is a freedom of choice of the methods used for the evaluation. The variable reduction_interoperation is used to control which method is used, and its value is given in brackets as the options are explained.

The simplest choice (0) is to use Samurai to reduce the integrals directly to scalars, and to call these integrals from QCDLoop [78] or OneLOop [79]. An alternative is also provided, which is to project out the tensor integrals using tensorial reconstruction [63], and then either use golem95 (1) to calculate the tensor integrals or Samurai (3) to find the coefficients of the scalar integrals, and then call them as above. A common method of usage, and that which is used in this thesis, is to use the former option by default, and switch to tensorial reconstruction and golem95 for

desired.

[2] At this stage the overall sign of diagrams containing Majorana fermions [28, 29] is also determined, as QGRAF's implementation is not reliable.

phase-space points at which Samurai's reduction fails (2)[3]. A further option uses tensorial reconstruction throughout, but after that Samurai by default and golem95 (4) as a rescue system.

The result is given as a four-component object: the Born part (squared), and the finite, ϵ^{-1} and ϵ^{-2} parts of the one-loop part after interference with the Born part. GoSam is also capable of performing loop-induced processes, i.e. those with no tree level, as is used in Section 7.4.2. The results provided have certain prefactors assumed as detailed in Section 2.5 of [151].

A table of processes for which GoSam has been run and checked on a phase-space point level against external programmes (which are cited) is given as Figure 7.1. This is taken from [151][4].

Finally, it is worth noting that GoSam is fully compatible with the Binoth Les Houches Interface (see Section 7.3.4), and the later parts of this chapter concern such an interfacing.

Process	Checked with Ref.	Process	Checked with Ref.
$e^+e^- \to u\overline{u}$	[167]	$u\overline{d} \to e^-\overline{\nu}_e\, g$	[170]
$e^+e^- \to t\overline{t}$	[47, 168]	$e^+e^- \to e^+e^-\gamma$ (QED)	[176]
$u\overline{u} \to d\overline{d}$	[169, 170]	$pp \to H\, t\overline{t}$	[170]
$gg \to gg$	[171]	$pp \to W^+W^+jj$	[177]v3
$gg \to gZ$	[172]	$pp \to W^\pm\, j$ (QCD corr.)	MCFM [110, 173]
$d\overline{d} \to t\overline{t}$	[170], MCFM [110, 173]	$pp \to b\overline{b}b\overline{b}$	[178, 179]
$gg \to t\overline{t}$	[170], MCFM [110, 173]	$pp \to W^+W^-b\overline{b}$	[170, 180]
$bg \to H\, b$	[170, 174]	$u\overline{u} \to t\overline{t}b\overline{b}$	[170, 180]
$\gamma\gamma \to \gamma\gamma$	[175]	$gg \to t\overline{t}b\overline{b}$	[170, 180]
$u\overline{d} \to e^-\overline{\nu}_e$	[170]	$u\overline{d} \to W^+ggg$	[180]

Table 7.1: List of processes performed by GoSam and checked against the literature, from [151].

[3]For example, approximately 1 point in 4000 fails for the $gg \to 4l$ process of Section 7.4.2

[4]The process $pp \to W^\pm\, j$ (EW corr.) was removed from the table, as only the IR poles had been checked. The process $e^+e^- \to t\overline{t}$ was also checked against a private analytic calculation.

Complex masses

GoSam can work with propagators with complex masses, either within[5] or outside the loops: complex numerators are implemented. However, the complex coupling constants and mixing angles, required for the use of the complex-mass scheme, are not currently implemented in the case where they cannot be pulled out as an overall factor. Only QCD corrections are included in the calculation later in this chapter, i.e. as an EW calculation it is only leading order, and so a fixed-width scheme (see Section 6.1) is used for the boson propagators.

7.3 Monte Carlo Event Generators and Sherpa

In this thesis so far, we have considered partonic matrix elements for a given phase space point: we have had a fixed number of quarks and gluons in the initial and final states, which had fixed momenta. However, as discussed in Section 2.6, states of this kind are not observable:

- for a physical observable, we will have to take account of the existence of additional, unresolved particles;
- due to colour confinement, we do not see the partons, but only hadrons in initial and final states;
- because at the LHC we have composite initial states, we do not know the incoming partons' momenta when observing a particular event's final state. In addition, if we want to gain any statistical reach, we must integrate over ranges of final momenta.

We therefore need to do a great deal of work before our partonic matrix element can give an observable, and for this we use a Monte Carlo Event generator, specifically Sherpa [181–183]. Because of asymptotic freedom, the important quantity is the scale at which we are operating: we have a non-perturbative regime within

[5]For this, either Samurai with OneLOop, or the golem95 limb can be used, but Samurai with QCDLoop cannot be used as the latter does not support complex masses.

the proton (low scale), then a hard partonic interaction, described by perturbative QCD, and any partons in the final state will evolve down in energy by radiation of coloured particles until they reach a scale at which they hadronise again.

7.3.1 Initial State Partons

At the LHC, partons from within each proton will collide, and after this point, the partonic cross section is relevant. However, neither the identities, nor the momenta of the incident partons are known *a priori*, nor are they directly measurable from the final state. Instead, we describe the probability of a particular parton i having a particular fraction of the momentum of the proton x using a Parton Distribution Function (PDF) $f_i(x, \mu_F^2)$, where μ_F^2 is a factorisation scale[6]. The PDFs are non-perturbative quantities, whose values must be fitted from data. Several groups, including CTEQ [184], NNPDF [185] and MSTW [186] produce PDF sets, each using different fitting methods and different input data. An example is given from the last group in Figure 7.3.1.

If we have a set of PDFs at one scale, we can evolve it to any other scale using DGLAP equations[7] [187–189]. The DGLAP method rests on the concept that in moving between scales, all flavours of parton will radiate. This changes all the PDFs in an interdependent way. For any parton i at a scale μ_F^2 we have, to first order (Equations 27 and 28 of [189])[8]:

$$2\mu_F^2 \frac{df_i(x,\mu_F^2)}{d\mu_F^2} = \frac{\alpha_s(\mu_R)}{2\pi} \int_x^1 \frac{dy}{y} \sum_j \kappa_{ij}(y) f_j(\tfrac{x}{y}, \mu_F^2), \tag{7.3.1}$$

where we have introduced the splitting kernel κ_{ij} which, schematically, is the likelihood of a parent parton j splitting and producing a parton i which carries a fraction y of its momentum. The kernels are obtained by calculating any process, and repeating the calculation with one extra emission, then taking a ratio in the collinear

[6]The place and relevance of factorisation scales is explained in Section 2.6.1.

[7]So-called as they were found independently by Dokshitzer, Gribov and Lipatov, and Altarelli and Parisi.

[8]The μ_R-dependence of the right-hand side is usually ignored in the literature. Clearly, if the two scales are set to be equal, it need not be made explicit.

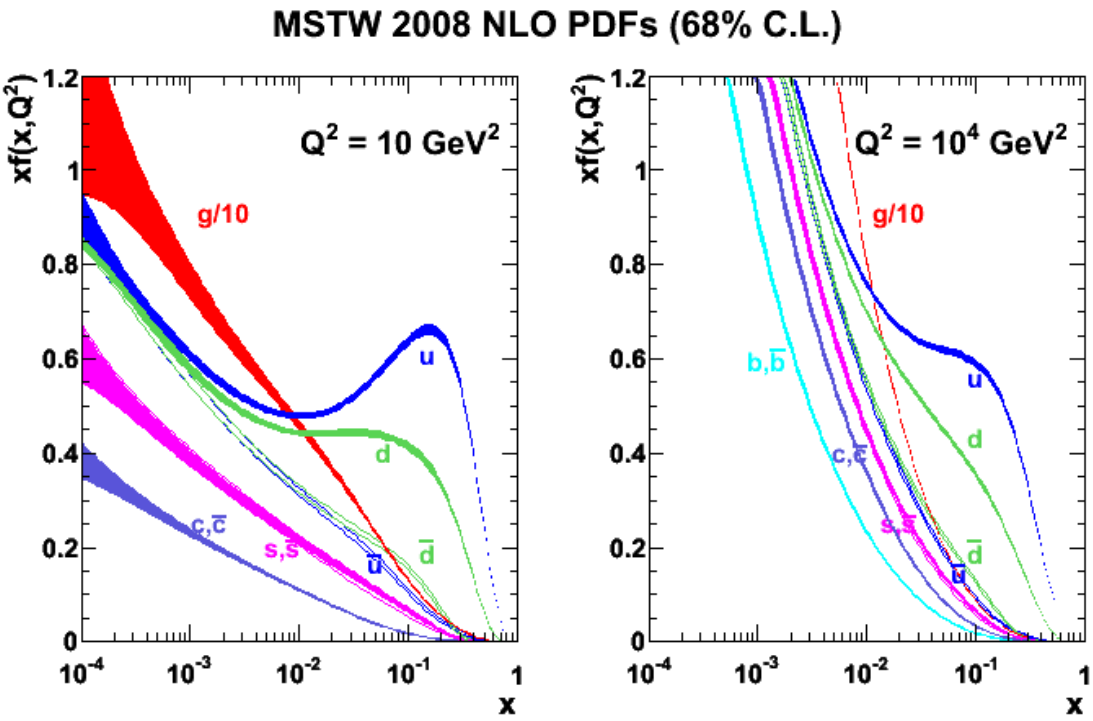

Figure 7.1: PDFs of quarks and the gluon, evaluated at two factorisation scales, taken from [186]

limit. They are now available to three-loop level [190, 191].

Once we have a set of PDFs for our colliding hadrons a and b, we then require a partonic cross section $\hat{\sigma}(x_1, x_2, \mu_R^2, \mu_F^2)$ for all possible initial states, in principle valid for all possible parton momenta. We integrate over the momenta, with PDFs folded in, and sum over the possible initial states. We will then have a total cross section $\sigma(\mu_R^2, \mu_F^2)$

$$\sigma(\mu_R^2, \mu_F^2) = \sum_{i,j} \int dx_i dx_j f_i^{(a)}(x_i, \mu_F^2) f_j^{(b)}(x_j, \mu_F^2) \hat{\sigma}(x_i, x_j, \mu_R^2, \mu_F^2). \tag{7.3.2}$$

7.3.2 Parton Showering

If we have any final-state partons, they will have been produced by hard-scale QCD, in a regime with a small strong coupling constant. Then, moving away from the event, they will radiate near-collinear partons and the scale will reduce [192–194]. In order to implement this evolution, we form a probability [195] that there will be

no branching in the evolution of a parton p from a scale[9] t to t' by integrating and exponentiating Equation (7.3.1):

$$P^{(p)}(x,t,t') = \exp\left\{ -\int_t^{t'} \frac{d\tau}{\tau} \int_x^{y_{max}} \frac{\alpha_s(y,\tau)}{2\pi} \frac{dy}{y} \sum_j \kappa_{ij}(y,\tau) \frac{f_j(\frac{x}{y},\tau)}{f_j(x,\tau)} \right\}, \quad (7.3.3)$$

where we recognise that there is a scale at which the parton will hadronise (see the following section), which gives the maximum energy fraction y_{max}. Using this technique, one hard parton produced in the event will be evolved down to several partons with hadronisation-scale energies.

7.3.3 Hadronisation

In Section 7.3.1, we moved from hadrons to initial state partons. Now that, after showering, we have final state partons, we must hadronise to model the particles which will be seen in the detector: as it is non-perturbative, this process is performed by phenomenological models, for example the Lund string model [196] and the cluster model [197].

7.3.4 Les Houches Interface

In order to interface a one-loop matrix element programme (OLP), with a Monte Carlo event generator (MC), which will perform the tree-level parts of the calculation, the subtraction terms and the phase-space integration, the Binoth Les Houches Accord has been developed [198][10]

In this accord, there are two phases: initialisation and runtime. In the initialisation phase, the MC produces an order file in a standard format, containing a list of subprocesses (such as different quark initial states in a proton collider) and a number of commands describing the desired characteristics of the calculation, such

[9] Different techniques use different definitions of this scale quantity: the angle between the partons and their relative transverse momentum p_T are two popular choices. Sherpa takes the latter.

[10] This follows on from accords dealing firstly with the interface between matrix element event generators on the one hand and parton shower and hadronisation event generators on the other [199], and secondly with standard event files [200].

as the model and the type of correction (QCD or EW). This file is read by the OLP, which returns a contract file with statements on which of the options are acceptable, and error messages if any are not. After these errors have been addressed by the user and the contract file shows no errors, it is passed to the MC. The OLP provides functions that can be called by the MC: `GoSam` does this by generating the code required for the process, and supplying a library to be linked by the MC.

At the runtime phase, the MC will call an initialisation routine for the OLP and then a routine to calculate each point desired by the MC. This process is shown in Figure 7.2, taken from [151].

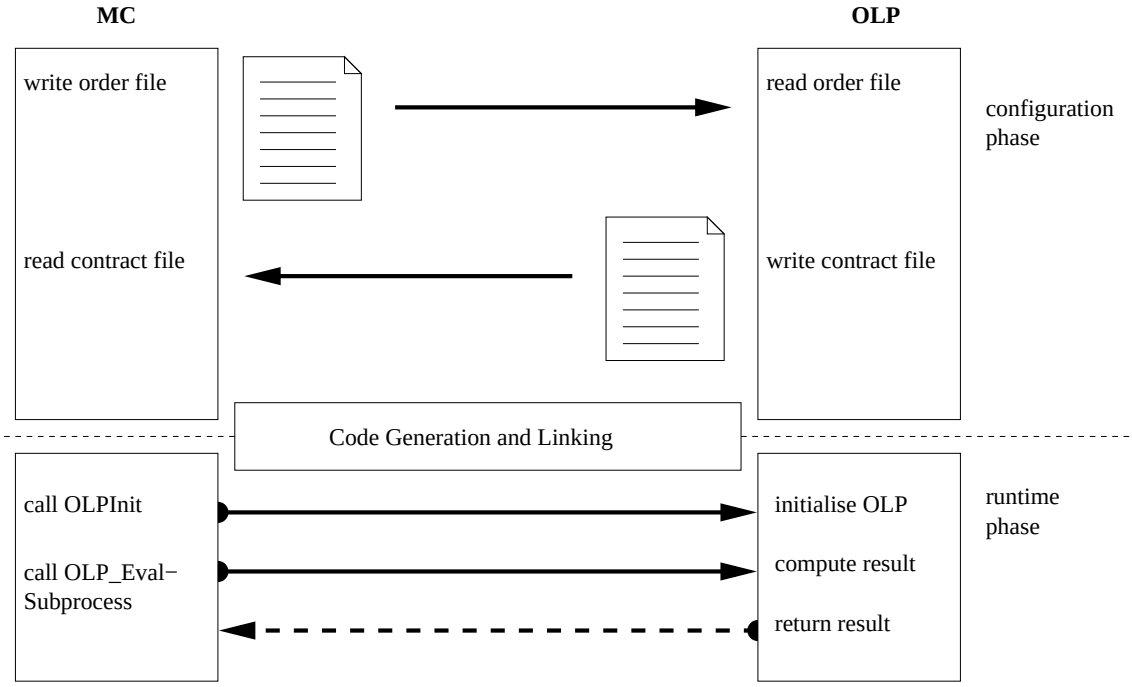

Figure 7.2: The interaction between Monte Carlo event generator and One Loop Programme using the Binoth Les Houches Accord, from [151].

7.4 Four Charged Lepton production $pp \to e^+e^-\mu^+\mu^-$

In this section, we describe the NLO calculation of the production of four charged leptons at the LHC, using `GoSam` coupled to `Sherpa`. In the work of this thesis, two components of the calculation, quark-initiated and gluon-initiated, were performed

separately and summed, as in [145]. This gives the best estimate of the cross section that can be obtained without a full NNLO calculation.

Throughout, we used the parameters in Appendix A of [201], which are given in Appendix A.2 for ease of reference. In this section, two distinct pairs of values for Higgs mass and width are used in different comparisons, as explained in the text.

7.4.1 Quark-initiated Process

This part of the calculation is of the classic type detailed in Chapter 3. There is a tree-level cross-section at $\mathcal{O}(\alpha^4)$, with diagrams like those in Figure 7.3. Then we also calculate the one-loop diagrams involving a gluon, such as in Figure 7.4, and also strong real emission diagrams, as in Figure 7.5, which only come from initial state radiation. This is then an $\mathcal{O}(\alpha_s\alpha^4)$ cross-section calculation. The neutral vector boson can be Z or γ, and we have both resonant and non-resonant diagrams[11] (as in Figure 7.3, left and right respectively). For this process, it was possible to use

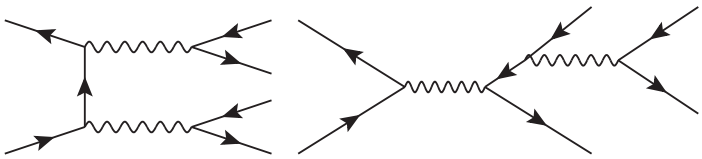

Figure 7.3: Two leading order diagrams.

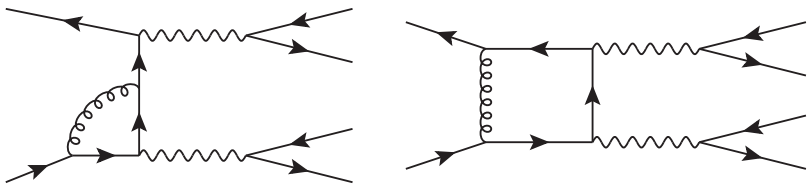

Figure 7.4: Two one-loop diagrams.

[11]The terms *resonant* and *non-resonant* are used in this thesis to refer to the left and right-hand diagrams of Figure 7.3 respectively: some authors would use the terms *doubly-resonant* and *singly-resonant* respectively, but this distinction is not needed here as we have no diagrams which have no resonance at all. We then refer to the contribution from each diagram in the same way, and so, for example, the contribution from the left-hand diagram of Figure 7.3 when we have one off-shell photon and one off-shell Z-boson is part of our *resonant* contribution.

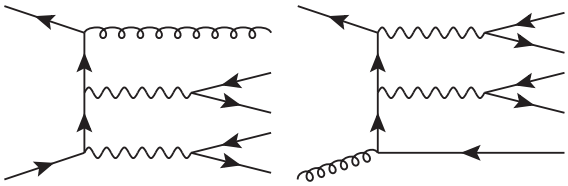

Figure 7.5: Two real emission diagrams.

the Binoth Les Houches Interface (see Section 7.3.4) to combine `GoSam` and `Sherpa`. The tree-level and real emission contributions, and the phase space integration (using `Amegic` [202]), were performed by `Sherpa`, which called `GoSam` for the one-loop part[12].

7.4.2 Gluon-initiated Process

This calculation includes all the channels for the $gg \to e^+e^-\mu^+\mu^-$ cross-section at $\mathcal{O}(\alpha_s^2\alpha_{QED}^4)$. The charged leptons originate from neutral vector bosons (Z or γ): either these are produced via a quark box, or a Higgs boson is produced via a b- or t-quark triangle and decays into two Z-bosons (Figure 7.6, left and right respectively). No effective vertices are included. No approximation is made in the decays of the neutral vector bosons into the leptons, so spin correlations are fully included.

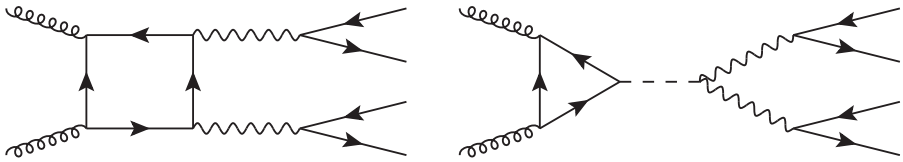

Figure 7.6: Two gluon-initiated one-loop diagrams.

Those diagrams with a triangle with one external electroweak vector boson, of the type of Figure 7.7, are suppressed by the Landau-Yang theorem [203, 204], and we do not include them.

[12] `GoSam` calculates the one-loop interference term with its own implementation of the Born matrix element, so `Sherpa` takes the `GoSam` one-loop value, divides by `GoSam`'s Born result and multiplies by `Sherpa`'s Born result.

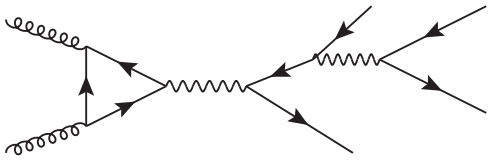

Figure 7.7: A diagram which is suppressed due to the Landau-Yang theorem.

This process, having no tree level and so contributing as $|\mathcal{M}_{1loop}|^2$, is formally NNLO[13] in α_s. However, for high proton energy environments, such as in the LHC, the gluon PDF (see Section 7.3.1) is very large, giving a sufficient enhancement for this component to be significant. We find it to give a 7% contribution to the overall cross-section for our cuts (see Table 7.4).

For this process, because `Sherpa` cannot process a loop-induced amplitude, it was necessary to write a process-specific interface for `Sherpa`, using the Les Houches library files of `GoSam`, and the `Sherpa` phase-space integrator `Comix` [205].

7.4.3 Comparison with `gg2VV`

The programme `gg2VV` [148] is both a one-loop integrator and an event generator for the processes $gg \to VV$, with $V = W, Z$, including the Higgs boson channel. Before we performed the comparison detailed below, of the `GoSam+Sherpa` cross-section (integrated over phase space) with the published result, one of the authors kindly provided results for a few phase space points that we were able to use for checking our implementation. One such point is given in Table 7.2: the agreement is very good, with deviations on the 10^{-7} level.

In [148] the calculation $gg \to e^+e^-\mu^+\mu^-$ is performed, with a Higgs boson of mass 400 GeV and width 29.16 GeV, for $\sqrt{s} = 7$ TeV and $\mu_F = \mu_R = 200$ GeV. Two sets of cuts are used:

[13] When seen as a contribution to $pp \to e^+e^-\mu^+\mu^-$: if instead we were considering the calculation purely of $gg \to e^+e^-\mu^+\mu^-$, then this would be an LO calculation.

ZZ standard: $p_{T,l} > 20\,\text{GeV}$; $|\eta_l| < 2.5$; $76\,\text{GeV} < M_{e^+e^-}, M_{\mu^+\mu^-} < 106\,\text{GeV}$

ZZ Higgs search: The above, plus $|M_{e^+e^-\mu^+\mu^-} - M_H| < \Gamma_H$

where $\eta = -\log\left(\tan\left(\frac{\theta}{2}\right)\right)$ is the pseudorapidity, with θ the angle from the beam-line. The PDF set used is MSTW2008LO with 1-loop running of α_s, which has $\alpha_s(M_Z) = 0.13939$. We performed the same calculation in `GoSam+Sherpa`, and in Table 7.3, the cross-section results are compared. We see that the results are consistent, and that our integration errors are much larger.

Particle	Energy	p_x	p_y	p_z
g_1	1699.6232364577	0.0000000000000	0.0000000000000	1699.6232364577
g_2	16.394675394750	0.0000000000000	0.0000000000000	-16.394675394750
e^+	801.30664127984	-115.74320293321	86.268438448558	788.19642276630
e^-	34.234962490356	-17.086266666690	-9.4233544743312	28.129922476999
μ^+	47.037479680574	4.6603922623004	-2.5256841121306	46.737845034058
μ^-	833.43882840158	128.16907733758	-74.319399862087	820.16437078550

	without Higgs	$m_H = 400\,\text{GeV}$
`gg2VV`	$7.6430935 \times 10^{-13}$	$1.4272669 \times 10^{-13}$
`GoSam`	$7.6430963 \times 10^{-13}$	$1.4272667 \times 10^{-13}$

Table 7.2: Comparison of a phase-space point from `gg2VV` with our own calculation.

	`gg2VV` σ/fb	`GoSam+Sherpa` σ/fb
Standard	0.7012(8)	0.691(14)
Higgs search	0.2867(3)	0.291(5)

Table 7.3: Comparison of cross-sections from [148] with our own, for cuts given in the text.

7.4.4 Results and Comparison with MCFM

In this section, the results for this process are presented for the 7 TeV LHC. We continue to use the ZZ standard cuts from [148] (see Section 7.4.3), and the PDF detailed there is used for the gluon-initiated process. For the quark-initiated component, the MSTW2008NLO set[14] is used with two-loop running and $\alpha_s(M_Z) = 0.12018$.

The results produced by MCFM [173] do not include the Higgs, and so the results in this section refer to a Higgsless calculation. The bottom quark is taken to be massless, and a five-flavour scheme for the proton is used.

The programme MCFM includes a process which it refers to as ZZ production [110, 144], but which includes decays to charged leptons, non-resonant contributions, and the contribution of off-shell photons, which renders it the same process as we are calculating.

For the quark-initiated process, the programmes were of comparable speed, with GoSam+Sherpa taking 5ms per phase space point (averaged over Born, virtual[15] and real phase spaces), and MCFM requiring 20ms per point in the Born+virtual phase space and 6ms in the real phase space. However for the gluon-initiated process, due both to the bespoke and unoptimised way in which GoSam's calculation was interfaced to Sherpa, and to the comparison of a numerical double one-loop calculation with the evaluation of an analytic expression, GoSam+Sherpa's evaluation was more than two orders of magnitude slower than that of MCFM (900ms and 3ms per phase-space point respectively). However, in order to reduce the error estimates for the values in the histograms to a comparable level, much larger runs were required in MCFM, so the total running times of the two programmes were comparable[16].

In MCFM, the leptons are not marked with their flavour, so it is not known which

[14] Interfaced using LHAPDF [206].

[15] In this section we include the calculation of Catani-Seymour subtraction terms [46] within the virtual and real components (we use a Nagy α-parameter 0.01 [207]).

[16] Here, we have excluded the time for generation of GoSam's one-loop amplitude code, which of course only has to be performed once. It was highly parallelised, but required approximately 250 hours of computing time in total.

	MCFM		GoSam+Sherpa	
	qq	gg	qq	gg
σ/fb	5.2059(7)	0.35573(15)	5.226(11)	0.358(4)
Points	8×10^7	10^7	10^7	10^6

Table 7.4: Comparison of cross-sections from MCFM with our own, for cuts given in the text. The MCFM qq-initiated points are approximately 10% Born+virtual calls, the rest being real.

lepton flavour pair is which. Instead, we talk of the same-flavour opposite-sign pairs as *first and second* leptons and *third and fourth* leptons. Due to the symmetry of the problem, a comparison of any MCFM lepton with any GoSam+Sherpa one is fair, and so we compare the electron with the first lepton and the electron-positron pair with the first-second pair. It should be noted that this implied ordering is merely bookkeeping: it does not, for example, imply that the first lepton is the one with the highest p_T.

At the end of this chapter, Figures 7.8–7.12 are given, comparing the results of GoSam+Sherpa and MCFM. In these, a "Ratio" is also given, which is the difference of the GoSam+Sherpa and MCFM values in that bin, normalised to the MCFM value. We find very good agreement between the results of the programmes, providing a solid confirmation of the GoSam+Sherpa implementation.

The scale variation is also shown on these plots, with the central value being $\mu_R = \mu_F = \mu = H_T$ and the range being $\frac{1}{2}H_T < \mu < 2H_T$, where H_T is the scalar sum of the transverse momenta of event's final state particles.

One difference between the implementations is that MCFM uses an overall factor scheme for its complex masses, whereas we use a fixed width (see Section 6.1). Given the closeness of the results, it can be seen that this scheme difference does not produce a significant deviation.

7.4.5 Higgs Interference

When considering a specific signal process, experimentalists often consider it and and any background process to be separate. However, in taking $pp \to H \to ZZ$ as a signal and $pp \to ZZ$ excluding the Higgs as background, an artificial split is made, and it is important to consider not only these two processes in isolation, but also the interference between them, as in [148].

In order to investigate this, we performed a calculation with a Higgs of mass $m_H = 125\,\text{GeV}$ and width $\Gamma_H = 4.03$ MeV (taken from [100]). Because the proton was taken to contain a massless b-quark, the only impact was on the gluon-initiated case (although there, the coupling of the b-quark to the Higgs was included).

In order to assess the interference, the full calculation is compared with the sum of the calculations $pp \to ZZ$ without Higgs and $pp \to H \to ZZ$, including a plot of the full calculation minus the sum, normalised to the full cross-section. This is a measure of the interference effect. For comparison, the size of the signal divided by the full calculation result is also given. The results are plotted in Figures 7.13–7.22.

We can see that, for the variables shown, interference effect is not clearly discernible in the calculation including both quark and gluon initial states. In the purely gluon-initiated case, however, there is a negative interference effect on the percent level, particularly clear on the ratio plots (Figures 7.14, 7.16, 7.18, 7.20 and 7.22). This is consistent with the negative interference on the percent level found in [148], although better precision will be required to prove and quantify this effect: this will form part of future work.

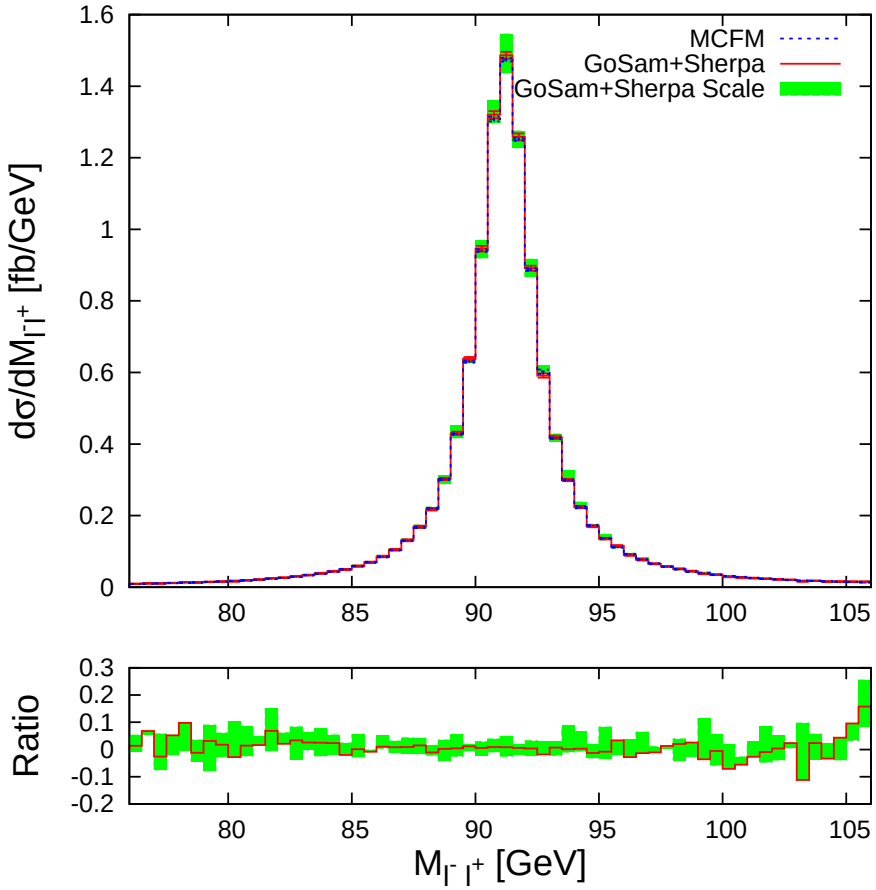

Figure 7.8: For the process $pp \to e^+e^-\mu^+\mu^-$, a comparison plot of the distribution of the invariant mass of the electron pair calculated with `MCFM` (blue dotted line), and with `GoSam+Sherpa` (red solid line), including the latter's scale uncertainty (green fill). The factorisation and renormalisation scales are taken to be equal and to vary in the range $\frac{1}{2}H_T < \mu < 2H_T$. The qq-initiated subprocess is calculated to NLO, and the one-loop-induced gg-initiated process is included. Integration error bars are shown, but are too small to be visible on many points. The lower plot shows the "Ratio", defined as ((`GoSam+Sherpa` value) - (`MCFM` value))/`MCFM` value, along with its scale variation.

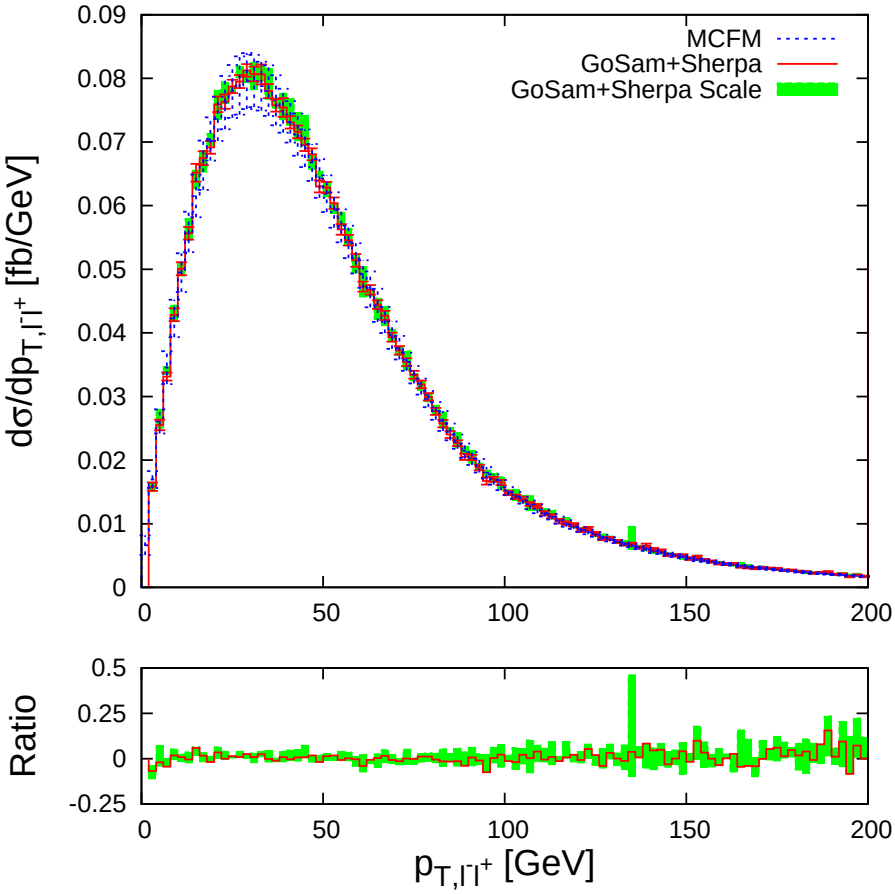

Figure 7.9: The p_T of the electron pair, in the process $pp \to e^+e^-\mu^+\mu^-$, comparing `MCFM` (blue dotted line) with `GoSam+Sherpa` (red solid line), including scale uncertainty (green fill). The details are the same as for Figure 7.8. This plot is constructed using a larger `MCFM` run, 3.8×10^8 points, in order to reduce its errors.

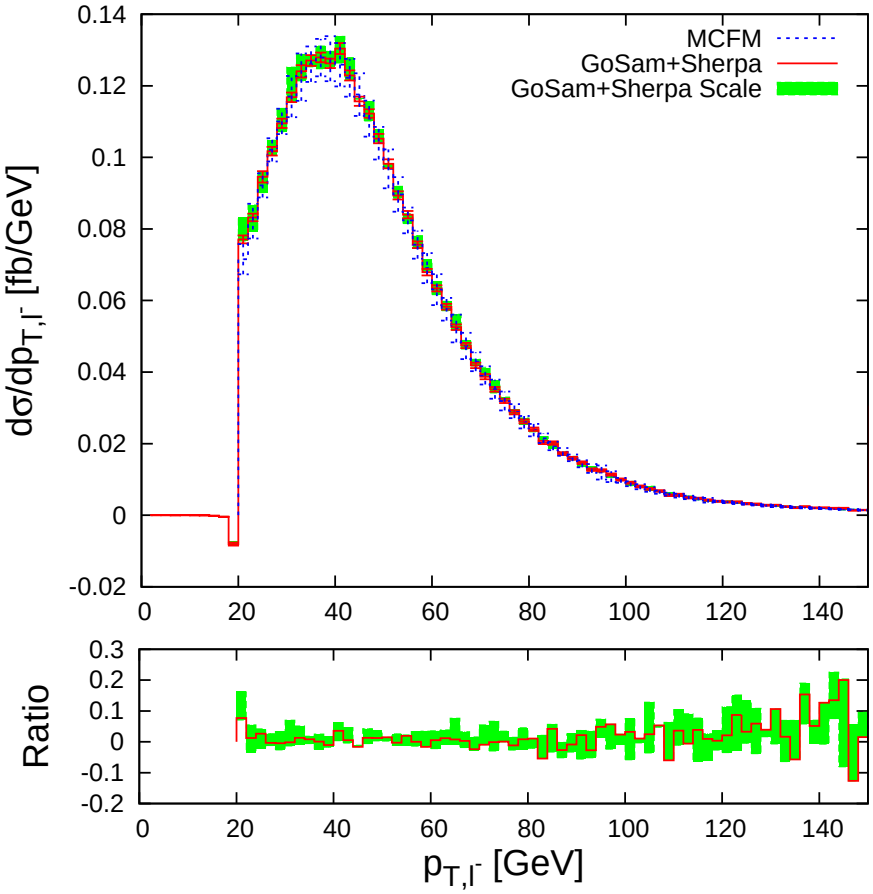

Figure 7.10: The p_T of the electron, in the process $pp \to e^+e^-\mu^+\mu^-$, comparing `MCFM` (blue dotted line) with `GoSam+Sherpa` (red solid line), including scale uncertainty (green fill). The details are the same as for Figure 7.8. The negative value in the bins below the electron cut value are due to a numerical issue: p_T values calculated at the event-generation level, which determine which events pass these cuts, can be different from the analysis-level calculations by a small amount, allowing "leakage" to below 20GeV.

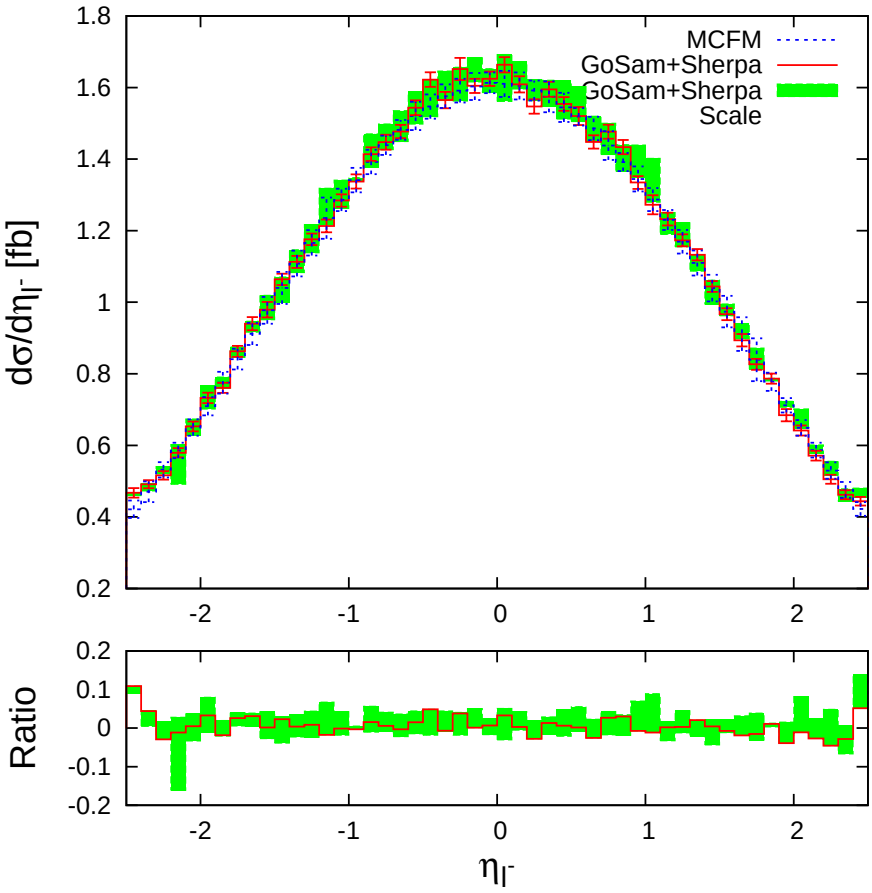

Figure 7.11: The pseudorapidity η of the electron, in the process $pp \to e^+e^-\mu^+\mu^-$, comparing `MCFM` (blue dotted line) with `GoSam+Sherpa` (red solid line), including scale uncertainty (green fill). The details are the same as for Figure 7.8.

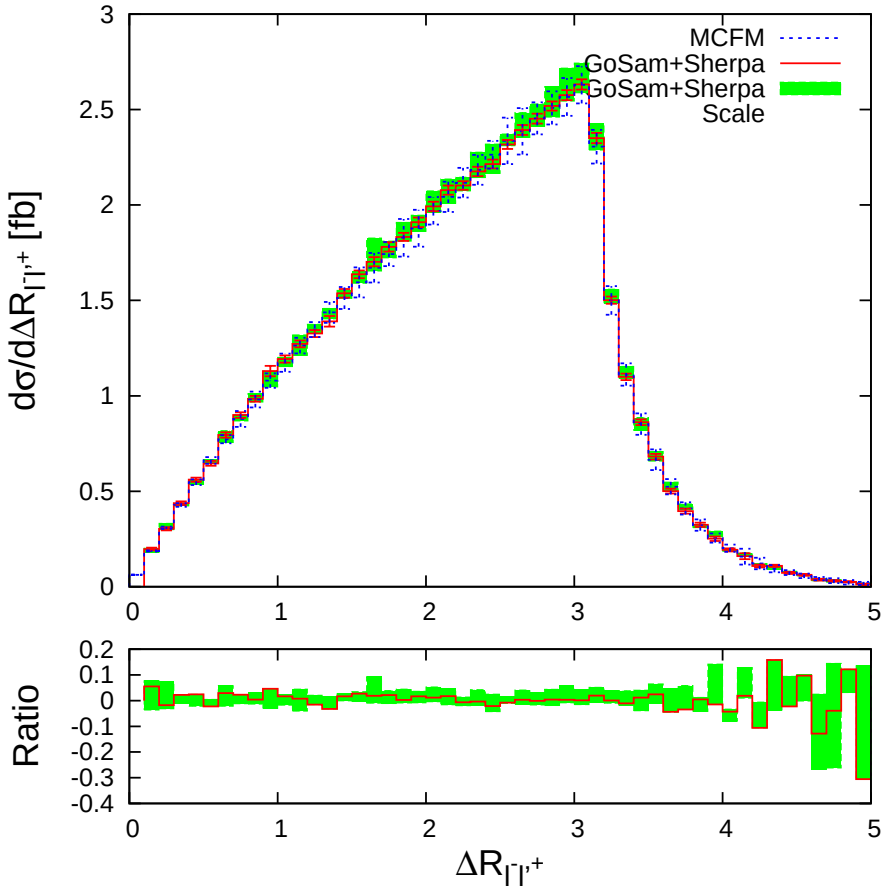

Figure 7.12: The $\Delta R = \sqrt{(\Delta\phi)^2 + (\Delta\eta)^2}$, with ϕ the azimuthal angle between the electron and the antimuon, in the process $pp \to e^+e^-\mu^+\mu^-$, comparing `MCFM` (blue dotted line) with `GoSam+Sherpa` (red solid line), including scale uncertainty (green fill). The details are the same as for Figure 7.8.

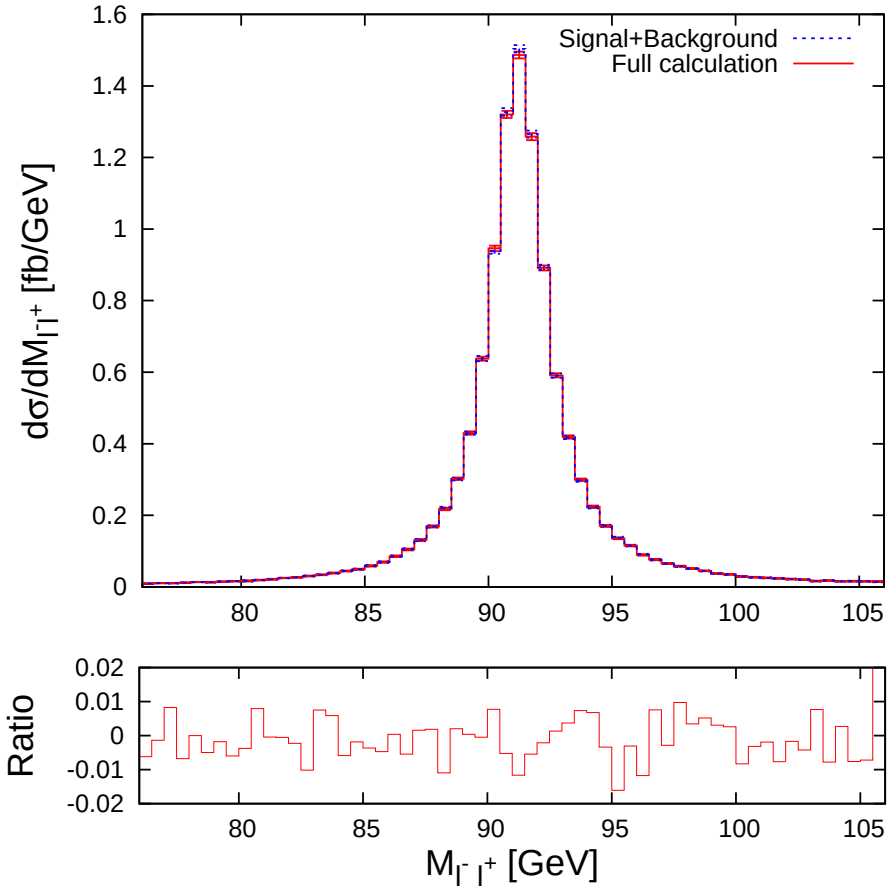

Figure 7.13: The invariant mass of the electron pair with `GoSam+Sherpa`, for the process $pp \to e^+e^-\mu^+\mu^-$. Both the qq-initiated subprocess (calculated to NLO), and the one-loop-induced gg-initiated process are included. The plot shows the sum of the results without the Higgs and the Higgs contribution ("Signal+Background" blue dotted line), and a full calculation (red solid line). Integration error bars are shown. The lower plot shows the normalised difference between the two lines, Ratio $\equiv$ ((Signal+Background)-(Full calculation))/(Full calculation), in order to show the size of the negative interference.

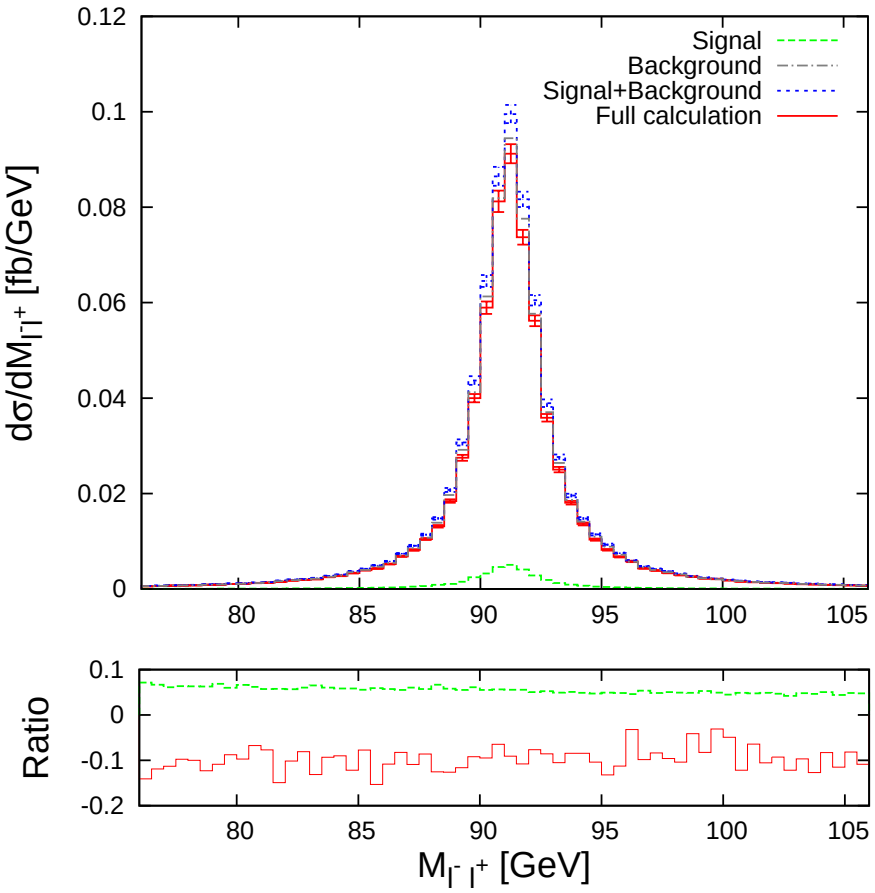

Figure 7.14: For the gluon-initiated channel only in $e^+e^-\mu^+\mu^-$ production: the invariant mass of the electron pair with `GoSam+Sherpa`. Without the Higgs ("Background" grey, dot-dash line), only the Higgs contribution ("Signal" green, dashed line), their sum (blue dotted line), and a full calculation (red solid line). Integration error bars are shown only for the latter two cases. On the lower plot, as well as Ratio $\equiv$ ((Signal+Background)-(Full calculation))/(Full calculation), which shows the size of the negative interference, the ratio of signal to full cross-section is shown (green dashed line).

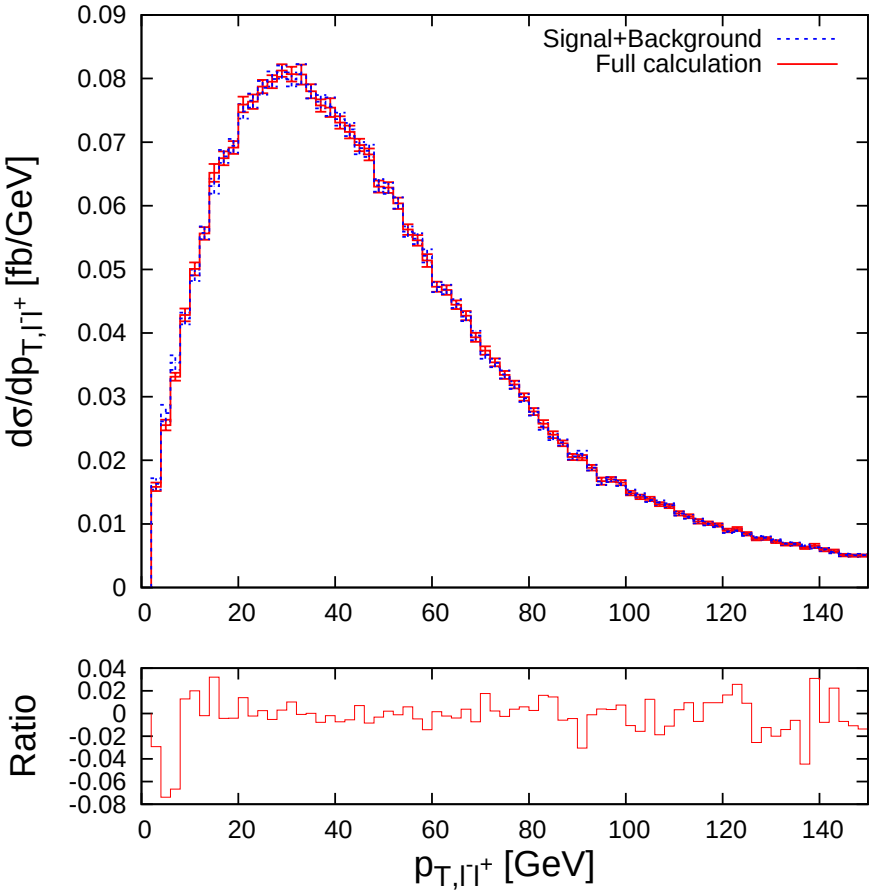

Figure 7.15: The p_T of the electron pair from `GoSam+Sherpa`, for the process $pp \to e^+e^-\mu^+\mu^-$. The sum of the results without the Higgs and the Higgs contribution ("Signal+Background" blue dotted line), and a full calculation (red solid line), as in Figure 7.13.

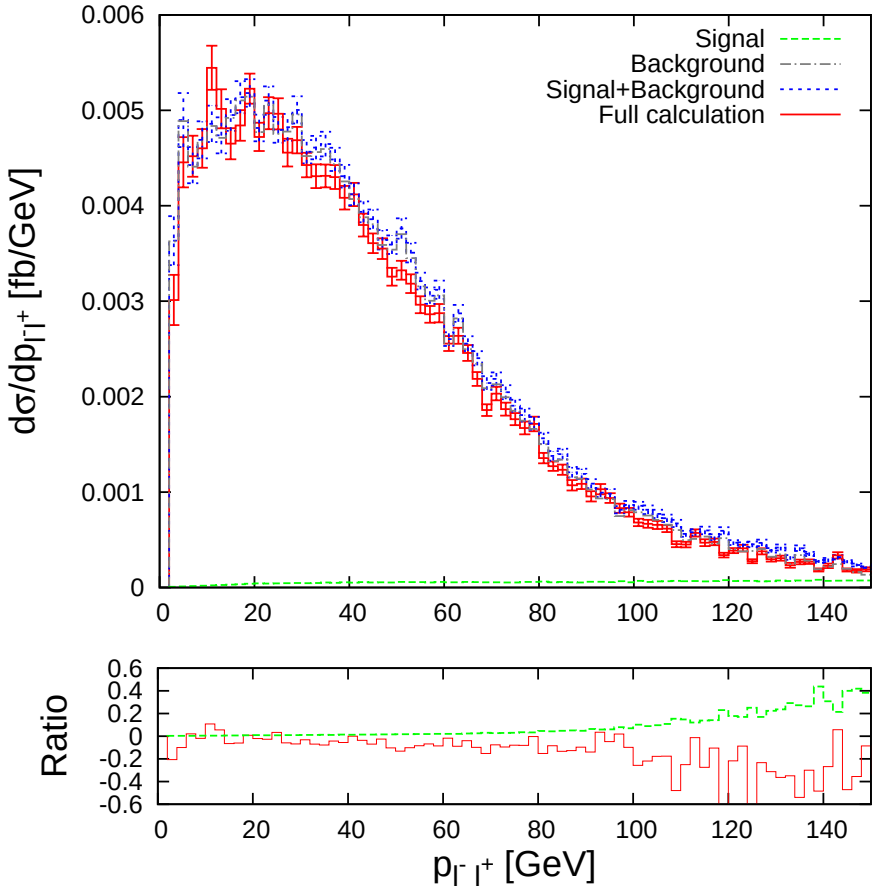

Figure 7.16: For the gluon-initiated channel only in $e^+e^-\mu^+\mu^-$ production: the p_T of the electron pair from `GoSam+Sherpa`. Without the Higgs ("Background" grey, dot-dash line), only the Higgs contribution ("Signal" green, dashed line), their sum (blue dotted line), and a full calculation (red solid line), as in Figure 7.14.

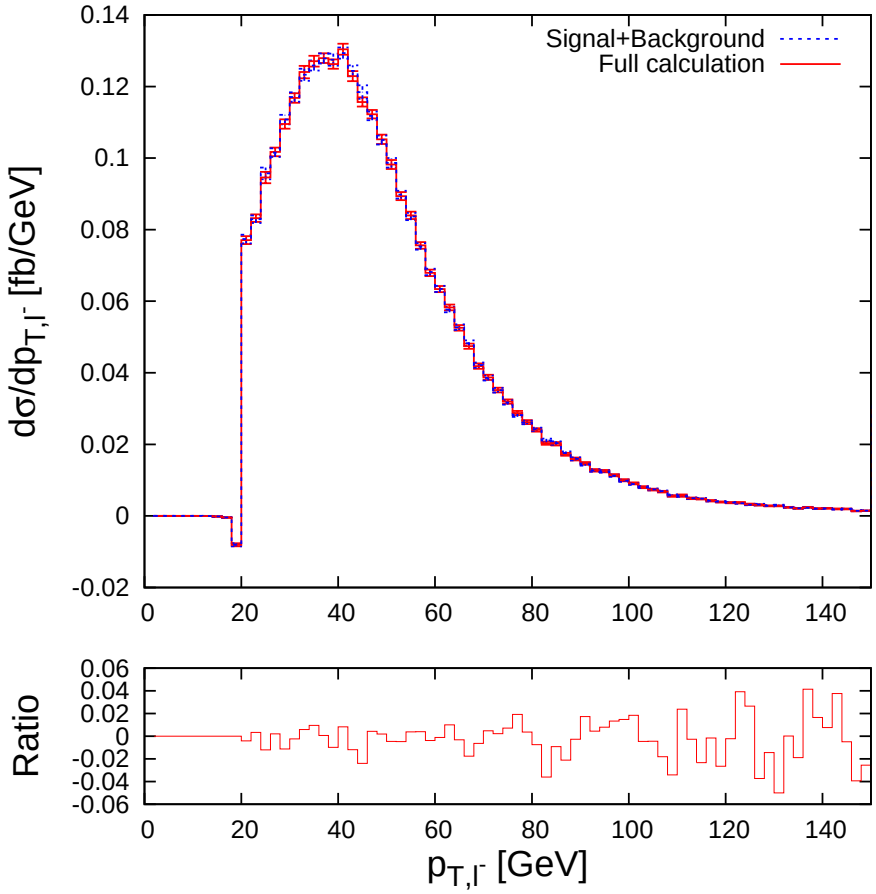

Figure 7.17: The p_T of the electron from `GoSam+Sherpa`, for the process $pp \to e^+e^-\mu^+\mu^-$. The sum of the results without the Higgs and the Higgs contribution ("Signal+Background" blue dotted line), and a full calculation (red solid line), as in Figure 7.13. The negative bin issue occurs, as in Figure 7.10

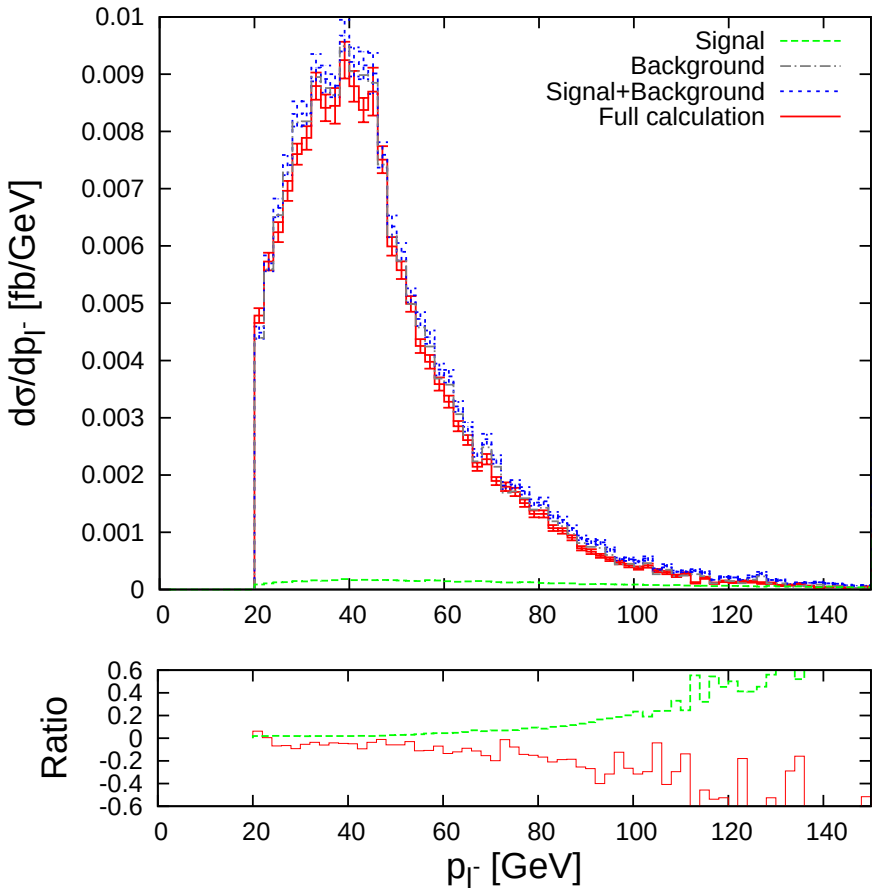

Figure 7.18: For the gluon-initiated channel only in $e^+e^-\mu^+\mu^-$ production: the p_T of the electron from `GoSam+Sherpa`. Without the Higgs ("Background" grey, dot-dash line), only the Higgs contribution ("Signal" green, dashed line), their sum (blue dotted line), and a full calculation (red solid line), as in Figure 7.14.

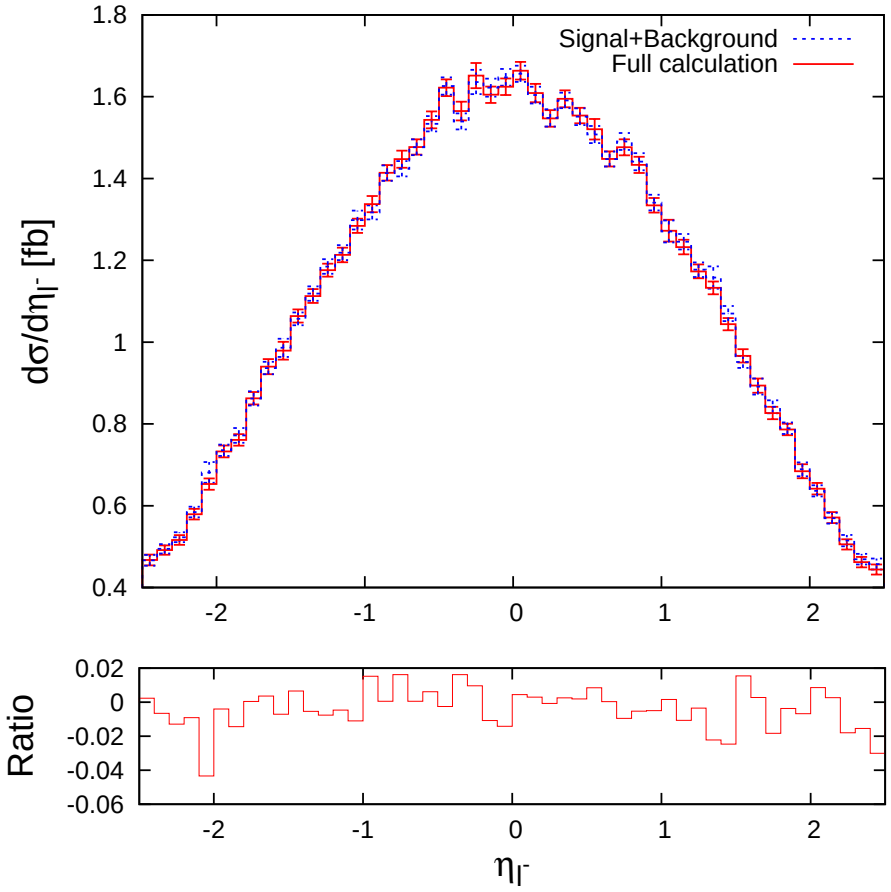

Figure 7.19: The pseudorapidity η of the electron from `GoSam+Sherpa`, for the process $pp \to e^+e^-\mu^+\mu^-$. The sum of the results without the Higgs and the Higgs contribution ("Signal+Background" blue dotted line), and a full calculation (red solid line), as in Figure 7.13.

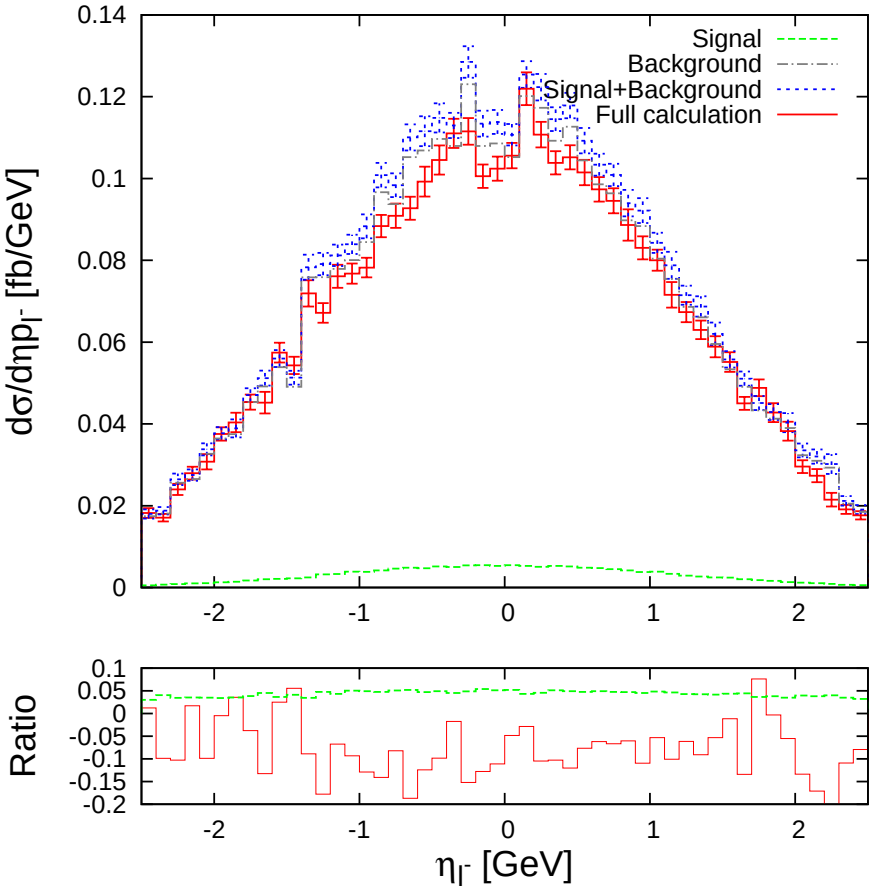

Figure 7.20: For the gluon-initiated channel only in $e^+e^-\mu^+\mu^-$ production: the pseudorapidity η of the electron from `GoSam+Sherpa`. Without the Higgs ("Background" grey, dot-dash line), only the Higgs contribution ("Signal" green, dashed line), their sum (blue dotted line), and a full calculation (red solid line), as in Figure 7.14.

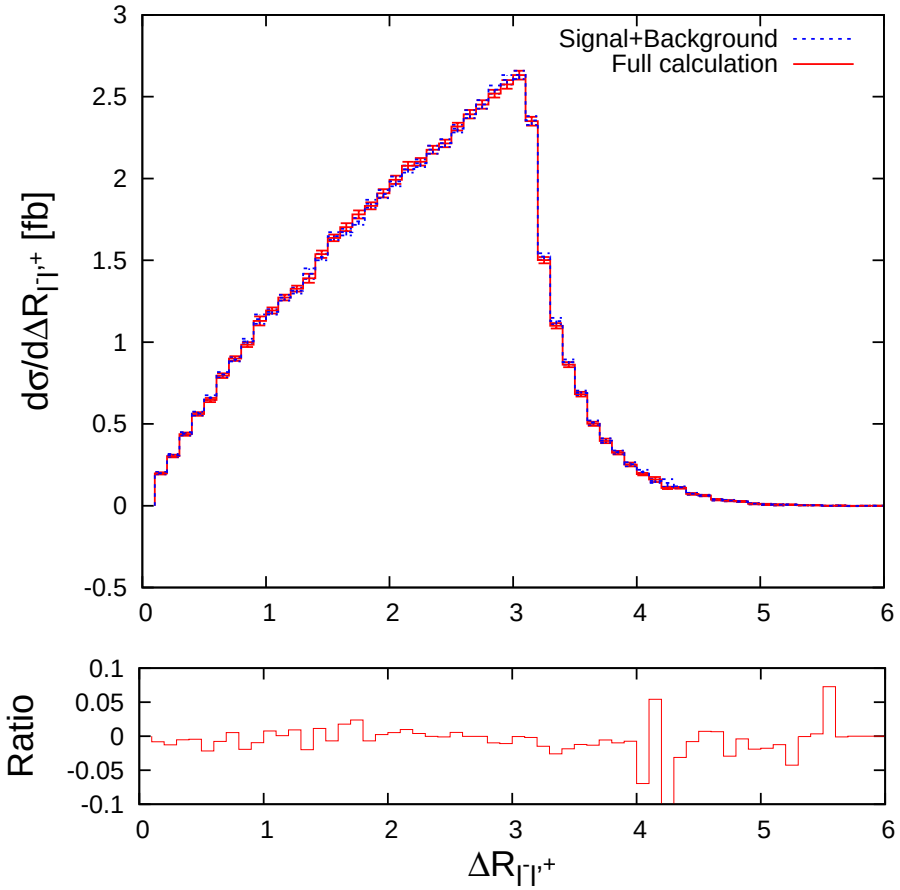

Figure 7.21: The $\Delta R = \sqrt{(\Delta\phi)^2 + (\Delta\eta)^2}$ between the electron and the antimuon from `GoSam+Sherpa`, for the process $pp \to e^+e^-\mu^+\mu^-$. The sum of the results without the Higgs and the Higgs contribution ("Signal+Background" blue dotted line), and a full calculation (red solid line), as in Figure 7.13.

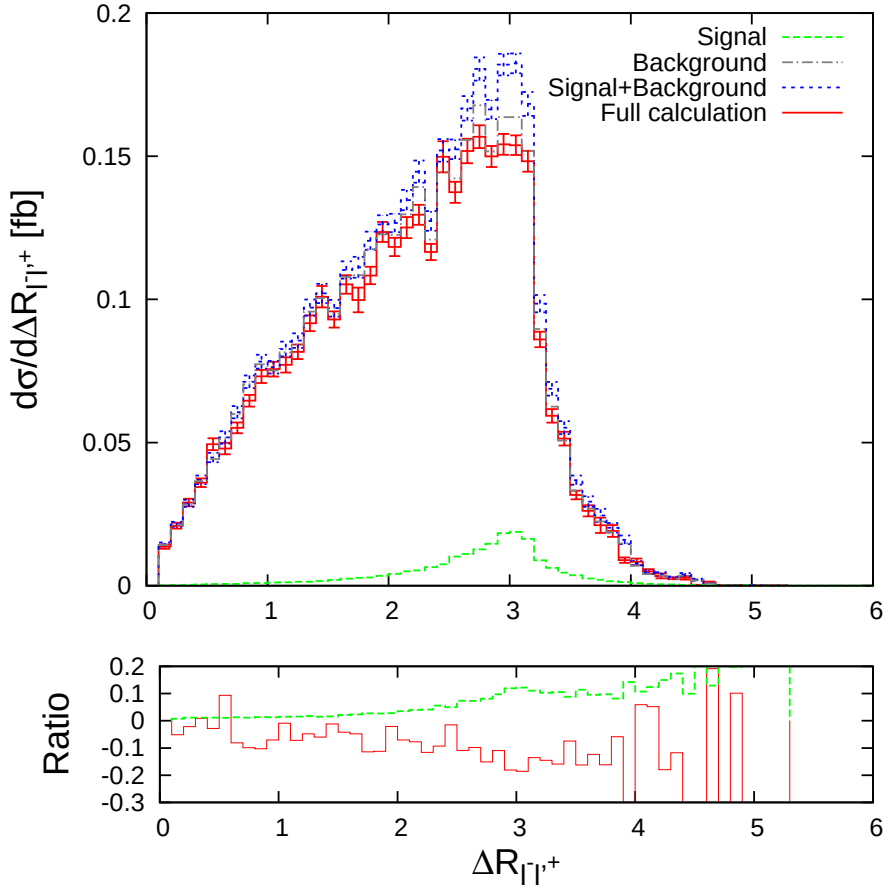

Figure 7.22: For the gluon-initiated channel only in $e^+e^-\mu^+\mu^-$ production: the $\Delta R = \sqrt{(\Delta\phi)^2 + (\Delta\eta)^2}$ between the electron and the antimuon from `GoSam+Sherpa`. Without the Higgs ("Background" grey, dot-dash line), only the Higgs contribution ("Signal" green, dashed line), their sum (blue dotted line), and a full calculation (red solid line), as in Figure 7.14.

Chapter 8

Conclusions

In this thesis we have laid out the process of tensor reduction and the construction of a library of integrals for the automated calculation of multiparticle processes at particle colliders. The methods in Chapters 4, 5 and 6 of this thesis are used to construct a numerically stable one-loop matrix element for a general process.

The methods increasing the numerical stability have come in three forms:

- using numerical integration as an alternative to the production of inverse Gram determinants, at both tensor-integral and scalar-integral level;
- using reexpressions of the functions which have better numerical behaviour in the required region; and
- using complex masses to avoid Landau singularities in cases with unstable particles.

Once we have constructed a one-loop matrix element, we can combine it with the tree-level, subtraction and real parts, provided externally, and then in order to obtain a physical observable we must integrate over phase-space. Because we are dealing with hadron colliders, the phase-space integration must be performed with the structure of the colliding protons folded in.

We were able to demonstrate the functioning of this full chain of tools by calculating the process $pp \to e^+e^-\mu^+\mu^-$, proceeding via neutral vector bosons, to NLO, with the additional inclusion of the (formally NNLO) loop-induced component $gg \to e^+e^-\mu^+\mu^-$. We used the Binoth Les Houches Accord to connect `GoSam`

with `Sherpa`: for the quark-initiated case it was possible to use the standard interface, but for the gluon-initiated process, a bespoke interfacing of the Les Houches library files was developed. Our calculation showed good agreement with another programme, `MCFM`, and the literature (specifically the numbers from `gg2VV`). We showed that this method can lead to a study of the interference effects of the Higgs to ZZ decay signal with the diboson background.

There are some excellent possibilities to expand this work in future. In terms of the production of two neutral vector bosons, it will be possible to expand this work to include other final states, particularly τ-lepton decays, which are not found in the literature. In addition, the interface gives us access to `Sherpa`'s parton shower machinery, allowing a specific study including both showering and the Higgs corrections, which is not yet available in the literature.

In addition, the general and powerful set of linked programmes that have been developed will permit us to explore further processes with a range of mass scales and up to six external legs: this is particularly relevant in the era of the LHC, which creates many processes with multiple mass scales.

Bibliography

[1] P.A.M. Dirac. The Quantum theory of the electron. *Proc.Roy.Soc.Lond.*, A117:610–624, 1928.

[2] E. Fermi. Quantum theory of radiation. *Rev. Mod. Phys.*, 4:87–132, Jan 1932.

[3] C.-N. Yang and R. L. Mills. Conservation of Isotopic Spin and Isotopic Gauge Invariance. *Phys.Rev.*, 96:191–195, 1954.

[4] P. W. Higgs. Broken symmetries, massless particles and gauge fields. *Phys.Lett.*, 12:132–133, 1964.

[5] P. W. Higgs. Broken Symmetries and the Masses of Gauge Bosons. *Phys.Rev.Lett.*, 13:508–509, 1964.

[6] F. Englert and R. Brout. Broken Symmetry and the Mass of Gauge Vector Mesons. *Phys.Rev.Lett.*, 13:321–323, 1964.

[7] G.S. Guralnik, C.R. Hagen, and T.W.B. Kibble. Global Conservation Laws and Massless Particles. *Phys.Rev.Lett.*, 13:585–587, 1964.

[8] S.L. Glashow. Partial Symmetries of Weak Interactions. *Nucl.Phys.*, 22:579–588, 1961.

[9] S. Weinberg. A Model of Leptons. *Phys.Rev.Lett.*, 19:1264–1266, 1967.

[10] A. Salam. Weak and Electromagnetic Interactions. *Conf.Proc.*, C680519:367–377, 1968.

[11] M. Gell-Mann. A Schematic Model of Baryons and Mesons. *Phys.Lett.*, 8:214–215, 1964.

[12] G. Zweig. An SU(3) model for strong interaction symmetry and its breaking. 1964.

[13] J.J. Aubert et al. Experimental Observation of a Heavy Particle J. *Phys.Rev.Lett.*, 33:1404–1406, 1974.

[14] J.E. Augustin et al. Discovery of a Narrow Resonance in e+ e- Annihilation. *Phys.Rev.Lett.*, 33:1406–1408, 1974.

[15] K. A. Brueckner. Meson-Nucleon Scattering and Nucleon Isobars. *Phys.Rev.*, 86:106–109, 1952.

[16] O.W. Greenberg. Spin and Unitary Spin Independence in a Paraquark Model of Baryons and Mesons. *Phys.Rev.Lett.*, 13:598–602, 1964.

[17] M.Y. Han and Y. Nambu. Three Triplet Model with Double SU(3) Symmetry. *Phys.Rev.*, 139:B1006–B1010, 1965.

[18] G. Aad et al. Observation of a new particle in the search for the Standard Model Higgs boson with the ATLAS detector at the LHC. *Phys.Lett.B*, 2012, hep-ex/1207.7214.

[19] S. Chatrchyan et al. Observation of a new boson at a mass of 125 GeV with the CMS experiment at the LHC. *Phys.Lett.B*, 2012, hep-ex/1207.7235.

[20] Precision electroweak measurements on the Z resonance. *Phys.Rept.*, 427:257–454, 2006, hep-ex/0509008.

[21] M. E. Peskin and D. V. Schroeder. An Introduction to quantum field theory. 1995.

[22] P. Z. Skands. QCD for Collider Physics. 2011, hep-ph/1104.2863.

[23] R. Brock et al. Handbook of perturbative QCD: Version 1.0. *Rev.Mod.Phys.*, 67:157–248, 1995.

[24] A. Denner. Techniques for calculation of electroweak radiative corrections at the one loop level and results for W physics at LEP-200. *Fortsch.Phys.*, 41:307–420, 1993, hep-ph/0709.1075.

[25] M. Srednicki. Quantum field theory. 2007.

[26] T. Plehn. Lectures on LHC Physics. *Lect.Notes Phys.*, 844:1–193, 2012, hep-ph/0910.4182.

[27] R.P. Feynman. Space - time approach to quantum electrodynamics. *Phys.Rev.*, 76:769–789, 1949.

[28] A. Denner, H. Eck, O. Hahn, and J. Kublbeck. Feynman rules for fermion number violating interactions. *Nucl.Phys.*, B387:467–484, 1992.

[29] A. Denner, H. Eck, O. Hahn, and J. Kublbeck. Compact Feynman rules for Majorana fermions. *Phys.Lett.*, B291:278–280, 1992.

[30] J.A.M. Vermaseren. Axodraw. *Comput.Phys.Commun.*, 83:45–58, 1994.

[31] D. Binosi and L. Theussl. JaxoDraw: A Graphical user interface for drawing Feynman diagrams. *Comput.Phys.Commun.*, 161:76–86, 2004, hep-ph/0309015.

[32] W. Pauli and F. Villars. On the Invariant regularization in relativistic quantum theory. *Rev.Mod.Phys.*, 21:434–444, 1949.

[33] A. Denner and S. Dittmaier. Reduction schemes for one-loop tensor integrals. *Nucl.Phys.*, B734:62–115, 2006, hep-ph/0509141.

[34] G. 't Hooft and M.J.G. Veltman. Regularization and Renormalization of Gauge Fields. *Nucl.Phys.*, B44:189–213, 1972.

[35] C.G. Bollini and J.J. Giambiagi. Dimensional Renormalization: The Number of Dimensions as a Regularizing Parameter. *Nuovo Cim.*, B12:20–25, 1972.

[36] A. Signer and D. Stoeckinger. Using Dimensional Reduction for Hadronic Collisions. *Nucl.Phys.*, B808:88–120, 2009, hep-ph/0807.4424.

[37] F.J. Dyson. The Radiation theories of Tomonaga, Schwinger, and Feynman. *Phys.Rev.*, 75:486–502, 1949.

[38] J.C. Taylor. Ward Identities and Charge Renormalization of the Yang-Mills Field. *Nucl.Phys.*, B33:436–444, 1971.

[39] A.A. Slavnov. Ward Identities in Gauge Theories. *Theor.Math.Phys.*, 10:99–107, 1972.

[40] J.A.M. Vermaseren, S.A. Larin, and T. van Ritbergen. The four loop quark mass anomalous dimension and the invariant quark mass. *Phys.Lett.*, B405:327–333, 1997, hep-ph/9703284.

[41] M. Czakon. The Four-loop QCD beta-function and anomalous dimensions. *Nucl.Phys.*, B710:485–498, 2005, hep-ph/0411261.

[42] L.D. Faddeev and V.N. Popov. Feynman Diagrams for the Yang-Mills Field. *Phys.Lett.*, B25:29–30, 1967.

[43] J. C. Collins, D. E. Soper, and G. F. Sterman. Factorization of Hard Processes in QCD. *Adv.Ser.Direct.High Energy Phys.*, 5:1–91, 1988, hep-ph/0409313.

[44] T. Kinoshita. Mass singularities of Feynman amplitudes. *J.Math.Phys.*, 3:650–677, 1962.

[45] T.D. Lee and M. Nauenberg. Degenerate Systems and Mass Singularities. *Phys.Rev.*, 133:B1549–B1562, 1964.

[46] S. Catani and M.H. Seymour. A General algorithm for calculating jet cross-sections in NLO QCD. *Nucl.Phys.*, B485:291–419, 1997, hep-ph/9605323.

[47] S. Catani, S. Dittmaier, M. H. Seymour, and Z. Trocsanyi. The Dipole formalism for next-to-leading order QCD calculations with massive partons. *Nucl.Phys.*, B627:189–265, 2002, hep-ph/0201036.

[48] D. A. Kosower. Antenna factorization of gauge theory amplitudes. *Phys.Rev.*, D57:5410–5416, 1998, hep-ph/9710213.

[49] J. M. Campbell, M.A. Cullen, and E.W. N. Glover. Four jet event shapes in electron - positron annihilation. *Eur.Phys.J.*, C9:245–265, 1999, hep-ph/9809429.

[50] S. Frixione, Z. Kunszt, and A. Signer. Three jet cross-sections to next-to-leading order. *Nucl.Phys.*, B467:399–442, 1996, hep-ph/9512328.

[51] S. Frixione. A General approach to jet cross-sections in QCD. *Nucl.Phys.*, B507:295–314, 1997, hep-ph/9706545.

[52] D. B. Melrose. Reduction of Feynman Diagrams. *Il Nuovo Cimento X*, 40:181–213, 1965.

[53] G. Passarino and M.J.G. Veltman. One Loop Corrections for e+ e- Annihilation Into mu+ mu- in the Weinberg Model. *Nucl.Phys.*, B160:151, 1979.

[54] W.L. van Neerven and J.A.M. Vermaseren. LARGE LOOP INTEGRALS. *Phys.Lett.*, B137:241, 1984.

[55] T. Binoth, J.-Ph. Guillet, G. Heinrich, E. Pilon, and T. Reiter. Golem95: A Numerical program to calculate one-loop tensor integrals with up to six external legs. *Comput.Phys.Commun.*, 180:2317–2330, 2009, hep-ph/0810.0992.

[56] G. Ossola, C. G. Papadopoulos, and R. Pittau. Reducing full one-loop amplitudes to scalar integrals at the integrand level. *Nucl.Phys.*, B763:147–169, 2007, hep-ph/0609007.

[57] G. Ossola, C. G. Papadopoulos, and R. Pittau. CutTools: A Program implementing the OPP reduction method to compute one-loop amplitudes. *JHEP*, 0803:042, 2008, hep-ph/0711.3596.

[58] F. del Aguila and R. Pittau. Recursive numerical calculus of one-loop tensor integrals. *JHEP*, 0407:017, 2004, hep-ph/0404120.

[59] P. Mastrolia, G. Ossola, T. Reiter, and F. Tramontano. Scattering AMplitudes from Unitarity-based Reduction Algorithm at the Integrand-level. *JHEP*, 1008:080, 2010, hep-ph/1006.0710.

[60] Z. Bern, L.J. Dixon, D.C. Dunbar, and D.A. Kosower. One loop n point gauge theory amplitudes, unitarity and collinear limits. *Nucl.Phys.*, B425:217–260, 1994, hep-ph/9403226.

[61] C.F. Berger, Z. Bern, L.J. Dixon, F. Febres Cordero, D. Forde, et al. An Automated Implementation of On-Shell Methods for One-Loop Amplitudes. *Phys.Rev.*, D78:036003, 2008, hep-ph/0803.4180.

[62] W.T. Giele and G. Zanderighi. On the Numerical Evaluation of One-Loop Amplitudes: The Gluonic Case. *JHEP*, 0806:038, 2008, hep-ph/0805.2152.

[63] G. Heinrich, G. Ossola, T. Reiter, and F. Tramontano. Tensorial Reconstruction at the Integrand Level. *JHEP*, 1010:105, 2010, hep-ph/1008.2441.

[64] T. Binoth, J.P. Guillet, and G. Heinrich. Reduction formalism for dimensionally regulated one loop N point integrals. *Nucl.Phys.*, B572:361–386, 2000, hep-ph/9911342.

[65] T. Binoth, J.-Ph. Guillet, G. Heinrich, E. Pilon, and C. Schubert. An Algebraic/numerical formalism for one-loop multi-leg amplitudes. *JHEP*, 0510:015, 2005, hep-ph/0504267.

[66] J.R. Andersen et al. The SM and NLO Multileg Working Group: Summary report. pages 21–189, 2010, hep-ph/1003.1241.

[67] G. Cullen, N. Greiner, A. Guffanti, J.-Ph. Guillet, G. Heinrich, et al. Recent Progress in the Golem Project. *Nucl.Phys.Proc.Suppl.*, 205-206:67–73, 2010, hep-ph/1007.3580.

[68] T. Reiter, G. Cullen, N. Greiner, A. Guffanti, J.-Ph. Guillet, et al. Modern Feynman Diagrammatic One-Loop Calculations. *PoS*, CPP2010:003, 2010, hep-ph/1011.6632.

[69] S. Barnett. *Matrices: Methods and Applications, Chapter 10.* Oxford Applied Mathematics and Computing Sciences Series. Clarendon Press, Oxford, 1990.

[70] G. Dahlquist & Å. Björk. *Numerical Methods (trad. N. Anderson), Section 5.2.5.* Prentice-Hall series in automatic computations, 1974.

[71] G. Källén. Elementary Particle Physics. 1964.

[72] L.D. Landau. On analytic properties of vertex parts in quantum field theory. *Nucl.Phys.*, 13:181–192, 1959.

[73] A. I. Davydychev. A Simple formula for reducing Feynman diagrams to scalar integrals. *Phys.Lett.*, B263:107–111, 1991.

[74] Z. Bern, L.J. Dixon, and D.A. Kosower. Dimensionally regulated one loop integrals. *Phys.Lett.*, B302:299–308, 1993, hep-ph/9212308.

[75] George F. Sterman. Partons, factorization and resummation, TASI 95. 1995, hep-ph/9606312.

[76] S. Dittmaier. Separation of soft and collinear singularities from one loop N point integrals. *Nucl.Phys.*, B675:447–466, 2003, hep-ph/0308246.

[77] W.T. Giele and E.W.N. Glover. A Calculational formalism for one loop integrals. *JHEP*, 0404:029, 2004, hep-ph/0402152.

[78] R.K. Ellis and G. Zanderighi. Scalar one-loop integrals for QCD. *JHEP*, 0802:002, 2008, hep-ph/0712.1851.

[79] A. van Hameren. OneLOop: For the evaluation of one-loop scalar functions. *Comput.Phys.Commun.*, 182:2427–2438, 2011, hep-ph/1007.4716.

[80] T. Hahn and M. Rauch. News from FormCalc and LoopTools. *Nucl.Phys.Proc.Suppl.*, 157:236–240, 2006, hep-ph/0601248.

[81] G. 't Hooft and M.J.G. Veltman. Scalar One Loop Integrals. *Nucl.Phys.*, B153:365–401, 1979.

[82] W. Giele, E.W.N. Glover, and G. Zanderighi. Numerical evaluation of one-loop diagrams near exceptional momentum configurations. *Nucl.Phys.Proc.Suppl.*, 135:275–279, 2004, hep-ph/0407016.

[83] J. Fleischer and T. Riemann. A Complete algebraic reduction of one-loop tensor Feynman integrals. *Phys.Rev.*, D83:073004, 2011, hep-ph/1009.4436.

[84] W. H. Press, S. A. Teukolsky, W. T. Vetterling, and B. P. Flannery. *Numerical Recipes*. Cambridge University Press, 2007.

[85] D.I. Olive R.J. Eden, P.V. Landshoff and J.C. Polkinghorne. *The analytic S-matrix*. CUP, Cambridge, 1966.

[86] G. Cullen, J.-Ph. Guillet, G. Heinrich, T. Kleinschmidt, E. Pilon, et al. Golem95C: A library for one-loop integrals with complex masses. *Comput.Phys.Commun.*, 182:2276–2284, 2011, hep-ph/1101.5595.

[87] G.J. van Oldenborgh and J.A.M. Vermaseren. New Algorithms for One Loop Integrals. *Z.Phys.*, C46:425–438, 1990.

[88] M.J.G. Veltman. Unitarity and causality in a renormalizable field theory with unstable particles. *Physica*, 29:186–207, 1963.

[89] F. Scheck. Electroweak and strong interactions: An introduction to theoretical particle physics. 1996.

[90] A. Sirlin. Theoretical considerations concerning the Z0 mass. *Phys.Rev.Lett.*, 67:2127–2130, 1991.

[91] A. Sirlin. Observations concerning mass renormalization in the electroweak theory. *Phys.Lett.*, B267:240–242, 1991.

[92] R.G. Stuart. Gauge invariance, analyticity and physical observables at the Z0 resonance. *Phys.Lett.*, B262:113–119, 1991.

[93] R.G. Stuart. The Structure of the Z^0 resonance and the physical properties of the Z^0 boson. *Phys.Rev.Lett.*, 70:3193–3196, 1993.

[94] M. Passera and A. Sirlin. Analysis of the Z0 resonant amplitude in the general R(xi) gauges. *Phys.Rev.Lett.*, 77:4146–4149, 1996, hep-ph/9607253.

[95] P. Gambino and P.A. Grassi. The Nielsen identities of the SM and the definition of mass. *Phys.Rev.*, D62:076002, 2000, hep-ph/9907254.

[96] P. A. Grassi, B. A. Kniehl, and A. Sirlin. Width and partial widths of unstable particles in the light of the Nielsen identities. *Phys.Rev.*, D65:085001, 2002, hep-ph/0109228.

[97] N. Kauer. Narrow-width approximation limitations. *Phys.Lett.*, B649:413–416, 2007, hep-ph/0703077.

[98] D. Berdine, N. Kauer, and D. Rainwater. Breakdown of the Narrow Width Approximation for New Physics. *Phys.Rev.Lett.*, 99:111601, 2007, hep-ph/0703058.

[99] C.F. Uhlemann and N. Kauer. Narrow-width approximation accuracy. *Nucl.Phys.*, B814:195–211, 2009, hep-ph/0807.4112.

[100] N. Kauer and G. Passarino. Inadequacy of zero-width approximation for a light Higgs boson signal. 2012, hep-ph/1206.4803.

[101] Y. Kurihara, D. Perret-Gallix, and Y. Shimizu. e+ e- → e- anti-electron-neutrino u anti-d from LEP to linear collider energies. *Phys.Lett.*, B349:367–374, 1995, hep-ph/9412215.

[102] E.N. Argyres, W. Beenakker, G.J. van Oldenborgh, A. Denner, S. Dittmaier, et al. Stable calculations for unstable particles: Restoring gauge invariance. *Phys.Lett.*, B358:339–346, 1995, hep-ph/9507216.

[103] W. Beenakker, G.J. van Oldenborgh, A. Denner, S. Dittmaier, J. Hoogland, et al. The Fermion loop scheme for finite width effects in e^+e^- annihilation into four fermions. *Nucl.Phys.*, B500:255–298, 1997, hep-ph/9612260.

[104] G. Passarino. Unstable particles and nonconserved currents: A Generalization of the fermion loop scheme. *Nucl.Phys.*, B574:451–494, 2000, hep-ph/9911482.

[105] E. Accomando, A. Ballestrero, and E. Maina. Nonconserved currents and gauge restoring schemes in single W production. *Phys.Lett.*, B479:209–217, 2000, hep-ph/9911489.

[106] U. Baur and D. Zeppenfeld. Finite width effects and gauge invariance in radiative W productions and decay. *Phys.Rev.Lett.*, 75:1002–1005, 1995, hep-ph/9503344.

[107] G. Passarino. WTO : A Deterministic approach to 4 fermion physics. *Comput.Phys.Commun.*, 97:261–303, 1996, hep-ph/9602302.

[108] A. Ballestrero. Fermion loops, conserved currents and single-W. *Nucl.Phys.Proc.Suppl.*, 89:25–30, 2000, hep-ph/0005325.

[109] U. Baur, J.A.M. Vermaseren, and D. Zeppenfeld. Electroweak vector boson production in high-energy ep collisions. *Nucl.Phys.*, B375:3–44, 1992.

[110] J. M. Campbell and R. K. Ellis. An Update on vector boson pair production at hadron colliders. *Phys.Rev.*, D60:113006, 1999, hep-ph/9905386.

[111] H. G.J. Veltman. Mass and width of unstable gauge bosons. *Z.Phys.*, C62:35–52, 1994.

[112] R.G. Stuart. Production cross-sections for unstable particles. *Nucl.Phys.*, B498:28–38, 1997, hep-ph/9504215.

[113] A. Aeppli, G.J. van Oldenborgh, and D. Wyler. Unstable particles in one loop calculations. *Nucl.Phys.*, B428:126–146, 1994, hep-ph/9312212.

[114] W. Beenakker, F.A. Berends, and A.P. Chapovsky. An Effective Lagrangian approach for unstable particles. *Nucl.Phys.*, B573:503–535, 2000, hep-ph/9909472.

[115] W. Beenakker, A.P. Chapovsky, A. Kanaki, C.G. Papadopoulos, and R. Pittau. Towards an effective Lagrangian approach to fermion loop corrections. *Nucl.Phys.*, B667:359–393, 2003, hep-ph/0303105.

[116] M. Beneke, A.P. Chapovsky, A. Signer, and G. Zanderighi. Effective theory approach to unstable particle production. *Phys.Rev.Lett.*, 93:011602, 2004, hep-ph/0312331.

[117] M. Beneke, A.P. Chapovsky, A. Signer, and G. Zanderighi. Effective theory calculation of resonant high-energy scattering. *Nucl.Phys.*, B686:205–247, 2004, hep-ph/0401002.

[118] M. Beneke, N. Kauer, A. Signer, and G. Zanderighi. Towards pair production near threshold with unstable particle effective theory. *Nucl.Phys.Proc.Suppl.*, 152:162–167, 2006, hep-ph/0411008.

[119] A. Denner, S. Dittmaier, M. Roth, and D. Wackeroth. Predictions for all processes $e^+e^- \to 4$ fermions + gamma. *Nucl.Phys.*, B560:33–65, 1999, hep-ph/9904472.

[120] A. Denner, S. Dittmaier, M. Roth, and L.H. Wieders. Electroweak corrections to charged-current $e^+e^- \to 4$ fermion processes: Technical details and further results. *Nucl.Phys.*, B724:247–294, 2005, hep-ph/0505042.

[121] G. Lopez Castro, J.L. Lucio, and J. Pestieau. W+- and Z0 propagators on the resonance region. *Mod.Phys.Lett.*, A6:3679–3682, 1991.

[122] S. Actis, G. Passarino, C. Sturm, and S. Uccirati. Two-Loop Threshold Singularities, Unstable Particles and Complex Masses. *Phys.Lett.*, B669:62–68, 2008, hep-ph/0809.1302.

[123] G. Passarino, C. Sturm, and S. Uccirati. Higgs Pseudo-Observables, Second Riemann Sheet and All That. *Nucl.Phys.*, B834:77–115, 2010, hep-ph/1001.3360.

[124] S. Actis and G. Passarino. Two-Loop Renormalization in the Standard Model Part III: Renormalization Equations and their Solutions. *Nucl.Phys.*, B777:100–156, 2007, hep-ph/0612124.

[125] S. Goria, G. Passarino, and D. Rosco. The Higgs Boson Lineshape. 2011, hep-ph/1112.5517.

[126] A. Aeppli, F. Cuypers, and G.J. van Oldenborgh. O(Gamma) corrections to W pair production in e+ e- and gamma gamma collisions. *Phys.Lett.*, B314:413–420, 1993, hep-ph/9303236.

[127] A. Denner, S. Dittmaier, M. Roth, and D. Wackeroth. O(alpha) corrections to e+ e- → W W → four fermions (+ gamma): First numerical results from RACOON W W. *Phys.Lett.*, B475:127–134, 2000, hep-ph/9912261.

[128] S. Dittmaier and M. Roth. LUSIFER: A LUcid approach to six FERmion production. *Nucl.Phys.*, B642:307–343, 2002, hep-ph/0206070.

[129] J.D. Bjorken and S.D. Drell. Relativistic quantum fields. 1965.

[130] F. Boudjema and L. D. Ninh. b anti-b H production at the LHC: Yukawa corrections and the leading Landau singularity. *Phys.Rev.*, D78:093005, 2008, hep-ph/0806.1498.

[131] A. Denner, S. Dittmaier, and T. Hahn. Radiative corrections to $ZZ \to ZZ$ in the electroweak standard model. *Phys.Rev.*, D56:117–134, 1997, hep-ph/9612390.

[132] T. Binoth and G. Heinrich. Numerical evaluation of phase space integrals by sector decomposition. *Nucl.Phys.*, B693:134–148, 2004, hep-ph/0402265.

[133] R.W. Brown and K.O. Mikaelian. W+ W- and Z0 Z0 Pair Production in e+ e-, p p, p anti-p Colliding Beams. *Phys.Rev.*, D19:922, 1979.

[134] J. Ohnemus and J.F. Owens. An Order $\alpha^{-}s$ calculation of hadronic ZZ production. *Phys.Rev.*, D43:3626–3639, 1991.

[135] B. Mele, P. Nason, and G. Ridolfi. QCD radiative corrections to Z boson pair production in hadronic collisions. *Nucl.Phys.*, B357:409–438, 1991.

[136] L.J. Dixon and A. Signer. Complete O (alpha-s**3) results for e+ e- → (gamma, Z) → four jets. *Phys.Rev.*, D56:4031–4038, 1997, hep-ph/9706285.

[137] D. A. Dicus, C. Kao, and W.W. Repko. GLUON PRODUCTION OF GAUGE BOSONS. *Phys.Rev.*, D36:1570, 1987.

[138] J.J. van der Bij and E.W. N. Glover. PHOTON Z BOSON PAIR PRODUCTION VIA GLUON FUSION. *Phys.Lett.*, B206:701, 1988.

[139] E.W. N. Glover and J.J. van der Bij. Z BOSON PAIR PRODUCTION VIA GLUON FUSION. *Nucl.Phys.*, B321:561, 1989.

[140] U. Baur, E.W. N. Glover, and J.J. van der Bij. HADRONIC PRODUCTION OF ELECTROWEAK VECTOR BOSON PAIRS AT LARGE TRANSVERSE MOMENTUM. *Nucl.Phys.*, B318:106, 1989.

[141] E.W. N. Glover and J.J. van der Bij. HIGGS BOSON PAIR PRODUCTION VIA GLUON FUSION. *Nucl.Phys.*, B309:282, 1988.

[142] T. Matsuura and J.J. van der Bij. Characteristics of leptonic signals for Z boson pairs at hadron colliders. *Z.Phys.*, C51:259–266, 1991.

[143] C. Zecher, T. Matsuura, and J.J. van der Bij. Leptonic signals from off-shell Z boson pairs at hadron colliders. *Z.Phys.*, C64:219–226, 1994, hep-ph/9404295.

[144] J. M. Campbell, R. K. Ellis, and C. Williams. Vector boson pair production at the LHC. *JHEP*, 1107:018, 2011, hep-ph/1105.0020.

[145] J.M. Campbell, E. Castaneda-Miranda, Y. Fang, N. Kauer, B. Mellado, et al. Normalizing Weak Boson Pair Production at the Large Hadron Collider. *Phys.Rev.*, D80:054023, 2009, hep-ph/0906.2500.

[146] R. Frederix, S. Frixione, V. Hirschi, F. Maltoni, R. Pittau, et al. Four-lepton production at hadron colliders: aMC@NLO predictions with theoretical uncertainties. *JHEP*, 1202:099, 2012, hep-ph/1110.4738.

[147] T. Binoth, N. Kauer, and P. Mertsch. Gluon-induced QCD corrections to pp $\to$ ZZ $\to l\bar{l}l'\bar{l}'$. *Progress in High Energy Physics*, 2:142, 2008, hep-ph/0807.0024.

[148] N. Kauer. Signal-background interference in $gg \to H \to VV$. 2012, hep-ph/1201.1667.

[149] G. Aad et al. Search for the standard model higgs boson in the decay channel $H \to ZZ^{(*)} \to 4l$ with 4.8 fb-1 of pp collision data at sqrt(s) = 7 tev with atlas. *Phys.Lett.*, B710:383–402, 2012, hep-ex/1202.1415.

[150] S. Chatrchyan et al. Search for the standard model Higgs boson in the decay channel H to ZZ to 4 leptons in pp collisions at sqrt(s) = 7 TeV. *Phys. Rev. Lett. 108,*, 111804, 2012, hep-ex/1202.1997.

[151] G. Cullen, N. Greiner, G. Heinrich, G. Luisoni, P. Mastrolia, et al. Automated One-Loop Calculations with GoSam. *Eur.Phys.J.*, C72:1889, 2012, hep-ph/1111.2034.

[152] P. Nogueira. Automatic Feynman graph generation. *J.Comput.Phys.*, 105:279–289, 1993.

[153] J.A.M. Vermaseren. New features of FORM. 2000, math-ph/0010025.

[154] J. Kuipers, T. Ueda, J.A.M. Vermaseren, and J. Vollinga. FORM version 4.0. 2012, hep-ph/1203.6543.

[155] A. Semenov. LanHEP - a package for automatic generation of Feynman rules from the Lagrangian. Updated version 3.1. 2010, hep-ph/1005.1909.

[156] C. Degrande, C. Duhr, B. Fuks, D. Grellscheid, O. Mattelaer, et al. UFO - The Universal FeynRules Output. *Comput.Phys.Commun.*, 183:1201–1214, 2012, hep-ph/1108.2040.

[157] F. A. Berends, R. Kleiss, P. De Causmaecker, R. Gastmans, and T. T. Wu. Single Bremsstrahlung Processes in Gauge Theories. *Phys.Lett.*, B103:124, 1981.

[158] F. A. Berends, R. Kleiss, P. De Causmaecker, R. Gastmans, W. Troost, et al. Multiple Bremsstrahlung in Gauge Theories at High-Energies. 2. Single Bremsstrahlung. *Nucl.Phys.*, B206:61, 1982.

[159] M. Caffo and E. Remiddi. EVALUATION OF TRANSITION AMPLITUDES BETWEEN DIRAC SPINORS. *Helv.Phys.Acta*, 55:339, 1982.

[160] Z. Xu, D.-H. Zhang, and L. Chang. HELICITY AMPLITUDES FOR MULTIPLE BREMSSTRAHLUNG IN MASSLESS NONABELIAN GAUGE THE-

ORY. 1. NEW DEFINITION OF POLARIZATION VECTOR AND FORMULATION OF AMPLITUDES IN GRASSMANN ALGEBRA. 1984.

[161] Z. Xu, D.-H. Zhang, and L. Chang. Helicity Amplitudes for Multiple Bremsstrahlung in Massless Nonabelian Gauge Theories. *Nucl.Phys.*, B291:392, 1987.

[162] R. Kleiss and W. J. Stirling. Spinor Techniques for Calculating p anti-p $\to$ $W^{\pm}Z^{0}$ + Jets. *Nucl.Phys.*, B262:235–262, 1985.

[163] J.F. Gunion and Z. Kunszt. Improved Analytic Techniques for Tree Graph Calculations and the G g q anti-q Lepton anti-Lepton Subprocess. *Phys.Lett.*, B161:333, 1985.

[164] D. Maitre and P. Mastrolia. S@M, a Mathematica Implementation of the Spinor-Helicity Formalism. *Comput.Phys.Commun.*, 179:501–574, 2008, hep-ph/0710.5559.

[165] G. Cullen, M. Koch-Janusz, and T. Reiter. Spinney: A Form Library for Helicity Spinors. *Comput.Phys.Commun.*, 182:2368–2387, 2011, hep-ph/1008.0803.

[166] T. Reiter. Optimising Code Generation with haggies. *Comput.Phys.Commun.*, 181:1301–1331, 2010, hep-ph/0907.3714.

[167] R. K. Ellis, W. J. Stirling, and B.R. Webber. QCD and collider physics. *Camb.Monogr.Part.Phys.Nucl.Phys.Cosmol.*, 8:1–435, 1996.

[168] J. Jersak, E. Laermann, and P.M. Zerwas. Electroweak Production of Heavy Quarks in e+ e- Annihilation. *Phys.Rev.*, D25:1218, 1982.

[169] R. K. Ellis and J.C. Sexton. Qcd radiative corrections to parton parton scattering. *Nucl.Phys.*, B269:445, 1986.

[170] V. Hirschi, R. Frederix, S. Frixione, M. V. Garzelli, F. Maltoni, et al. Automation of one-loop QCD corrections. *JHEP*, 1105:044, 2011, hep-ph/1103.0621.

[171] T. Binoth, J.-Ph. Guillet, and G. Heinrich. Algebraic evaluation of rational polynomials in one-loop amplitudes. *JHEP*, 0702:013, 2007, hep-ph/0609054.

[172] J.J. van der Bij and E.W. N. Glover. Z BOSON PRODUCTION AND DECAY VIA GLUONS. *Nucl.Phys.*, B313:237, 1989.

[173] J. M. Campbell and R. K. Ellis. Radiative corrections to Z b anti-b production. *Phys.Rev.*, D62:114012, 2000, hep-ph/0006304.

[174] J. M. Campbell, R. K. Ellis, F. Maltoni, and S. Willenbrock. Higgs-Boson production in association with a single bottom quark. *Phys.Rev.*, D67:095002, 2003, hep-ph/0204093.

[175] G.J. Gounaris, P.I. Porfyriadis, and F.M. Renard. The gamma gamma $\to$ gamma gamma process in the standard and SUSY models at high-energies. *Eur.Phys.J.*, C9:673–686, 1999, hep-ph/9902230.

[176] S. Actis, P. Mastrolia, and G. Ossola. NLO QED Corrections to Hard-Bremsstrahlung Emission in Bhabha Scattering. *Phys.Lett.*, B682:419–427, 2010, hep-ph/0909.1750.

[177] T. Melia, K. Melnikov, R. Rontsch, and G. Zanderighi. Next-to-leading order QCD predictions for W^+W^+jj production at the LHC. *JHEP*, 1012:053, 2010, hep-ph/1007.5313.

[178] T. Binoth, N. Greiner, A. Guffanti, J. Reuter, J.-Ph. Guillet, et al. Next-to-leading order QCD corrections to pp $\to$ b anti-b b anti-b + X at the LHC: the quark induced case. *Phys.Lett.*, B685:293–296, 2010, hep-ph/0910.4379.

[179] N. Greiner, A. Guffanti, T. Reiter, and J. Reuter. NLO QCD corrections to the production of two bottom-antibottom pairs at the LHC. *Phys.Rev.Lett.*, 107:102002, 2011, hep-ph/1105.3624.

[180] A. van Hameren, C.G. Papadopoulos, and R. Pittau. Automated one-loop calculations: A Proof of concept. *JHEP*, 0909:106, 2009, hep-ph/0903.4665.

[181] T. Gleisberg, S. Hoeche, F. Krauss, A. Schalicke, S. Schumann, et al. SHERPA 1. alpha: A Proof of concept version. *JHEP*, 0402:056, 2004, hep-ph/0311263.

[182] T. Gleisberg, S. Hoeche, F. Krauss, M. Schonherr, S. Schumann, et al. Event generation with SHERPA 1.1. *JHEP*, 0902:007, 2009, hep-ph/0811.4622.

[183] F. Siegert. Monte-Carlo event generation for the LHC. *Doctoral thesis, Durham University*, 2010.

[184] H.-L. Lai et al. New parton distributions for collider physics. *Phys. Rev.*, D82:074024, 2010, 1007.2241.

[185] R. D. Ball et al. A first unbiased global NLO determination of parton distributions and their uncertainties. *Nucl. Phys.*, B838:136–206, 2010, 1002.4407.

[186] A.D. Martin, W.J. Stirling, R.S. Thorne, and G. Watt. Parton distributions for the LHC. *Eur.Phys.J.*, C63:189–285, 2009, hep-ph/0901.0002.

[187] Y. L. Dokshitzer. Calculation of the Structure Functions for Deep Inelastic Scattering and e+ e- Annihilation by Perturbation Theory in Quantum Chromodynamics. *Sov.Phys.JETP*, 46:641–653, 1977.

[188] V.N. Gribov and L.N. Lipatov. Deep inelastic e p scattering in perturbation theory. *Sov.J.Nucl.Phys.*, 15:438–450, 1972.

[189] G. Altarelli and G. Parisi. Asymptotic Freedom in Parton Language. *Nucl.Phys.*, B126:298, 1977.

[190] S. Moch, J. A. M. Vermaseren, and A. Vogt. The three-loop splitting functions in QCD: The non-singlet case. *Nucl. Phys.*, B688:101–134, 2004, hep-ph/0403192.

[191] A. Vogt, S. Moch, and J.A.M. Vermaseren. The Three-loop splitting functions in QCD: The Singlet case. *Nucl.Phys.*, B691:129–181, 2004, hep-ph/0404111.

[192] Z. Nagy and Davison E. Soper. Matching parton showers to NLO computations. *JHEP*, 0510:024, 2005, hep-ph/0503053.

[193] Z. Nagy and Davison E. Soper. A New parton shower algorithm: Shower evolution, matching at leading and next-to-leading order level. pages 101–123, 2006, hep-ph/0601021.

[194] S. Schumann and F. Krauss. A Parton shower algorithm based on Catani-Seymour dipole factorisation. *JHEP*, 0803:038, 2008, hep-ph/0709.1027.

[195] T. Sjostrand. A Model for Initial State Parton Showers. *Phys.Lett.*, B157:321, 1985.

[196] B. Andersson, G. Gustafson, G. Ingelman, and T. Sjostrand. Parton Fragmentation and String Dynamics. *Phys.Rept.*, 97:31–145, 1983.

[197] M. Bahr, S. Gieseke, M.A. Gigg, D. Grellscheid, K. Hamilton, et al. Herwig++ Physics and Manual. *Eur.Phys.J.*, C58:639–707, 2008, hep-ph/0803.0883.

[198] T. Binoth, F. Boudjema, G. Dissertori, A. Lazopoulos, A. Denner, et al. A Proposal for a standard interface between Monte Carlo tools and one-loop programs. *Comput.Phys.Commun.*, 181:1612–1622, 2010, hep-ph/1001.1307.

[199] E. Boos, M. Dobbs, W. Giele, I. Hinchliffe, J. Huston, et al. Generic user process interface for event generators. 2001, hep-ph/0109068.

[200] J. Alwall, A. Ballestrero, P. Bartalini, S. Belov, E. Boos, et al. A Standard format for Les Houches event files. *Comput.Phys.Commun.*, 176:300–304, 2007, hep-ph/0609017.

[201] S. Dittmaier et al. Handbook of LHC Higgs Cross Sections: 1. Inclusive Observables. 2011, hep-ph/1101.0593.

[202] F. Krauss, R. Kuhn, and G. Soff. AMEGIC++ 1.0: A Matrix element generator in C++. *JHEP*, 0202:044, 2002, hep-ph/0109036.

[203] L. D. Landau. *Dokl. Akad. Nawk.*, 60:207, 1948.

[204] C.-N. Yang. Selection Rules for the Dematerialization of a Particle Into Two Photons. *Phys.Rev.*, 77:242–245, 1950.

[205] T. Gleisberg and S. Hoeche. Comix, a new matrix element generator. *JHEP*, 0812:039, 2008, hep-ph/0808.3674.

[206] M.R. Whalley, D. Bourilkov, and R.C. Group. The Les Houches accord PDFs (LHAPDF) and LHAGLUE. 2005, hep-ph/0508110.

[207] Z. Nagy. Next-to-leading order calculation of three jet observables in hadron hadron collision. *Phys.Rev.*, D68:094002, 2003, hep-ph/0307268.

[208] J.P. Guillet. Private communication.

Appendix A

Notation and Conventions

In this thesis, we use the mostly-minus metric tensor $g^{\mu\nu}$

$$\mathbf{g} = \begin{pmatrix} 1 & 0 & 0 & 0 \\ 0 & -1 & 0 & 0 \\ 0 & 0 & -1 & 0 \\ 0 & 0 & 0 & -1 \end{pmatrix}. \tag{A.0.1}$$

We use Feynman slash notation: for a lorentz four-vector a^μ:

$$\not{a} \equiv \gamma_\mu a^\mu, \tag{A.0.2}$$

and except where stated otherwise, we use the Einstein summation convention

$$a_i b_i \equiv \sum_i a_i b_i. \tag{A.0.3}$$

A.1 Units and Dimensions

Throughout this thesis, natural units $\hbar = c = 1$ are used. This leaves us with only one dimensionful quantity, which is taken to be mass. We can count the dimension (denoted with square brackets) of all quantities in terms of this mass dimension:

$$[\text{Mass}] = [\text{Energy}] = [\text{Momentum}] = 1 \tag{A.1.4}$$

$$[\text{Distance}] = [\text{Time}] = -1. \tag{A.1.5}$$

A.2 LHC parameters

The list of parameters used in the calculation of Chapter 7, taken from Appendix A of [201], is given below.

Parameter	Value
G_F	$1.16637 \times 10^5\,\mathrm{GeV}^2$
b mass	4.16 GeV
t mass	172.5 GeV
W mass	80.398 GeV
W width	2.141 GeV
Z mass	91.1876 GeV
Z width	2.4952 GeV

Table A.1: Standard Model parameters.

Our parameters deviate from [201] in that everything lighter than a b-quark (and in some cases also the b-quark itself, as explained in the text) is taken to be massless.

Appendix B

Useful Mathematical Objects

B.1 The Dirac Matrices γ^μ

This is a set of four matrices, which together can be treated as a relativistic four-vector. In this section, we will treat each matrix as four-dimensional, and so each matrix carries two spinorial indices running from 1 to 4. They obey, as a defining equation:

$$\{\gamma^\mu, \gamma^\nu\} = 2\eta^{\mu\nu} I \tag{B.1.1}$$

with $\eta^{\mu\nu}$ the Minkowski metric and I the 4×4 identity in spinor space.

Although often for practical calculations we do not need to write the matrices explicity, merely calculate a trace of a chain of them, we sometimes wish to write an explicit form. There are two common representations, the Dirac representation:

$$\gamma^0 = \begin{pmatrix} 1 & 0 & 0 & 0 \\ 0 & 1 & 0 & 0 \\ 0 & 0 & -1 & 0 \\ 0 & 0 & 0 & -1 \end{pmatrix} \gamma^1 = \begin{pmatrix} 0 & 0 & 0 & 1 \\ 0 & 0 & 1 & 0 \\ 0 & -1 & 0 & 0 \\ -1 & 0 & 0 & 0 \end{pmatrix}$$
$$\gamma^2 = \begin{pmatrix} 0 & 0 & 0 & -i \\ 0 & 0 & i & 0 \\ 0 & i & 0 & 0 \\ -i & 0 & 0 & 0 \end{pmatrix} \gamma^3 = \begin{pmatrix} 0 & 0 & 1 & 0 \\ 0 & 0 & 0 & -1 \\ 1 & 0 & 0 & 0 \\ 0 & -1 & 0 & 0 \end{pmatrix}, \tag{B.1.2}$$

and the *Weyl* representation, with the same γ^1, γ^2 and γ^3, but different γ^0:

$$\gamma^0 = \begin{pmatrix} 0 & 0 & 1 & 0 \\ 0 & 0 & 0 & 1 \\ 1 & 0 & 0 & 0 \\ 0 & 1 & 0 & 0 \end{pmatrix}. \tag{B.1.3}$$

B.2 The Dirac δ-functional

The Dirac δ-functional, $\delta(x)$, can be thought of physically as an infinite spike positioned at $x = 0$, with zero value elsewhere, such that its integral is unity. A more rigorous definition uses, with a slight abuse of notation, $\delta(x)dx$ as a measure:

$$\int_{-\infty}^{\infty} f(x)\delta(x - x_0)dx = f(x_0). \tag{B.2.4}$$

This definition can be used to prove several interesting properties, of which we will show the shifting property and the behaviour on composition with a function. We will then briefly consider the dimensions of $\delta(x)$.

Shifting property: $\delta(ax)$

For a real constant a, we can examine $\delta(ax)$ under an integral. First we note that the δ-functional is symmetric, so:

$$\int \delta(ax)dx = \int \delta(|a|x)dx = \int \delta(-|a|x)dx. \tag{B.2.5}$$

Now with a simple change of variables

$$\int \delta(ax)dx = \int \delta(y)\frac{dy}{|a|} \tag{B.2.6}$$

and a relabelling $y \to x$, we see that

$$\delta(ax) = \frac{1}{|a|}\delta(x). \tag{B.2.7}$$

Composition with a Function: $\delta\left(f(x)\right)$

Consider a real function $f(x)$ which has exactly one root, at $x = x_0$, and whose derivative is $f'(x)$. Let us use it in the following integral:

$$\mathcal{I}_f = \int \delta\left(f(x)\right)|f'(x)|\,dx. \tag{B.2.8}$$

The δ-functional will be zero except at $x = x_0$, so we could equally write this as

$$\mathcal{I}_f = \int \delta\left(f(x)\right) |f'(x_0)|\, dx. \tag{B.2.9}$$

Now let us again change variables in (B.2.8) to $y = f(x)$ so that $dy = f'(x)dx$

$$\mathcal{I}_f = \int \delta\left(y\right) dy, \tag{B.2.10}$$

so we have

$$\delta\left(f(x)\right) = \frac{1}{|f'(x_0)|}\delta(x) \tag{B.2.11}$$

and this expands in functions with more than one root to a sum of such terms on the right-hand side. Note that this function agrees with (B.2.7).

Dimensions

When considering physical situations, it is often useful to consider the dimensions of our objects. If we start from

$$\int \delta(x)dx = 1, \tag{B.2.12}$$

we see immediately that

$$[\delta(x)] = [x]^{-1}. \tag{B.2.13}$$

B.3 The Γ function

The Γ function is defined by

$$\Gamma(z) = \int_0^\infty e^{-t}t^{z-1}dt \tag{B.3.14}$$

and by integration by parts, one can show it has the property

$$\Gamma(z) = (z-1)\Gamma(z-1). \tag{B.3.15}$$

If z is a positive integer, by iterating this formula we can obtain

$$\Gamma(z) = (z-1)!. \tag{B.3.16}$$

The derivative of the function can be taken by using the property $\frac{d}{dx}t^x = \frac{d}{dx}\exp(x\log(t)) = \log(t)t^x$:

$$\frac{d}{dz}\Gamma(z) = \int_0^\infty e^{-t}\log(t)t^{z-1}dt, \tag{B.3.17}$$

so that

$$\Gamma'(1) = \int_0^\infty e^{-t}\log(t)dt \equiv -\gamma_E, \tag{B.3.18}$$

where $\gamma_E = 0.577215664901...$ is the Euler-Mascheroni constant.

From (B.3.16), we know that $\Gamma(1) = 1$, and we can now find $\Gamma(1+\epsilon)$ by Taylor expansion:

$$\Gamma(1+\epsilon) = \Gamma(1) + \epsilon\Gamma'(1) + \frac{1}{2}\epsilon^2\Gamma''(1) + \dots \tag{B.3.19}$$

$$= 1 - \epsilon\gamma_E + \mathcal{O}(\epsilon^2), \tag{B.3.20}$$

and by (B.3.15) we can also find

$$\Gamma(\epsilon) = \frac{\Gamma(1+\epsilon)}{\epsilon} = \frac{1}{\epsilon} - \gamma_E + \mathcal{O}(\epsilon). \tag{B.3.21}$$

B.4 The Euler Beta Function

We wish to prove

$$B(s,t) = \int_0^1 dy y^{s-1}(1-y)^{t-1} \tag{B.4.22}$$

$$= \frac{\Gamma(s)\Gamma(t)}{\Gamma(s+t)} \tag{B.4.23}$$

$$= \int_0^\infty dz \frac{z^{s-1}}{[z+1]^{(s+t)}}. \tag{B.4.24}$$

We may choose either (B.4.22) or (B.4.23) to be the definition of the function.

To prove

$$B(s,t) = \int_0^1 dy y^{s-1}(1-y)^{t-1} = \frac{\Gamma(s)\Gamma(t)}{\Gamma(s+t)}, \tag{B.4.25}$$

we start with the definition of the Γ-function (see Appendix B.3) to make the product $\Gamma(s)\Gamma(t)$:

$$\Gamma(s)\Gamma(t) = \int_{p=0}^\infty p^{s-1}e^{-p}dp \int_{q=0}^\infty q^{t-1}e^{-q}dq \;\; = \int_{p=0}^\infty \int_{q=0}^\infty dpdq p^{s-1}q^{t-1}e^{-p-q} \tag{B.4.26}$$

and make the substitution $p = xy$, $q = y(1-x)$ such that

$$\begin{pmatrix} p \\ q \end{pmatrix} = \begin{pmatrix} y & x \\ -y & 1-x \end{pmatrix} \begin{pmatrix} x \\ y \end{pmatrix}, \tag{B.4.27}$$

and so $dpdq = ydxdy$

$$\Gamma(s)\Gamma(t) = \int_{y=0}^{\infty} \int_{x=0}^{1} ydxdy(xy)^{s-1} \left(y(1-x)\right)^{t-1} e^{-y} \tag{B.4.28}$$

$$= \int_{y=0}^{\infty} dy y^{(s+t)-1} e^{-y} \int_{x=0}^{1} dx x^{s-1}(1-x)^{t-1} \tag{B.4.29}$$

$$= \Gamma(s+t)B(s,t) \tag{B.4.30}$$

and the equation is proven.

Now to show

$$B(s,t) = \int_0^1 dy y^{s-1}(1-y)^{t-1} = \int_0^{\infty} dz \frac{z^{s-1}}{[z+1]^{(s+t)}} \tag{B.4.31}$$

We use on the first integral the substitution

$$z = \frac{y}{(1-y)} \tag{B.4.32}$$

so that

$$y = \frac{z}{1+z}, \qquad (1-y) = \frac{1}{1+z}, \qquad dz = \frac{dy}{(1-y)^2}, \qquad dy = \frac{dz}{(1+z)^2}, \tag{B.4.33}$$

and therefore

$$B(s,t) = \int_{y=0}^{1} dy y^{s-1}(1-y)^{t-1} \tag{B.4.34}$$

$$= \int_{z=0}^{\infty} \frac{dz}{(1+z)^2} \left(\frac{z}{1+z}\right)^{s-1} \left(\frac{1}{1+z}\right)^{t-1} \tag{B.4.35}$$

$$= \int_{z=0}^{\infty} dz \frac{z^{s-1}}{(1+z)^{s+t}}. \tag{B.4.36}$$

Appendix C

Additional Derivations

C.1 Feynman Parameters

We start from (4.1.3):

$$\frac{1}{AB} = \int_0^1 dxdy\delta(1-x-y)\frac{1}{(xA+yB)^2}, \tag{C.1.1}$$

and differentiate with respect to B:

$$\begin{aligned}\frac{d}{dB}\left(\frac{1}{AB}\right) &= \int_0^1 dxdy\delta(1-x-y)\frac{d}{dB}\left(\frac{1}{(xA+yB)^2}\right)\\ \frac{1}{AB^2} &= \int_0^1 dxdy\delta(1-x-y)\left(\frac{2y}{(xA+yB)^3}\right).\end{aligned} \tag{C.1.2}$$

Now we can repeat this:

$$\begin{aligned}(-1)^{n-1}(n-1)!\frac{1}{AB^n} &= \int_0^1 dxdy\delta(1-x-y)\frac{d^{n-1}}{dB^{n-1}}\left(\frac{1}{(xA+yB)^2}\right)\\ \frac{1}{AB^n} &= \frac{(-1)^{n-1}}{(n-1)!}\int_0^1 dxdy\delta(1-x-y)(-1)^{n-1}n!y^{n-1}\frac{1}{(xA+yB)^{n+1}}\\ \frac{1}{AB^n} &= \int_0^1 dxdy\delta(1-x-y)\frac{ny^{n-1}}{(xA+yB)^{n+1}}.\end{aligned} \tag{C.1.3}$$

We wish to show (not using the summation convention):

$$\frac{1}{A_1A_2\ldots A_n} = \int_0^1 dx_1dx_2\ldots dx_n\delta\left(\sum_{i=1}^n x_i - 1\right)\frac{(n-1)!}{[x_1A_1+x_2A_2+\cdots+x_nA_n]^n}. \tag{C.1.4}$$

This can be proven by starting with

$$\frac{1}{A} = \int_0^\infty dt e^{-At}, \text{ and} \tag{C.1.5}$$

$$1 = \int_0^\infty ds\delta\left(s - \sum_{i=1}^n t_i\right), \tag{C.1.6}$$

and taking several copies of (C.1.5), left-multiplied by (C.1.6)

$$\frac{1}{A_1 A_2 \dots A_n} = \int_{s=0}^\infty ds\delta\left(s - \sum_{i=1}^n t_i\right) \int_{t_1=0}^\infty dt_1 e^{-A_1 t_1} \int_{t_2=0}^\infty dt_2 e^{-A_2 t_2} \dots \int_{t_n=0}^\infty dt_n e^{-A_n t_n}, \tag{C.1.7}$$

then setting $x_i = st_i$

$$\frac{1}{A_1 A_2 \dots A_n} = \int_{s=0}^\infty ds\delta\left(s - \sum_{i=1}^n sx_i\right) \int_{x_1=0}^\infty s dx_1 e^{-A_1 s x_1} \dots \int_{x_n=0}^\infty s dx_n e^{-A_n s x_n} \tag{C.1.8}$$

$$= \int_{s=0}^\infty ds s^{n-1}\delta\left(1 - \sum_{i=1}^n x_i\right) \int_{x_1=0}^\infty dx_1 e^{-A_1 s x_1} \dots \int_{x_n=0}^\infty dx_n e^{-A_n s x_n}, \tag{C.1.9}$$

where in moving to (C.1.9), we have moved a factor of s out of the δ-functional and multiplied by s^{-1}, using the shifting property[1]

The integral over s can then be done. For illustration, we perform this for $n = 2$, to return our original result 4.1.3:

$$\frac{1}{A_1 A_2} = \int_{x_1=0}^\infty dx_1 \int_{x_2=0}^\infty dx_2 \delta(1 - x_1 - x_2) \int_{s=0}^\infty ds s e^{-A_1 s x_1} e^{-A_2 s x_2} \tag{C.1.10}$$

$$= \int_{x_1=0}^\infty dx_1 \int_{x_2=0}^\infty dx_2 \delta(1 - x_1 - x_2) \times \left(\left[s\frac{e^{s(-A_1 x_1 - A_2 x_2)}}{(-A_1 x_1 - A_2 x_2)}\right]_0^\infty - \int_{s=0}^\infty ds \frac{e^{s(-A_1 x_1 - A_2 x_2)}}{(-A_1 x_1 - A_2 x_2)}\right) \tag{C.1.11}$$

$$= \int_{x_1=0}^\infty dx_1 \int_{x_2=0}^\infty dx_2 \delta(1 - x_1 - x_2) \left(0 - \frac{\left[e^{s(-A_1 x_1 - A_2 x_2)}\right]_0^\infty}{(-A_1 x_1 - A_2 x_2)^2}\right) \tag{C.1.12}$$

$$= \int_{x_1=0}^1 dx_1 \int_{x_2=0}^1 dx_2 \delta(1 - x_1 - x_2) \frac{1}{(A_1 x_1 + A_2 x_2)^2}, \tag{C.1.13}$$

[1] $\delta(ax) = \frac{1}{a}\delta(x)$: the Dirac δ-functional is explored in Appendix B.2.

where in the last step, the upper integration limits for x_1 and x_2 were set to 1, which is the effect from the δ-functional, as they must both be positive.

Now for higher values of n, the integration by parts will be repeated. An $(n-1)!$ will result after for the repeated differentiation of the ss in each step, and each step will also give a minus, which will cancel that from the argument of the exponential which is brought down. Therefore the result of the integration of (C.1.9) is:

$$\frac{1}{A_1 A_2 \dots A_n} = \int_0^1 dx_1 dx_2 \dots dx_n \delta\left(\sum_{i=1}^n x_i - 1\right) \frac{(n-1)!}{[x_1 A_1 + x_2 A_2 + \dots + x_n A_n]^n}, \tag{C.1.14}$$

which is what we wished to find.

If we wish to have repeated A_i in the denominator, then as before we can differentiate (C.1.14) repeatedly, giving the result

$$\frac{1}{A_1^{\nu_1} A_2^{\nu_2} \dots A_n^{\nu_n}} = \int_0^1 dx_1 dx_2 \dots dx_n \delta\left(\sum_{i=1}^n x_i - 1\right) \frac{\prod_{i=1}^n x_i^{\nu_i - 1}}{[\sum_{i=1}^n x_i A_i]^{\sum \nu_i}} \frac{\Gamma(\nu_1 + \nu_2 + \dots + \nu_n)}{\Gamma(\nu_1)\Gamma(\nu_2)\dots\Gamma(\nu_n)}. \tag{C.1.15}$$

C.2 Reduction Steps and Loop-momentum Shifts

In order to show the shift in loop momentum which is required by methods that have a "standard" form for their loop integrals, let us start with such an integral, and write the q_i as $k + r_i$, setting $r_N = 0$.

$$\mathcal{I}_N^{d,\mu_1\mu_2\dots\mu_r}(N, N, \dots, N) = \int \frac{d^d k}{i\pi^{d/2}} \frac{k^{\mu_1} k^{\mu_2} \dots k^{\mu_r}}{((k+r_1)^2 - m_1^2 + i\lambda)((k+r_2)_2^2 - m_2^2 + i\lambda)\dots(k^2 - m_N^2 + i\lambda)}. \tag{C.2.16}$$

Now let us work with a specific example: the rank two massless triangle, dropping the λs, with its k^μs contracted with r_1 and r_2.

$$r_{1\mu} r_{2\nu} \mathcal{I}_3^{d,\mu\nu}(N, N, \dots, N) = \int \frac{d^d k}{i\pi^{d/2}} \frac{(r_1 \cdot k)(r_2 \cdot k)}{((k+r_1)^2)((k+r_2)^2)(k^2)}. \tag{C.2.17}$$

Now we wish to cancel denominators, so we use the identity

$$r_1 \cdot k = \frac{1}{2}\left[2 r_i \cdot k + k^2 - k^2 + r_1 - r_1\right] = \frac{1}{2}\left[(k + r_i)^2 - k^2 - r_1\right], \tag{C.2.18}$$

and so we can write

$$r_{1\mu}r_{2\nu}\mathcal{I}_3^{d,\mu\nu}(N,N,\ldots,N) = \int \frac{d^dk}{i\pi^{d/2}} \frac{\frac{1}{2}\left[(k+r_i)^2-k^2-r_1\right] r_2\cdot k}{((k+r_1)^2)((k+r_2)^2)(k^2)} \tag{C.2.19}$$

$$= \frac{1}{2}\int \frac{d^dk}{i\pi^{d/2}} \frac{r_2\cdot k}{(((k+r_2)^2)(k^2)} - \frac{1}{2}\int \frac{d^dk}{i\pi^{d/2}} \frac{r_2\cdot k}{((k+r_1)^2)((k+r_2)^2)}$$

$$- \frac{r_1^2}{2}\int \frac{d^dk}{i\pi^{d/2}} \frac{r_2\cdot k}{((k+r_1)^2)((k+r_2)^2)(k^2)} \tag{C.2.20}$$

and in order to recover the standard form for the second term, we must shift the loop momentum $k \to k - r_2$, so we have

$$\int \frac{d^dk}{i\pi^{d/2}} \frac{r_2\cdot k}{((k+r_1)^2)((k+r_2)^2)} = \int \frac{d^dk}{i\pi^{d/2}} \frac{r_2\cdot k}{((k+(r_1-r_2))^2)(k^2)} \tag{C.2.21}$$

$$- r_2^2 \int \frac{d^dk}{i\pi^{d/2}} \frac{1}{((k+(r_1-r_2))^2)(k^2)} \tag{C.2.22}$$

so returning to the standard form has the cost of adding an extra term.

C.3 Splitting and Combining Logarithms

For positive, real arguments, it is trivial to split and combine logarithms, using the well-known rules:

$$\log(ab) = \log(a) + \log(b) \tag{C.3.23}$$

$$\log\left(\frac{a}{b}\right) = \log(a) - \log(b). \tag{C.3.24}$$

However, because for complex argument, the logarithm has a branch cut, chosen to be along the negative real axis, this situation becomes more complicated (with thanks to [208])[2]. We must either be careful to remain on the same branch or return to it by adding $\pm 2\pi i$. This is expressed in an η function which, with complex z_1 and z_2 is simply defined:

$$\eta(z_1,z_2) = \log(z_1z_2) - \log(z_1) - \log(z_1) \tag{C.3.25}$$

and has values $-2\pi i$, 0 and $2\pi i$, and notably is always zero if a and b have imaginary parts of opposite sign, or if either is a positive real.

[2]Although (C.3.23) still applies if a and b have imaginary parts of opposite signs, and (C.3.24) if the same sign.

Now in the context of our position on a branch, let us consider the case of the splitting of a logarithm of $z_1 = az_0$, with a real and z_0 complex

$$\log(z_1) = \log(az_0) = \begin{cases} \log(a) + \log(z_0) & a > 0 \\ \log(-a) + \log(-z_0) & a < 0. \end{cases} \tag{C.3.26}$$

In each case the first term is the logarithm of a positive real number, so no η functions enter.

Now consider moving from a general complex number Z to $-Z$. If $\mathrm{Im}(Z) < 0$, then to get to $-Z$ avoiding the branch cut, we must add π to the argument, and similarly we must subtract for $\mathrm{Im}(Z) > 0$. So

$$\log(-Z) = \log(Z) - i\pi\sigma_{\mathrm{Im}(Z)}, \tag{C.3.27}$$

where σ_x represents the sign of a variable x

Now let us examine again the case where $a < 0$. We apply (C.3.27) to $\log(-z_0)$ and note that $\sigma_{\mathrm{Im}(z_0)} = \sigma_a\sigma_{\mathrm{Im}(z_1)}$

$$\left.\begin{aligned} \log(z_1) &= \log(-a) + \log(z_0) - i\pi\sigma_{\mathrm{Im}(z_0)} \\ &= \log(-a) + \log(z_0) + i\pi\sigma_{\mathrm{Im}(z_1)} \end{aligned}\right\} a < 0, \tag{C.3.28}$$

but

$$\left.\begin{aligned} (a - i\lambda) &= |a|e^{-i\pi} \\ (a + i\lambda) &= |a|e^{+i\pi} \end{aligned}\right\} a < 0, \tag{C.3.29}$$

so

$$\left.\begin{aligned} \log(a + i\lambda\sigma_{\mathrm{Im}(z_1)}) &= \log(|a|) + i\pi\sigma_{\mathrm{Im}(z_1)} \\ \log(z_1) &= \log(a + i\lambda\sigma_{\mathrm{Im}(z_1)}) + \log(z_0) \end{aligned}\right\} a < 0, \tag{C.3.30}$$

but if $a > 0$, we can add a small imaginary part to $\log(a)$ without having any effect, so we have

$$\log(z_1) = \log(a + i\lambda\sigma_{\mathrm{Im}(z_1)}) + \log(z_0) \qquad \forall a \neq 0. \tag{C.3.31}$$

We will wish to apply this in Section 5.3 in the specific circumstance of splitting a logarithm with a real factor s:

$$\log(z) = \log(sx^2 + (-s + m_1^2 - m_2^2)x + m_2^2 - i\lambda) \tag{C.3.32}$$

$$= \log\left(s(x - x_1)(x - x_2)\right) \tag{C.3.33}$$

$$= \log(s + i\lambda\sigma_{\mathrm{Im}(z)}) + \log(x - x_1)(x - x_2) \tag{C.3.34}$$

$$= \log(s - i\lambda) + \log(x - x_1)(x - x_2), \tag{C.3.35}$$

because we have $\sigma_{\mathrm{Im}(z)} = -1$ for real or complex m_i: in the real case the only imaginary part is $-i\lambda$; and in the complex case, the imaginary part is $\mathrm{Im}(m_2)$ at $x = 0$ and $\mathrm{Im}(m_1)$ at $x = 1$, and interpolates between the two.

Now for real m_i, either x_1 and x_2 are real or they are complex with imaginary parts of opposite sign, so their logarithm can also be split with zero η function:

$$\log(z) = \log(s - i\lambda) + \log(x - x_1) + \log(x - x_2), \tag{C.3.36}$$

and for complex masses,

$$\log(z) = \log(s - i\lambda) + \log(x - x_1) + \log(x - x_2) + \eta(x - x_1, x - x_2) \tag{C.3.37}$$

$$= \log(s - i\lambda) + \log(x - x_1) + \log(x - x_2) + \eta(-x_1, -x_2), \tag{C.3.38}$$

as we know that $(x - x_1)(x - x_2)$ has a fixed sign imaginary part for all relevant values of x, namely $-\sigma_s$. Therefore the η function has throughout the same value as when $x = 0$.

C.4 n-dimensional Gaussian

Consider the integration of a gaussian in n-dimensional space. We can choose either to integrate the entire function in cartesians, or we can do only the radial integration and multiply by the "surface area" A.

$$\int_{-\infty}^{\infty} dx_1 \dots dx_n e^{-(x_1^2 + \dots + x_n^2)} = A \int_0^{\infty} dr e^{-r^2} r^{n-1}, \tag{C.4.39}$$

now use $\Gamma(n) = 2\int_0^{\infty} e^{-r^2} r^{2m-1} dr$ (found by simply substituting $t = r^2$ into the definition $\Gamma(n) = \int_0^{\infty} e^{-t} t^{n-1} dt$) to get

$$\left[\sqrt{\pi}\right]^n = A\frac{1}{2}\Gamma\left(\frac{n}{2}\right) \tag{C.4.40}$$

so

$$A = \frac{2\pi^{\frac{n}{2}}}{\Gamma\left(\frac{n}{2}\right)} \tag{C.4.41}$$

and we have an equation for the surface area of an n-sphere.

C.5 Relating $\det \mathcal{S}$ and $\det \mathcal{G}$ with α_i, β_i and γ_i

In Section 5.1.3 we asserted

$$(b_i \det \mathcal{S})^2 = 2\alpha_i \det \mathcal{S} - \det \mathcal{G} \left(\beta_i^2 - 4\alpha_i\gamma_i\right). \tag{C.5.42}$$

We have (5.1.33)-(5.1.34)

$$\begin{aligned} b_1 =& \frac{4ab + 2bd - c^2 - ce}{2bd^2 - 2cde + 2ae^2 - 8abf + 2c^2 f} = \frac{4ab + 2bd - c^2 - ce}{\det \mathcal{S}} \\ b_2 =& \frac{cd - 2ae}{2bd^2 - 2cde + 2ae^2 - 8abf + 2c^2 f} = \frac{cd - 2ae}{\det \mathcal{S}} \\ b_3 =& \frac{-2bd - cd + 2ae + ce}{2bd^2 - 2cde + 2ae^2 - 8abf + 2c^2 f} = \frac{-2bd - cd + 2ae + ce}{\det \mathcal{S}} \end{aligned} \tag{C.5.43}$$

and (5.1.39)

$$g_1(z) = bz^2 + (c+e)z + a + d + f \tag{C.5.44}$$

$$g_2(z) = az^2 + dz + f \tag{C.5.45}$$

$$g_3(z) = (a+b+c)z^2 + (d+e)z + f, \tag{C.5.46}$$

and can demonstrate this for the three cases:

$$\begin{aligned} (b_1 \det \mathcal{S})^2 + \det \mathcal{G} \left(\beta_1^2 - 4\alpha_1\gamma_1\right) =& (4ab + 2bd - c^2 - ce)^2 \\ &+ (4ab - c^2)((c+e)^2 - 4b(a+d+f)) && \text{(C.5.47)} \\ =& 2b(2bd^2 - 2cde + 2ae^2 - 8abf + 2fc^2) && \text{(C.5.48)} \\ =& 2\alpha_1(\det \mathcal{S}) && \text{(C.5.49)} \\ (b_2 \det \mathcal{S})^2 + \det \mathcal{G} \left(\beta_2^2 - 4\alpha_2\gamma_2\right) =& (cd - 2ae)^2 + (4ab - c^2)(d^2 - 4af) && \text{(C.5.50)} \\ =& 2a(-2ecd + 2ae^2 + 2fc^2 + 2bd^2 - 8abf) \\ & && \text{(C.5.51)} \\ =& 2\alpha_2(\det \mathcal{S}) && \text{(C.5.52)} \\ (b_3 \det \mathcal{S})^2 + \det \mathcal{G} \left(\beta_3^2 - 4\alpha_3\gamma_3\right) =& (-2bd - cd + 2ae + ce)^2 \\ &+ (4ab - c^2)((d+e)^2 - 4(a+b+c)f) && \text{(C.5.53)} \\ =& 2\alpha_3(\det \mathcal{S}). && \text{(C.5.54)} \end{aligned}$$

C.6 Small Imaginary Parts of $\mathcal{S}$

For $\mathcal{S}$, we can consider what the appropriate sign of the small imaginary parts should be. We find (see, e.g. Section 2.2 of [78]):

$$s_i \to s_i + i\lambda \tag{C.6.55}$$

$$s_{ij} \to s_{ij} + i\lambda \tag{C.6.56}$$

$$m_i^2 \to m_i^2 - i\lambda \tag{C.6.57}$$

which implies

$$\mathcal{S}_{ij} \to \mathcal{S}_{ij} + i\lambda. \tag{C.6.58}$$

Let us define the matrix H to have the same dimension as $\mathcal{S}$, and all of its entries unity. Then we can find the imaginary part of the determinant of $\mathcal{S}$:

$$\det \mathcal{S} \to \det\left(\mathcal{S} + i\lambda H\right) \tag{C.6.59}$$

$$= \det \mathcal{S} + i\lambda \sum_{ijk} \epsilon_{ijk}(\mathcal{S}_{1i}\mathcal{S}_{2j} + \mathcal{S}_{1i}\mathcal{S}_{3k} + \mathcal{S}_{2j}\mathcal{S}_{3k}) + \mathcal{O}(\lambda^2) \tag{C.6.60}$$

$$= \det \mathcal{S} + i\lambda \sum_{ijk} \epsilon_{ijk}(\mathcal{S}_{1i}\mathcal{S}_{2j} - \mathcal{S}_{1i}\mathcal{S}_{3j} + \mathcal{S}_{2i}\mathcal{S}_{3j}) + \mathcal{O}(\lambda^2) \tag{C.6.61}$$

$$\begin{aligned} = \det \mathcal{S} + i\lambda\big(&\mathcal{S}_{12}\mathcal{S}_{23} - \mathcal{S}_{12}\mathcal{S}_{33} + \mathcal{S}_{22}\mathcal{S}_{33} - \mathcal{S}_{13}\mathcal{S}_{22} + \mathcal{S}_{13}\mathcal{S}_{32} - \mathcal{S}_{23}\mathcal{S}_{32} \\ &- \mathcal{S}_{13}\mathcal{S}_{21} - \mathcal{S}_{13}\mathcal{S}_{31} + \mathcal{S}_{23}\mathcal{S}_{31} - \mathcal{S}_{11}\mathcal{S}_{23} + \mathcal{S}_{11}\mathcal{S}_{33} - \mathcal{S}_{21}\mathcal{S}_{33} \\ &- \mathcal{S}_{11}\mathcal{S}_{22} - \mathcal{S}_{11}\mathcal{S}_{32} + \mathcal{S}_{21}\mathcal{S}_{32} - \mathcal{S}_{12}\mathcal{S}_{21} + \mathcal{S}_{12}\mathcal{S}_{31} - \mathcal{S}_{22}\mathcal{S}_{31}\big) + \mathcal{O}(\lambda^2) \end{aligned} \tag{C.6.62}$$

$$\begin{aligned} = \det \mathcal{S} + i\lambda\big(&(\mathcal{S}_{11} - 2\mathcal{S}_{13} + \mathcal{S}_{33})(\mathcal{S}_{22} - 2\mathcal{S}_{23} + \mathcal{S}_{33}) \\ &- (\mathcal{S}_{12} - \mathcal{S}_{13} - \mathcal{S}_{23} + \mathcal{S}_{33})^2\big) + \mathcal{O}(\lambda^2) \end{aligned} \tag{C.6.63}$$

$$= \det \mathcal{S} + i\lambda \det \mathcal{G} + \mathcal{O}(\lambda^2), \tag{C.6.64}$$

which means that it is appropriate to equate:

$$\frac{2(bd^2 - cde + e^2a + c^2f - 4abf + i\lambda \det \mathcal{G})}{\det \mathcal{G}} = \frac{\det \mathcal{S}}{\det \mathcal{G}} = \frac{1}{\mathcal{B}}. \tag{C.6.65}$$